HOWARD UNIVERSITY
SCHOOL OF ENGINEERING
DEPARTMENT OF MECHANICAL ENGINEERING
WASHINGTON, D.C. 20059

FINAL REPORT

NASA GRANT: NSG-1414, Suppl. 3

THE DYNAMICS AND CONTROL OF LARGE FLEXIBLE SPACE STRUCTURES-IV

BY

Peter M. Bainum
Professor of Aerospace Engineering
Principal Investigator

and

V. K. Kumar
R. Krishna
A. S. S. R. Reddy
Graduate Research Assistants

AUGUST 1981

HOWARD UNIVERSITY
SCHOOL OF ENGINEERING
DEPARTMENT OF MECHANICAL ENGINEERING
WASHINGTON, D.C. 20059

FINAL REPORT

NASA GRANT: NSG-1414, Suppl. 3

THE DYNAMICS AND CONTROL OF LARGE FLEXIBLE SPACE STRUCTURES-IV

by

Peter M. Bainum
Professor of Aerospace Engineering
Principal Investigator

and

V.K. Kumar
R. Krishna
A.S.S.R. Reddy
Graduate Research Assistants

August 1981

ABSTRACT

The effects of solar radiation pressure as the main environmental disturbance torque have been incorporated into the model of the rigid orbiting shallow shell and computer simulation results indicate that within the linear range the rigid modal amplitudes are excited in proportion to the area to mass ratio. The effect of higher order terms in the gravity-gradient torque expressions previously neglected has been evaluated and found to be negligible for the size structures under consideration. A graph theory approach has been employed for calculating the eigenvalues of a large flexible system by reducing the system (stiffness) matrix to lower ordered submatrices. The related reachability matrix and term rank concepts are used to verify controllability and can be more effective than the alternate numerical rank tests. Control laws have been developed for the shape and orientation control of the orbiting flexible shallow shell and numerical results presented. Hybrid control systems consisting of point actuators and passive articulated dumbbell damping devices are evaluated for possible use with systems nominally oriented along the local horizontal and can result in improved fuel consumption and transient characteristics as compared with the active control system operating alone.

Contents

ABSTRACT

LIST OF FIGURES

CHAPTER 1 INTRODUCTION

CHAPTER 2 ENVIRONMENTAL DISTURBANCES

CHAPTER 3 GRAPH THEORY APPROACH TO THE EIGENVALUE PROBLEM OF LARGE SPACE STRUCTURES

CHAPTER 4 THE CONTROL OF LARGE FLEXIBLE ORBITING SHALLOW SPHERICAL SHELL STRUCTURES

CHAPTER 5 THE DYNAMICS OF LARGE FLEXIBLE EARTH POINTING STRUCTURES WITH A HYBRID CONTROL SYSTEM

CHAPTER 6 CONCLUSIONS AND RECOMMENDATIONS

LIST OF FIGURES

FIGURE NUMBER		Page Number
	CHAPTER 1	
1.1	Development of System Software for LSST Dynamics Analysis	1.2
	CHAPTER 2	
2.1	Beam Satellite	2.19
2.2	Influence of a Point Force on the Elastic Modes of a Free-Free Beam	2.20
2.3	Shallow Spherical Shell with Incident Solar Radiation	2.21
2.4	Geometry of Spherical Coordinate System	2.22
2.5	Shallow Spherical Shell with Dumbbell	2.23
2.6	Geometry of the Earth's Shadow	2.24
2.7	A Typical Variation of the Disturbance Torque, $C_z^{(s)}$, due to Solar Radiation Pressure	2.25
2.8a	Forced Pitch (θ) and Dumbbell Angle (γ) Response of the Gravitationally Stabilized Shallow Spherical Shell due to Solar Radiation Pressure	2.27
2.8b	Forced Roll (ϕ) Response of the Gravitationally Stabilized Shallow Spherical Shell due to Solar Radiation Pressure	2.28
2.8c	Forced Yaw Response of the Gravitationally Stabilized Shallow Spherical Shell due to Solar Radiation Pressure	2.29
2.9a	Forced Pitch (θ) and Dumbbell Angle (γ) Response of the Gravitationally Stabilized Shallow Spherical Shell due to Solar Radiation Pressure-Effect of Increase in the Area to Mass Ratio.	2.30
2.9b	Forced Roll (ϕ) Response of the Gravitationally Stabilized Shallow Spherical Shell due to Solar Radiation Pressure-Effect of Increase in The Area to Mass Ratio	2.31
2.9c	Forced Yaw (ψ) Response of the Gravitationally Stabilized Shallow Spherical Shell due to Solar Radiation Pressure-Effect of Increase in the Area to Mass Ratio	2.32

2.10	Boom Deflection Geometry (only half of total boom assembly shown)	2.33
A.1	Coordinate Frames	2.38
A.2	Euler Angle Rotations	2.39
A.3	Sequence of Rotation from τ_{10} to τ_2	2.39
B.1	Geometry of the Cross Section of a Shallow Spherical Shell	2.40
	CHAPTER 3	
1	Non-zero Element Pattern of the K-Matrix	3.6
2	Digraph of 16x16 K-Matrix	3.8
3a	Reachability Matrix for Free-Free Square Plate	3.9
3b	Reachability Matrix for Free-Free Square Plate after Separation of S_1, S_2, S_3 Submatrices	3.10
3c	Reachability Matrix for Free-Free Square Plate after Separation of S_1, S_2, S_3, S_4 Submatrices	3.11
3d	Reachability Matrix for Free-Free Square Plate after Separation of $S_1, S_2, S_3, S_4, S_5, S_6$ Sub-matrices	3.11
4	Location of Actuators	3.11
	CHAPTER 4	
4.1	Shallow Spherical Shell with Dumbbell and Location of Actuators	4.10
4.2	"A" Matrix for Shell without Dumbbell	4.11
4.3	"A" Matrix for Shell with Dumbbell	4.12
4.4	Time History of Control Forces without Dumbbell	4.13

	CHAPTER 5	
1a	Uniform Flexible Beam Nominally Oriented along the Local Horizontal	5.15
1b	Dumbbell Stabilized Flexible Beam Nominally Oriented along Local Horizontal with Passive and Active Controllers	5.15
2	Time Response of Flexible Beam with Active Control and No Dumbbell	5.16
3	Time Response of Dumbbell Stabilized Flexible Beam with Active Control	5.17
4	Dumbbell Stabilized Square Plate in Orbit	5.18
5	Nodal Patterns of the Free-Free Square Plate and the Actuator Locations	5.18
6	Time Response of Flexible Square Plate with Active Control and No Dumbbell	5.19
7	Time Response of Dumbbell Stabilized Flexible Square Plate with Active Control	5.20

I. INTRODUCTION

The present grant represents a continuation of the effort attempted in the previous grant years (May 1977-May 1980) and reported in Refs. 1.6.* Attitude control techniques for the pointing and stabilization of very large, inherently flexible spacecraft systems are being investigated. Control of both the orientation relative to the local vertical - local horizontal frame of reference and also the shape of the surface will often be required to meet the objectives of the various proposed LSST missions. These include: communications systems; earth observation and resource detection systems; orbitally based electronic mail systems; and also orbitally based platforms to be used for the collection of solar energy.

Figure 1.1 illustrates a plan of development of a system software capability for use in the analysis of LSST dynamics analysis. This plan can be subdivided into four different components: (1) system dyanmics; (2) structural dynamics; (3) application of control algorithms; and (4) the simulation of enviornmental disturbances.

Within the system dynamics block, a general formulation of the equation of motion of an arbitrary flexible body in orbit has been developed and includes also the effects of the Earth's gravity-gradient within the model. From this the equations of motion have been developed for homogeneous beams, plates, and shallow spherical shell-type structures.

---

*For references cited in this report, please see list of references after each chapter.

Fig. 1.1: DEVELOPMENT OF SYSTEM SOFTWARE FOR LSST DYNAMICS ANALYSIS

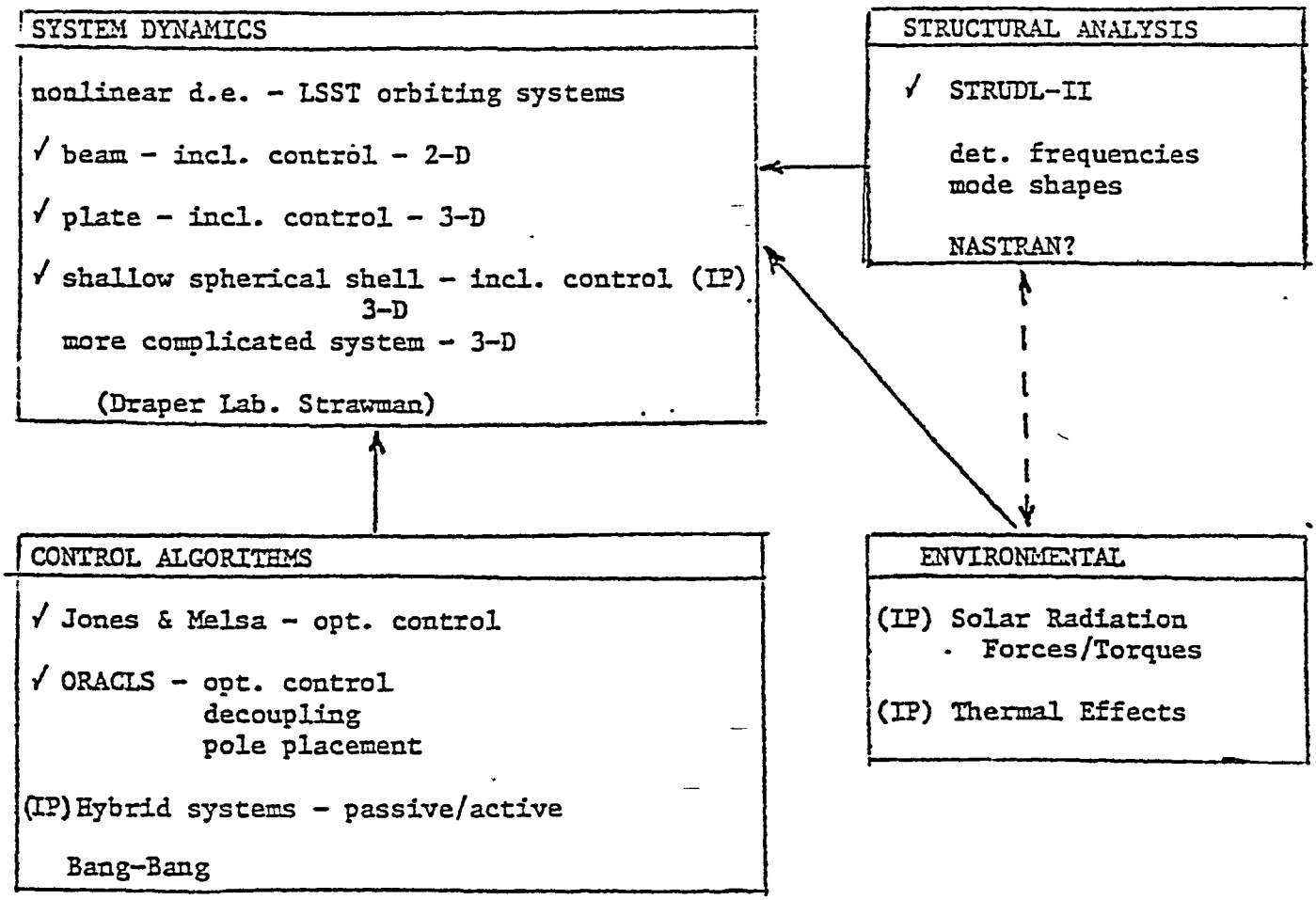

✓ operational

IP- in progress

For the simpler homogeneous structures such as unconstrained beams and circular plates the mode shape functions and elastic frequencies are available as relatively simple analytic expressions. For more complex systems such as a square or rectangular plate or non-isotropic systems these expressions must be calculated based on numerical techniques, usually finite element algorithms or numerical computations of rather complex analytical approximate relationships. For the complete simulation of the controlled dynamics of such systems, the frequencies and the modal shape functions of the retained modes are necessary inputs.

Once the uncontrolled dynamics and stability of these systems has been investigated various control algrithms are then used to establish controllability and develop control laws for the number and location of actuators assumed in the model. During the last grant year the acquisition of the ORACLS[7] software package, developed by NASA-Langley, has proved to be extremely useful in enabling us to develop control laws based on pole placement, decoupling, and optimal control theory techniques.

In accordance with our proposal to NASA dated January 15, 1980[8], we have also initiated a preliminary study of the disturbance forces which are primarily attributed to the effects of solar pressure forces and moments and the related problem of thermally induced deflections. The items indicated by a check mark have been essentially completed by the end of this grant year while those indicated by (IP) are still in progress at this time.

Chapter II of this report describes the results obtained to date in the study of the environmental disturbances and also an examination of the effect of higher order terms in the development of the gravity-gradient torque expressions which were previously neglected, in response to a question asked during last year's final oral presentation.

A paper presented at the Third VPI&SU/AIAA Symposium on the Dynamics and Control of Large Flexible Spacecraft, June 1981, forms the basis of Chapter III and illustrates how graph theoretic techniques can be used to facilitate the calculation of eigenvalues for large order systems and also to reduce the number of computations required to verify system controllability.

In Chapter IV control laws are developed for the shape and orientation control of the orbiting flexible shallow shell and typical required control forces are simulated. Attention is also given to the calculation of the modal frequencies of the shell which are seen to depend on the shell curvature as well as the material properties.

A second paper to be presented at the 1981 AAS/AIAA Astrodynamics Conference, August 1981, forms the basis of Chapter V, and examines the use of combinations of point actuators together with passive articulated dumbbell damping devices for large systems nominally pointing towards the Earth (i.e. - oriented along the local horizonal). The objective here is to demonstrate the improvement in fuel consumption and transient response characteristics which could be realized with such hybrid control systems.

Chapter VI describes the main general conclusions together with recommendations for further work.

References - Introduction

1. Bainum P.M. and Sellappan, R., "The Dynamics and Control of Large Flexible Space Structures," Final Report NASA Grant: NSG-1414, Part A: Discrete Model and Modal Control, Howard University, May 1978.

2. Bainum Peter M., Kumar, V.K., and James, Paul K., "The Dynamics and Control of Large Flexible Space Structures," Final Report, NASA Grant: NSG-1414, Part B: Development of Continuum Model and Computer Simulation, Howard University, May 1978.

3. Bainum, P.M. and Reddy, A.S.S.R., "The Dynamics and Control of Large Space Structures II," Final Report, NASA Grant NSG-1414, Suppl. I, Part A: Shape and Orientation Control Using Point Actuators, Howard University, June 1979.

4. Bainum, P.M., James P.K., Krishna, R., and Kumar, V.K., "The Dynamics and Control of Large Flexible Space Structures II" Final Report, NASA Grant NSG-1414, Suppl. 1, Part B: Model Development and Computer Simulation, Howard University, June 1979.

5. Bainum, P.M., Krishna, R., and James, P.K., "The Dynamics and Control of Large Flexible Space Structures III," Final Report, NASA Grant NSG-1414, Suppl. 2, Part A: Shape and Orientation Control of a Platform in Orbit using Point Actuators, Howard University, June 1980.

6. Bainum, P.M. and Kumar, V.K., "The Dynamics and Control of Large Flexible Space Structures III, Final Report, NASA Grant NSG-1414, Suppl. 2, Part B: The Modelling, Dynamics and Stability of Large Earth Pointing Orbiting Structures, Howard University, September 1980.

7. Armstrong, E.S., "ORACLS - A System for Linear Quadratic-Gaussian Control Law Design," NASA Technical Paper 1106, April 1978.

8. Bainum, P.M., "Proposal for Research Grant on: The Dynamics and Control of Large Flexible Space Structures IV," Howard University (Submitted to NASA), Jan. 15, 1980.

Chapter II

ENVIRONMENTAL DISTURBANCES

A spacecraft in orbit is subjected to many disturbance forces and torques which arise from the interaction between the spacecraft and the surrounding environment. The most common sources of such environmental disturbances are:

1. the earth's atmosphere;
2. the earth's magnetic field;
3. the earth's gravitational field;
4. meteorite impacts;
5. earth shine radiation;
6. solar radiation; and
7. influence of other planets and the sun.

At the orbits in which the proposed future space missions involving large space structures are flown, it is expected that the major source of disturbance is the solar radiation. However, since the dimensions of the proposed large structures are an order of magnitude larger than those of more conventional spacecraft, a reinvestigation into the gravity-gradient force and torque expressions which include higher order terms and higher harmonics of the earth's gravitational field is needed. Further, if gas jets are used for attitude and shape control, unwanted forces and torques may arise from the internal leaks in the system.

In section 2.1, the effects of point forces on a long, flexible beam are discussed. The method of approach can be extended to other types of structures. Also, some of the remarks made here also hold true, in general, for other types of structures.

An order of magnitude analysis of the gravity-gradient forces and torques due to the previously neglected higher order terms and higher harmonics of the earth's gravitational field is presented in section 2.2 for the class of large space structures currently proposed.

The effects of solar radiation pressure on the types of structures considered in Refs. 2.1-2.3 (i.e. beams, plates and shallow spherical shells) are discussed in section 2.3.

2.1. Point Force Acting on a Long, Flexible Beam

Consider the case of a long flexible orbiting beam which is nominally oriented along the local vertical, as shown in Fig. 2.1. The linearized equations of motion of this system with disturbances acting were obtained in Ref. 2.1 as,

$$\theta'' + 3\theta = C_y/J_y\omega_c^2 \tag{2.1}$$

$$\varepsilon_n'' + (\omega_n/\omega_c)^2\varepsilon_n = E_n/M_n\omega_c^2\ell \qquad (n = 1,2,\ldots) \tag{2.2}$$

where, θ = pitch

ε_n = nondimensional modal amplitude (A_n/ℓ)

ω_n = beam natural frequency; ω_c = orbital angular velocity

ℓ = length of the beam; M_n = n^{th} modal mass of the beam

C_y = pitch disturbance torque

E_n = n^{th} modal component of the external disturbance forces

J_y = pitch moment of inertia of the beam

$( )'$ = $d/d\tau$ and $\tau=\omega_c t$

t = time

It is assumed that a point force of magnitude, $F_1(t)$ is acting on the beam at $\zeta = \zeta_1$ as shown in Fig. 2.2.

The torque and the modal force components in eqns. (2.1) and (2.2) are given by,

$$(C_y/J_y\omega_c^2) = F_1\,\ell(\zeta_1 - \tfrac{1}{2})/J_y\omega_c^2 \;; \qquad E_n/M_n\omega_c^2\ell = \phi_z^{(n)}(\zeta_1)\; F_1/M_n\omega_c^2\ell$$

where, $\phi_z^{(n)}(\zeta)$ = n^{th} mode shape function of the beam.

By recalling, $J_y = m\ell^2/12$; $M_n = m$, where m is the mass of the beam, one arrives at,

$$C_y/J_y\omega_c^2 = 12(\zeta - \tfrac{1}{2})f_1 \;; \quad E_n/M_n\omega_c^2\ell = \phi_z^{(n)}(\zeta_1)f_1$$

where, $f_1 = F_1/m\omega_c^2\ell$; $\zeta = \xi_x/\ell + \tfrac{1}{2}$

Thus, one can rewrite eqns. (2.1) and (2.2) as,

$$\theta'' + 3\theta = 12(\zeta_1 - \tfrac{1}{2})f_1 \tag{2.3}$$

$$\varepsilon_n'' + (\omega_n/\omega_c)^2\varepsilon_n = \phi_1^{(n)}f_1 \tag{2.4}$$

where, $\phi_1^{(n)} = \phi_z^{(n)}(\zeta_1)$

The system of eqns. (2.3) and (2.4) may be represented by equivalent spring mass systems with forcing functions. Hence, one can define the following quantities for the above system assuming $f_1 = a_1 \sin(\frac{\omega}{\omega_c}\tau)$, where, ω = frequency of the point force, and $\tau = \omega_c t$

$$\theta_s = 4(\zeta - \tfrac{1}{2})a_1 \;; \quad \varepsilon_{n_s} = \phi_1^{(n)}a_1/(\omega_n/\omega_c)^2 \tag{2.5}$$

[θ_s and ε_{n_s} represent the deflections in each of the component modes of the system when a constant force of $f_1 = a_1$ is impressed on the system.]

By using eqn. (2.5) one can find the relative magnitudes of the influence of F_1 on each of the elastic modes for a given position of F_1. Fig. 2.2 shows the values of ε_{n_s} plotted against the position of F_1 for the first four elastic modes of the beam.

From this figure one can conclude that if the force F_1 is located at the nodal point of a mode, then that particular mode is not influenced by F_1. Also, one notes that, except for small regions near the nodal points of the first and second modes, for any postion of F_1 along the beam, the first and second modes are influenced quite significantly as compared to the other modes. Similar diagrams can be drawn when more than one force is acting on the beam. In the design of a controller which uses point actuators on the structures, such diagrams may be useful in a preliminary determination of actuator locations.

2.2. Gravity-Gradient Forces

In the studies presented in Refs. 2.1-2.3, the force at any point in the body due to the gravity-gradient was expressed as,

$$\bar{f} = \bar{f}_o + M\,\bar{r} \qquad (2.6)$$

where, $\bar{f}$ = gravity force intensity at the given point (force/mass) expressed in the body principal axes frame;

$\bar{f}_o$ = gravity force intensity at the center of mass of the body expressed in the body frame (force/mass);

$\bar{r}$ = instantaneous position vector of the given point with respect to the center of mass and expressed in the body frame;

M = matrix operator defined in eqn. (A.10) (Appendix A)

A brief development of eqn. (2.6) is presented in Appendix A. One can note that the terms containing $(\Delta\rho/\rho)^2$, $(\Delta\omega)^2$ and $(\Delta\eta)^2$ and higher powers are neglected in the derivation of eqn. (2.6) based on the assumption that they are very small as compared to unity.

One can estimate the order of magnitude of these quantities by noting that, $(\Delta\rho/\rho) \sim \mathcal{O}(\frac{\ell}{\rho_o})$; $\Delta\eta \sim \mathcal{O}(\frac{\ell}{\rho_o})$; $\Delta\omega \sim \mathcal{O}(\frac{\ell}{\rho_o})$, where, ℓ is the largest characteristic dimension of the structure and, ρ_o is the orbital radius. For currently proposed future large space structures the largest characteristic dimension is in the range of 100m to 10km. Hence, even if we consider the structure to be in a low altitude earth orbit (e.g. $\rho_o \sim$7000km), the magnitudes of $(\Delta\rho/\rho)$, $\Delta\eta$ and $\Delta\omega$ will be in the order of 10^{-5} to 10^{-4}. Thus, the quantities $(\Delta\rho/\rho)$, $\Delta\eta$ and $\Delta\omega$ are still much less than unity. Hence, one can neglect terms with $(\Delta\rho/\rho)^2$, $(\Delta\omega)^2$, $(\Delta\eta)^2$ and higher powers in the gravity force expression without introducing any significant error in the mathematical model.

The matrix M in eqn. (2.6) is the matrix defined in eqn. (A.9) and is given by,

$$M = M^{(o)} + \sum_{s=1}^{\infty} (\frac{a}{\rho_o})^s M^{(s)}; \frac{a}{\rho_o} < 1 \qquad (2.7)$$

where, $M^{(o)}$ = matrix defined in eqn. (A.11) of Appendix A; and

$$M^{(s)} = \frac{\nu a^2}{\rho_o^3} T_1 T_2 B^{(s)} (T_1 T_2)^{-1}$$

The term $M^{(o)}$ corresponds to a spherically symmetric gravitational field. The contributions due to higher harmonics of the gravitational field are represented by, $M^{(s)}$ (s = 1,2,...).

If we consider the contribution due to the zonal harmonics, one can easily show that, $M^{(1)} = 0$ if the origin of the inertial coordinate frame is chosen at the center of mass of the earth. The contribution due to the second zonal harmonic is given by,

$$M^{(2)} = \frac{\nu a^2}{\rho_o^3} T_1 T_2 B^{(2)} (T_1 T_2)^{-1} \qquad (2.8)$$

where,

$$B^{(2)} = J_2 \begin{bmatrix} 3(3c2\eta+1) & 6c2\eta & 0 \\ 6c2\eta & -\frac{3}{4}(7c2\eta+1) & 0 \\ 0 & 0 & -3(c2\eta+\frac{1}{2}) \end{bmatrix}$$

and $J_2 = 1.08263 \times 10^{-3}$, the second zonal harmonic coefficient.

A comparison of the elements of $M^{(2)}$ with the elements of $M^{(o)}$ show that each element of $M^{(2)}$ is three orders of magnitude smaller than the corresponding element in $M^{(o)}$. Further, it has been estimated by Bainum[2.4] that the percent error involved in evaluating force or moment expressions by neglecting the earth's oblateness (i.e. second zonal harmonic) is about 3.76×10^{-3} at synchronous altitudes. Thus, one can conclude that the contributions of higher order terms and higher harmonic components of the earth's gravity potential in the gravity-gradient force and torque expressions are negligible, even for the currently proposed large space structures.

2.3 Solar Radiation

At the orbital altitudes suggested for the proposed future large space systems one of the major sources of environmental disturbances would be due to solar radiation pressure. Karymov[2.5] has developed vector expressions for the forces and moments due to solar radiation pressure on a body. It is shown that the magnitude of the force and of the moment due to solar radiation on a sphere is independent of the direction of the incident radiation and also the surface properties of the sphere. Several investigators have considered the effect of solar radiation pressure on the dynamics of spacecraft.[2.6-2.12]

The majority of the spacecraft considered by these investigators consisted of a small central rigid satellite to which flat plate appendages were assumed to be attached. Since, the centers of the solar radiation pressure on these appendages are not usually located at the center of mass of the entire system, torques are exerted on the system. One can utilize the moments thus generated for attitude control of the spacecraft,[2.6-2.10] by controlling the orientation of the plates and/or vanes which can rotate at the ends of the appendages. In the case of large space structures, due to the inherently large surface area of the system, a significant amount of disturbance torque may be generated due to solar radiation pressure. In addition, the deformations induced by thermal stress due to solar heating may give rise to additional disturbance torques due to the interaction of the incident solar radiation on the deformed surface. A preliminary analysis of these effects of solar radiation on a rigid orbiting shallow spherical shell is presented here. To the authors' knowledge this is the first such analysis to consider the effect of solar radiation on an orbiting shallow spherical shell.

The expression for forces and moments due to solar radiation pressure on a shallow spherical shell structure are derived using the approach presented in Ref. 2.5. One can easily show that the moment due to solar radiation pressure on rigid beams and flat plate structures with uniform surface properties is zero. The force due to solar radiation pressure is given by,[2.5]

$$\bar{F}_s = \int_s d\bar{f}_s \tag{2.9}$$

where, $d\bar{f}_s = \hat{f}_s df_s$; $df_s = w(1+\varepsilon^2+2\varepsilon\cos 2\nu)^{\frac{1}{2}} \cos\nu \, ds$

$$\hat{f}_s = \frac{(1-\varepsilon)\hat{\tau} + 2\varepsilon(\hat{\tau}\cdot\hat{n})\hat{n}}{[(1-\varepsilon)^2 + 4\varepsilon^2(\hat{\tau}\cdot\hat{n})^2]^{\frac{1}{2}}}$$

ε = reflectivity

$\hat{\tau}$ = unit vector in the direction opposite to that of incident light flux

$\hat{n}$ = unit outward normal to the surface

$\frac{\pi}{2} - \nu$ = angle between $\hat{\tau}$ and $\hat{n}$

w = light energy density = 4.72×10^{-8} gms/cm^2 (for spacecraft orbiting in the vicinity of the earth, i.e. at or near the earth's distance from the sun).

The forces and torques due to solar radiation pressure on a shallow spherical shell are derived in the following section.

2.3A. Moments Due to Solar Radiation Pressure on a Rigid Shallow Spherical Shell

Fig. 2.3 shows a shallow spherical shell with the direction of incident radiation indicated by $-\hat{\tau}$. The moment due to solar radiation pressure can be expressed as,[2.5]

$$\bar{M}_s = (1-\varepsilon)\bar{M}_s^A + \varepsilon\bar{M}_s^R \qquad (2.10)$$

where, $\bar{M}_s^A$ = moment as calculated by assuming a totalling absorbing surface i.e. $\varepsilon = 0$; $\bar{M}_s^R$ = moment as calculated by assuming a totally reflective surface, i.e. ε=1.

Evaluation of $\bar{M}_s^A$:

The moment, $\bar{M}_s^A$ for a completely illuminated shallow shell (Fig. 2.3) is given by,[2.5]

$$\bar{M}_s^A = h_o \, s_2 \, \bar{r}_o(\hat{\tau} \times \hat{i}'') \qquad (2.11)$$

where, h_o = constant ($=4.64 \times 10^{-8}$ N/sq. m)

s_2 = projected area of the shell on a plane normal to $\hat{\tau}$

$\hat{i}''$ = unit vector perpendicular to $\hat{\tau}$ in the plane of $\hat{i}$ and $\hat{\tau}$

r_o = distance between the center of mass and the center of pressure.

After expressing, $\hat{\tau} = a_o\hat{i}+b_o\hat{j}+c_o\hat{k}$, one can easily derive from Fig. 2.3 that,

$$\left.\begin{aligned} S_2 &= \pi\ell^2 a_o \quad ; \quad r_o = \frac{H}{2}(1-a_o^2)^{\frac{1}{2}} \\ \text{and,} \quad (\hat{\tau}\times\hat{i}'') &= (1-a_o^2)^{\frac{1}{2}}(c_o\hat{j}-b_o\hat{k}) \end{aligned}\right\} \qquad (2.12)$$

After substituting eqn. (2.12) into eqn. (2.11) one obtains,

$$\bar{M}_s^A = \pi\ell^2 h_o \frac{H}{2} a_o(c_o\hat{j}-b_o\hat{k}) \qquad (2.13)$$

Evaluation of $\bar{M}_s^R$:

The moment due to solar radiation pressure on a totally reflecting surface is given by,[2.5]

$$\bar{M}_s^R = 2h_o\int_s(\hat{n}\times\bar{r})(\hat{\tau}.\hat{n})^2 ds \qquad (2.14)$$

where, $\hat{n}$ = outward normal to the surface of the shell at any point:

$\bar{r}$ = position vector from the center of mass of the shell.

One can express the vectors in eqn. (2.14) as (see Fig. 2.4),

$$\bar{r} = -p\hat{i}+R\hat{e}_n \quad ; \quad \hat{n} = \hat{e}_n \qquad (2.15)$$

$$\begin{aligned} \hat{\tau} = {} & (a_o c\beta_1+b_o c\beta s\rho_1+c_o s\beta s\beta_1)\hat{e}_n+(-a_o s\beta_1 \\ & +b_o c\beta_1 c\beta+c_o s\beta c\beta_1)\hat{e}_{\beta_1}+(-b_o s\beta+c_o c\beta)\hat{e}_\beta \end{aligned} \qquad (2.16)$$

where, $p = R-H/R$; $\hat{e}_n = c\beta_1\hat{i}+c\beta s\beta_1\hat{j}+s\beta s\beta_1\hat{k}$

$\hat{e}_{\beta_1} = -s_{\beta_1}\hat{i}+c\beta c\beta_1\hat{j}+s\beta c\beta_1\hat{k}$; $\hat{e}_\beta = -s\beta\hat{j}+c\beta\hat{k}$

a_o, b_o, c_o = direction cosines of $\hat{\tau}$ in the body frame, τ_3

Hence,

$$\left.\begin{aligned} \hat{n}\times\bar{r} &= p\,s\beta_1\hat{e}_\beta \\ (\hat{\tau}\cdot\hat{n})^2 &= (a_o c\beta_1+b_o c\beta s\beta_1+c_o s\beta s\beta_1)^2 \end{aligned}\right\} \qquad (2.17)$$

After substituting the results of eqn. (2.17) into eqn. (2.14) one obtains,

$$\begin{aligned} \bar{M}_s^R = 2h_o R^2(R-\frac{H}{2}) \int_{\beta_1=0}^{\beta_1'} \int_{\beta=0}^{2\pi} & (a_o c\beta_1+b_o c\beta s\beta_1 \\ & +c_o s\beta s\beta_1)^2 \hat{e}_\beta s^2\beta_1 d\beta d\beta_1 \end{aligned}$$

where, β_1' = maximum value of β_1 (see Fig. 2.4)

After performing the required integration,

$$\bar{M}_s^R = \pi h_o R^3 (1-H/2R) \left[2\frac{H}{R} - \frac{H^2}{R^2} \right]^2 a_o(b_o\hat{k}-c_o\hat{j}) \qquad (2.18)$$

Eqn. (2.18) can be further simplified for small values of H/ℓ by noting that, $H/R \tilde{=} 2H^2/\ell^2$ (as $R \tilde{=} \ell^2/2H$ see Fig. 2.5), i.e.

$$M_s^R \tilde{=} 16\pi h_o R^3 \left(\frac{H}{\ell}\right)^4 a_o(b_o\hat{k}-c_o\hat{j}) \qquad (2.19)$$

After substituting the results of eqns. (2.13) and (2.19) into eqn. (2.10) and noting, $R/\ell \tilde{=} \ell/2H$, (as $R \tilde{=} \ell^2/2H$, see Fig. 2.5), one obtains

$$\bar{M}_s = \frac{\pi}{2} h_o \ell^3 (H/\ell)(1-5\varepsilon) a_o(c_o\hat{j}-b_o\hat{k}) \qquad (H/\ell<<1) \qquad (2.20)$$

If the concave surface of the shell is facing towards the Sun, then $\bar{M}_s^R$ is obtained by multiplying the expression given in eqn. (2.19) by -1. Thus, for the case of the sun shining on the concave surface of the shell

$$\bar{M}_s = \frac{\pi}{2} h_o \ell^3 (H/\ell)(1-3\varepsilon) a_o(c_o\hat{j}-b_o\hat{k}) \qquad (H/\ell<<1) \qquad (2.21)$$

If the shell is moving in the earth's shadow, then, $\bar{M}_s=0$. Fig. 2.6 shows the geometry of the earth's shadow. For low altitude earth orbits, sufficiently accurate results can be obtained by approximating the earth's shadow to be a cylindrical shadow of radius equal to that of the earth (see Fig. 2.6). The following conditions determine whether the spacecraft is in the earth's shadow or not.

$$(\hat{\tau}\cdot\hat{\rho}_o) < 0 \ ; \text{ and, } [1-(\hat{\tau}\cdot\hat{\rho}_o)^2]^{\frac{1}{2}} \leq \frac{\rho_e}{\rho_o} \qquad (2.22)$$

where, $\hat{\rho}_o$ - unit vector along the line joining the earth and spacecraft and pointing towards the spacecraft.

ρ_e - earth radius.

If the spacecraft is moving in a circular orbit and if the spacecraft orbital angular position is measured from the spacecraft positon when the spacecraft is in the plane containing $\hat{\tau}$ and the orbit normal (and $\hat{\tau}\cdot\hat{\rho}_o > 0$ then the above conditions can be expressed as,

$$|(1-b_o^2)^{\frac{1}{2}}| \cos\tau < 0 \text{ ; and } (\sin^2\tau + b_o^2\cos^2\tau)^{\frac{1}{2}} \leq \rho_e/\rho_o \qquad (2.23)$$

where, $\tau = \omega_c t$ and b_o = component of $\hat{\tau}$ along the orbit normal.

The forced response of a rigid shallow shell with gravity stabilizing dumbbell due to solar radiation disturbance torques can be obtained by solving the following set of equations. The homogeneous form of these equations have been developed previously in Ref. 2.3

$$\theta'' - 3\Omega_y\theta - \bar{c}_y\gamma' - \bar{k}_y\gamma = C_y^{(s)} \qquad (2.24a)$$

$$\gamma'' + \bar{c}_y(1+c_1)\gamma' + \{3+\bar{k}_y(1+c_1)\}\gamma + 3(1+\Omega_y)\theta = Q_\gamma \qquad (2.24b)$$

$$\psi'' - \Omega_x\psi - (1+\Omega_x)\phi' = 0 \qquad (2.24c)$$

$$\phi'' + 4\Omega_z\phi + (1-\Omega_z)\psi' = C_z^{(s)} \qquad (2.24d)$$

$$\delta'' + \bar{c}_z(1+c_2)\delta' + \{4+\bar{k}_z(1+c_2)\}\delta + 4(1-\Omega_z)\phi - (1-\Omega_z)\psi' = Q_\delta \qquad (2.24e)$$

where,

$$C_y^{(s)} = (\bar{M}_s\cdot\hat{j})/J_y\omega_c^2 = \begin{cases} \delta_s\, a_o c_o(1-5\varepsilon) \text{ , } a_o>0 \\ \delta_s\, a_o c_o(1-3\varepsilon) \text{ , } a_o<0 \\ 0, \text{ when the spacecraft is in the Earth shadow.} \end{cases}$$

$$C_z^{(s)} = (\bar{M}_s\cdot\hat{k})/J_z\omega_c^2 = \begin{cases} \delta_s\, a_o b_o(1-5\varepsilon) \text{ , } a_o>0 \\ \delta_s\, a_o b_o(1-3\varepsilon) \text{ , } a_o<0 \\ 0, \text{ when the spacecraft is is in the Earth shadow.} \end{cases}$$

$$\delta_s = 2(\pi\ell^2/m)(H/\ell)\left(\frac{h_o}{\ell\omega_c^2}\right)$$

Q_γ, Q_δ = torques due to solar radiation on the dumbbell.

Figs. 2.7a and b show the nature of the disturbance torques, due to solar radiation, $C_y^{(s)}$ and $C_z^{(s)}$, for a spacecraft with an area to mass ratio of 0.02 m^2/kg and orbiting in a 250 n. mile altitude circular orbit, with the orbit normal oriented at an angle of 45 degrees to the earth-sun line. It can be noted from these figures that these torques are periodic. The average value of the pitch torque, $C_y^{(s)}$, over one orbit is noted to be zero. However, it is seen that the average value of the roll torque, $C_z^{(s)}$, over one orbit is not zero.

If the dumbbell is assumed to be rigid then the net torques on the dumbbell due to solar radiation pressure are zero, i.e., $Q_\gamma = 0$ and $Q_\delta = 0$.

Figs. 2.8-2.9 show the response of the rigid shallow shell-rigid dumbbell system subjected to the torques due to solar radiation pressure. The following numerical values for the constants have been assumed in obtaining these response plots.

$$h_o = 4.64 \times 10^{-6} N/m^2 \; ; \; (H/\ell) = 0.02 \; ; \; \ell = 50m \; ; \; \varepsilon = 0.5$$

In all these cases initial conditions are assumed to be zero. In Figs. 2.8 and 2.9 one can observe the beat phenomenon in the roll and yaw responses of the system. This indicates that some of the frequencies of the forcing functions are close to at least one of the system natural frequencies. One can also note that with an increase in the value of area to mass ratio, the amplitudes of pitch, roll, yaw, γ and δ responses increase in direct proportion.

Effect of the Thermal Deflection of the Stabilizing Boom

Due to the heating effect of the solar radiation, thermal stresses are induced in the structure. Thermal deformations are introduced in the structure because of these thermal stresses. It is assumed that the surface of the shallow spherical shell is controlled to be within the required accuracy limits although the control dynamics is not considered here. It is expected that the torque due to solar radiation pressure on the deformed shell is almost the same as that corresponding to the torque on an undeformed shell. However, since it is expected that there will be no control present to control the shape of the stabilizing boom, the boom will undergo thermal deformations due to solar heating. Additional torques may arise due to solar radiation pressure acting on the thermally deformed boom. In the present work, the boom is assumed to be a hollow tube of uniform cross section. The following additional simplifying assumptions are made in this preliminary investigation:

1. The boom cross section is of uniform thickness.

2. Boom deflections occur only in the plane containing the sunline and the boom's undeflected axis.

3. The temperature of the boom is independent of the boom's axial coordinate and the axial boom deflection is of higher order.

4. The energy exchange between the deflected boom and the satellite surface is negligible.

5. The earth radiation input may be neglected at the higher altitudes under consideration.

6. The inherent time lags in the heat transfer process are neglected.

7. Changes of moments of inertia and center of mass shift due to thermal deflections are neglected.

8. Boom deflections occur such that each differential element on the boom has the same constant radius of curvature.

In Ref. 2.4 an expression for the torque due to solar radiation pressure on a thermally bent pair of booms hinged at the center of the undeformed boom set has been derived based on the assumptions (1)-(8). The expression for the torque is given as[2.4],

$$\Delta N_s = \frac{2}{3} G' D \sin 2B_i \sin B_i \qquad (2.25)$$

where,

$G' = 2h_o \ell_d^2 r_d (1+ \frac{\varepsilon}{3})$; $D = \ell_d \alpha_o e q_s / 2kt_d$

$2\ell_d$ = length of the boom

r_d = radius of the tube; t_d = thickness of the tube;

ε = reflectivity ; e = emissivity

α_o = thermal absorptivity

B_i = Sun incidence angle between the sun direction and the undeflected boom axis (see Fig. 2.10)

The net torque attributed to solar pressure forces on the boom's tip masses is given by[2.4],

$$\Delta N_m = \frac{h_o S \ell_d}{2} D \sin 2 B_i \qquad (2.26)$$

where, S is the cross sectional spherical area.

If it is further assumed for this example that the Sun is shining in the orbit plane, then the net torque on the boom attributed to the solar radiation pressure on the thermally deflected boom is given by, $Q_\delta = 0$ and,

$$Q_\gamma = \Delta N_s + \Delta N_m \qquad (2.27)$$

By substituting eqn. (2.27) into eqn. (2.24b), one can solve eqns. (2.24a) and (2.24b) to obtain the pitch (θ) and dumbbell angle (γ) responses of the system for this case. In the present analysis a numerical integration procedure based on fourth order Runge-Kutta method was used in solving eqns. (2.24a) and (2.24b). For the example considered here, the following data has been assumed, boom material: beryllium copper.

$$\alpha_o = 0.15 \; ; \; e = 1.04\text{x}10^{-5}/^{o}\text{F} \; ; \; k = 36.3779 \text{k. cals/m-}^{o}\text{F-hr};$$

$$\varepsilon = 0.85 \; ; \; q_s = 1464.8 \text{ k.cals/hr-m}^2$$

In addition, $r_d/t_d = 1000$; $r_d = 5$cm ; tip mass = 0.5 (mass of the shell), have been assumed.

From the results of the numerical integration, it is noted that, for the set of data assumed in this particular example, the effect of the torque due to solar radiation pressure on a thermally deformed boom is negligible; thus, the pitch and dumbbell angle (γ) response in this case is essentially the same as that shown in Figs. 2.8-2.9 .

2.3B. Forces Due to Solar Radiation Pressure on a Rigid Shallow Spherical Shell

The force due to solar radiation pressure on a shallow spherical shell can be expressed in a similar fashion to eqn. (2.10), i.e.,

$$\bar{F}_s = (1-\varepsilon)\bar{F}_s^A + \varepsilon \bar{F}_s^R \qquad (2.28)$$

where, $\bar{F}_s^A$ = force as calculated by assuming a totally absorbing surface, i.e. $\varepsilon=0$;

$\bar{F}_s^R$ = force as calculated by assuming a totally reflective surface, i.e. $\varepsilon=1$.

Evaluation of $\bar{F}_s^A$:

The force, $\bar{F}_s^A$ for a completely illuminated shell is given by[2.5],

$$\bar{F}_s^A = -h_o s_2 \hat{\tau} \tag{2.29}$$

where, s_2 = projected area of the shell on a plane normal to $\hat{\tau} = \pi \ell^2 a_o$.

Hence, $\bar{F}_s^A = -\pi h_o \ell^2 a_o (a_o \hat{i} + b_o \hat{j} + c_o \hat{k})$ (2.30)

Evaluation of $\bar{F}_s^R$:

The force, $\bar{F}_s^R$ for a completely illuminated shell is given by[2.5],

$$\bar{F}_s^R = -2h_o \int_s \hat{n}(\hat{\tau}\cdot\hat{n})^2 \, ds \tag{2.31}$$

where, $\hat{n}$ = outward normal to the surface of the shell at any point.

By using the results in eqns. (2.15) and (2.16), one has,

$$\bar{F}_s^R = -2h_o R^2 \int_{\beta_1=0}^{\beta_1'} \int_{\beta=0}^{2\pi} (a_o c\beta_1 + b_o c\beta s\beta_1 + c_o s\beta s\beta_1)^2 \hat{e}_n s\beta_1 \, d\beta \, d\beta_1 \tag{2.32}$$

where, β_1' = maximum value of β_1.

After performing the required integration, one obtains,

$$\bar{F}_s^R = -\frac{\pi}{2} h_o R^2 \left[\left(2a_o^2 \left\{1-\left(1-\frac{H}{R}\right)^4\right\} + (b_o^2+c_o^2)\left(\frac{\ell}{R}\right)^4\right) \hat{i} + 2a_o(b_o\hat{j}+c_o\hat{k})\left(\frac{\ell}{R}\right)^4 \right] \tag{2.33}$$

Eqn. (2.33) can be further simplified for small values of (H/ℓ) by noting that, $(H/R) = 2(H/\ell)^2$ and $(\ell/R) = 2(H/\ell)$, i.e.,

$$\bar{F}_s^R \approx -8\pi h_o R^2 (H/\ell)^2 [a_o^2 \hat{i} + 2a_o(b_o\hat{j}+c_o\hat{k})(H/\ell)^2] \qquad (H/\ell \ll 1) \tag{2.34}$$

After substituting eqns. (2.30) and (2.34) into eqn. (2.28), one arrives at,

$$\overline{F}_s \approx -\pi h_o \ell^2 [(1+\varepsilon) a_o^2 \hat{i} + (1-\varepsilon) a_o (b_o \hat{j} + c_o \hat{k})] \quad (H/\ell << 1) \qquad (2.35)$$

If the concave surface of the shell is facing the sun, then, $\overline{F}_s^R$ is obtained by multiplying the expression in eqn. (2.34) by -1. Hence for the case of the sun shining on the concave surface of the shell,

$$\overline{F}_s \approx -\pi h_o \ell^2 [(1-3\varepsilon) a_o^2 \hat{i} + (1-\varepsilon) a_o (b_o \hat{j} + c_o \hat{k})] \quad (H/\ell << 1) \qquad (2.36)$$

The expressions in eqns. (2.35) and (2.36) might be useful in estimating the spacecraft orbit perturbations due to solar radiation pressure.

References

2.1. Bainum, P.M., Kumar, V.K., and James, P.K., "Dynamics and Control of Large Space Structures - Part B," Final Report, NASA Grant NSG-1414, Dept. of Mechanical Eng., Howard University, May 1978.

2.2 Bainum, P.M., James, P.K., Kumar, V.K., and Krishna, R., "The Dynamics and Control of Large Flexible Space Structures - II, Part B: Model Development and Computer Simulation," Final Report, NASA Grant NSG-1414, Suppl. 1, Dept. of Mechanical Eng., Howard University, June 1979.

2.3. Bainum, P.M. and Kumar, V.K., "The Dynamics and Stability of Large Flexible Space Structures - III, Part B: The Modelling, Dynamics and Stability of Large Earth Pointing Structures," Final Report, NASA Grant NSG-1414, Suppl. 2, Dept. of Mechanical Eng., Howard University, Sept. 1980.

2.4 Bainum P.M., "On the Motion and Stability of a Multiple Connected Gravity Gradient Satellite with Passive Damping," Technical Memorandum, TG-872, Johns Hopkins University, Appl. Phy. Lab., Jan. 1967, (Ph.D. Thesis, Catholic University of America, 1966).

2.5. Karymov, A.A., "Determination of Forces and Moments Due to Light Pressure Acting on a Body in Cosmic Space," PMM, Vol. 26, No. 5, 1962, pp. 867-876.

2.6. Crocker, M.C., "Attitude Control of a Sun Pointing Spinning Spacecraft by Means of Solar Radiation Pressure," J. of Spacecraft and Rockets, Vol. 7, No. 4, 1970, pp. 357.

2.7. Donlis, T.J. and Randall, J.C., "A Solar Vane Actuation System for Spacecraft Attitude Control," ASME Mech. Conf., Lafayette, Oct. 1964, paper no. 64.

2.8. Modi, V.J. and Pande, K.C., "Solar Pressure Control of a Dual Spin Satellite," J. of Spacecraft and Rockets, Vol. 10, 1973, pp. 355.

2.9. Modi, V.J. and Tschann, C., "On the Attitude and Librational Control of a Satellite Using Solar Radiation Pressure," presented at XXI IAF Congress, Konstanz, West Germany, Oct. 4-10, 1970.

2.10. Pande, K.C., Davis, M.S. and Modi, V.J., "Time Optimal Pitch Control of Satellites Using Solar Radiation Pressure," J. of Spacecraft and Rockets, Vol. 11, No. 8, 1974, pp. 601-603.

2.11. Clancy, T.F. and Mitchell, T.P., "Effects of Radiation Forces on the Attitude of an Artificial Earth Satellite," AIAA J., Vol. 2, No. 3, 1964, pp. 517-524.

2.12. Flanagan, R.S., and Modi, V.J., "Attitude Dynamics of a Gravity Gradient Satellite under the Influence of Solar Radiation Pressure," Aeronautical J., Vol. 74, Oct. 1970, pp. 835-841.

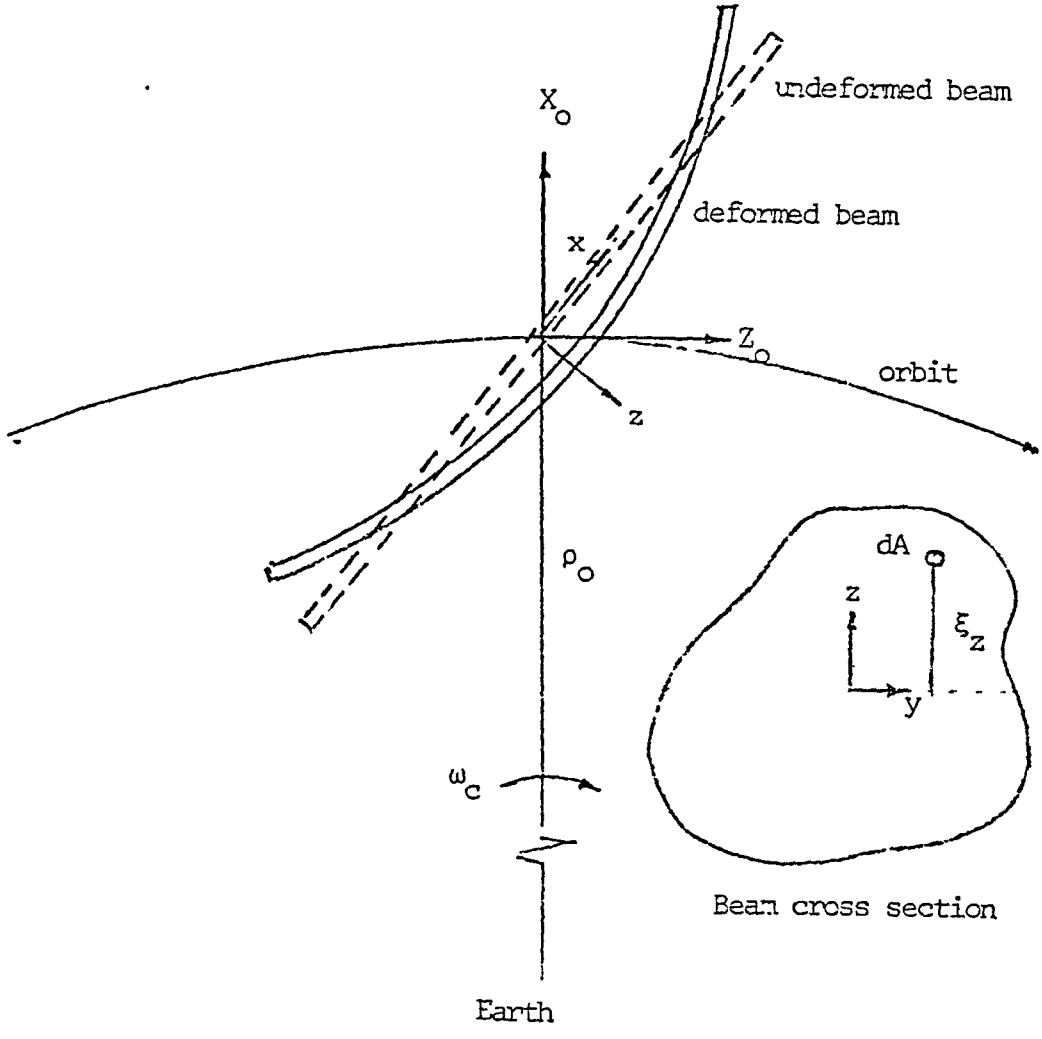

Fig. 2.1: Beam Satellite

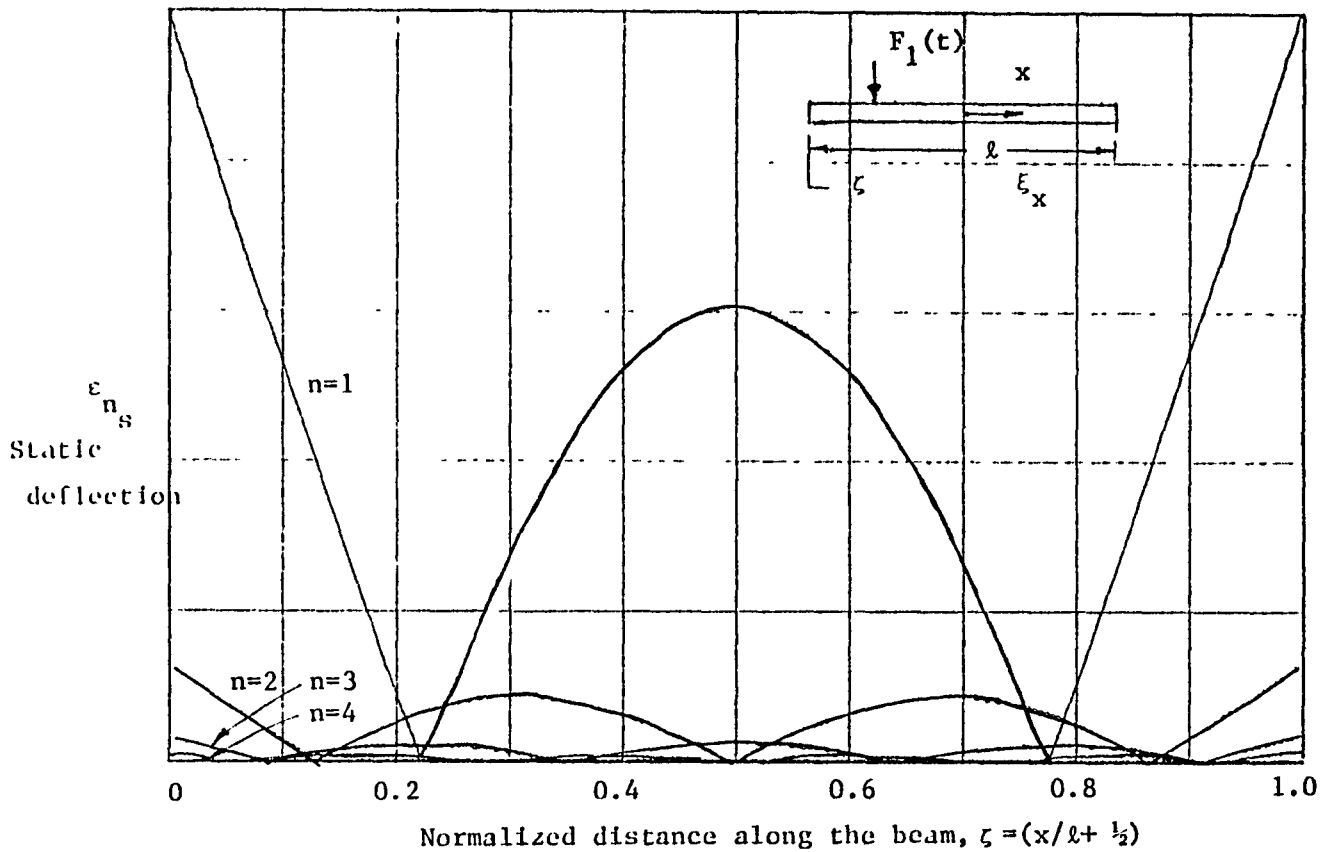

Fig. 2.2 : Influnce of a Point Force on the Elastic Modes of a Free-free Beam

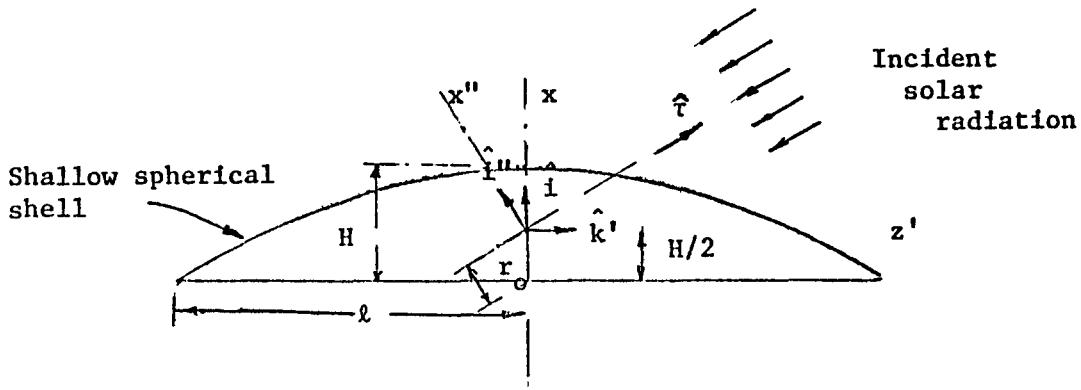

Fig. 2.3 : Shallow Spherical Shell with Incident Solar Radiation

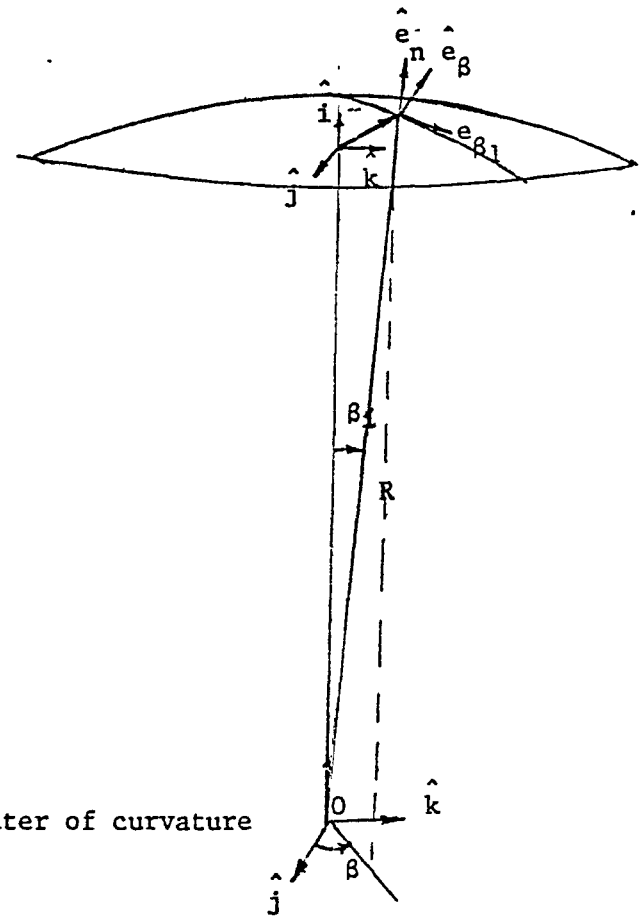

$\hat{e}_n, \hat{e}_\beta, \hat{e}_{\beta_1}$ are unit vectors of the spherical coordinate system centered at O.

Fig. 2.4: Geometry of Spherical Coordinate System

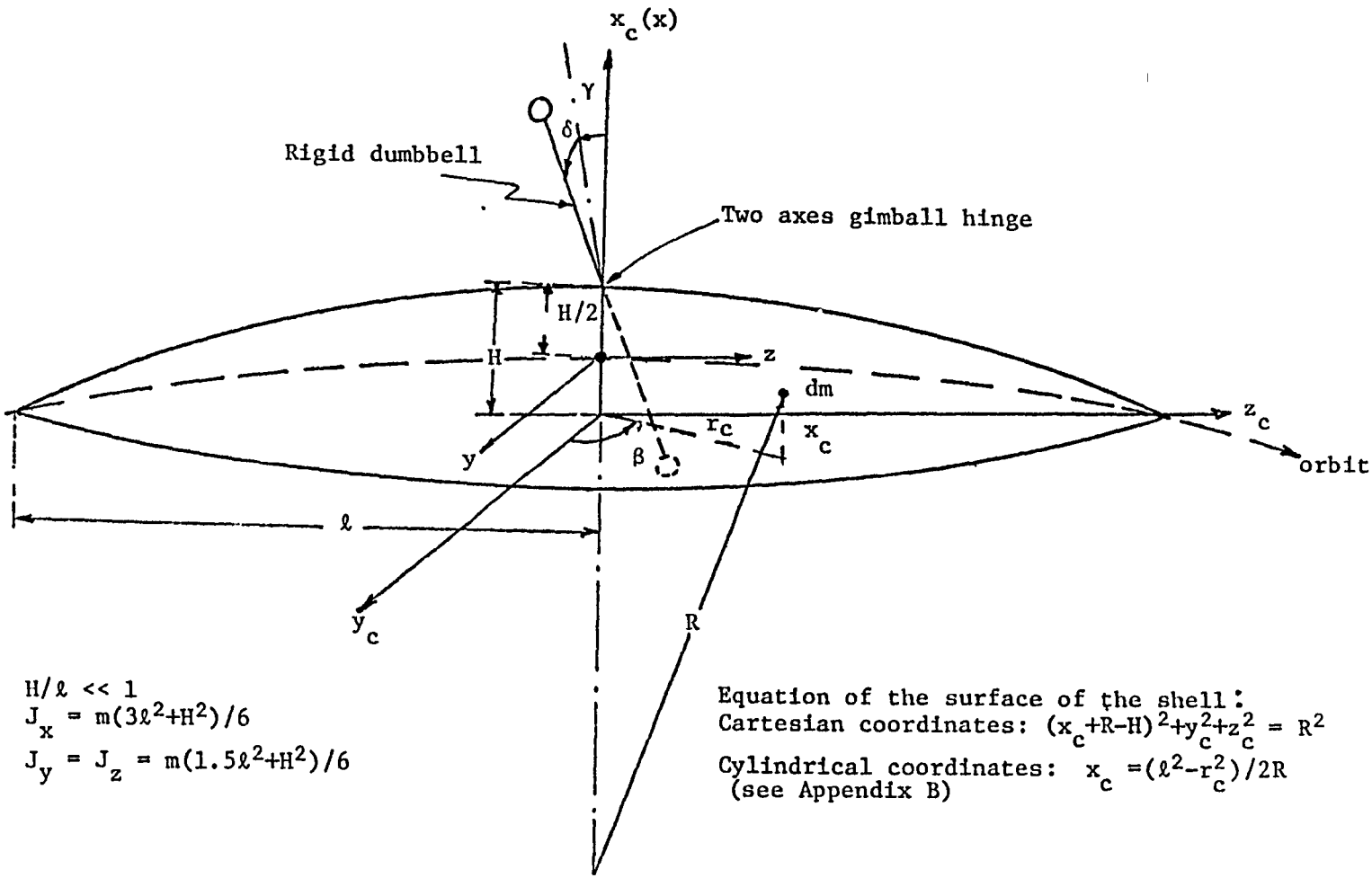

Fig. 2.5: Shallow Spherical Shell with Dumbbell.

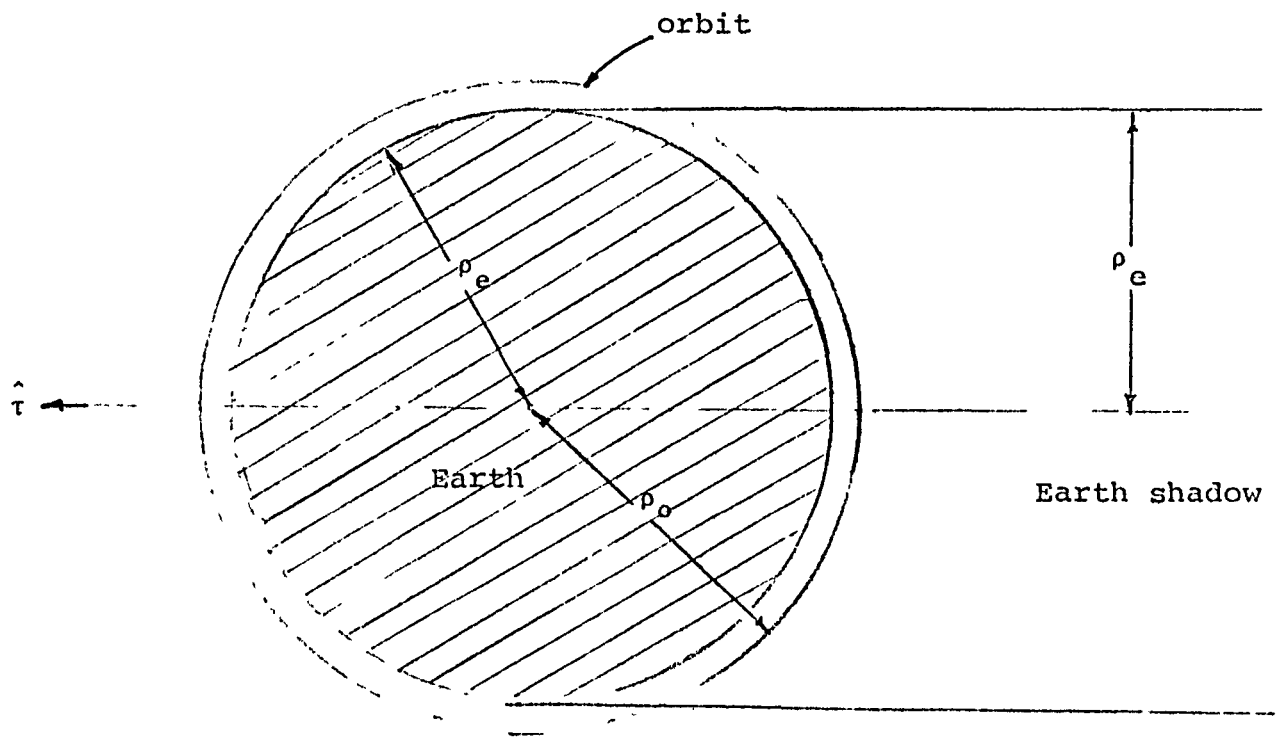

Fig. 2.6: Geometry of the Earth's Shadow

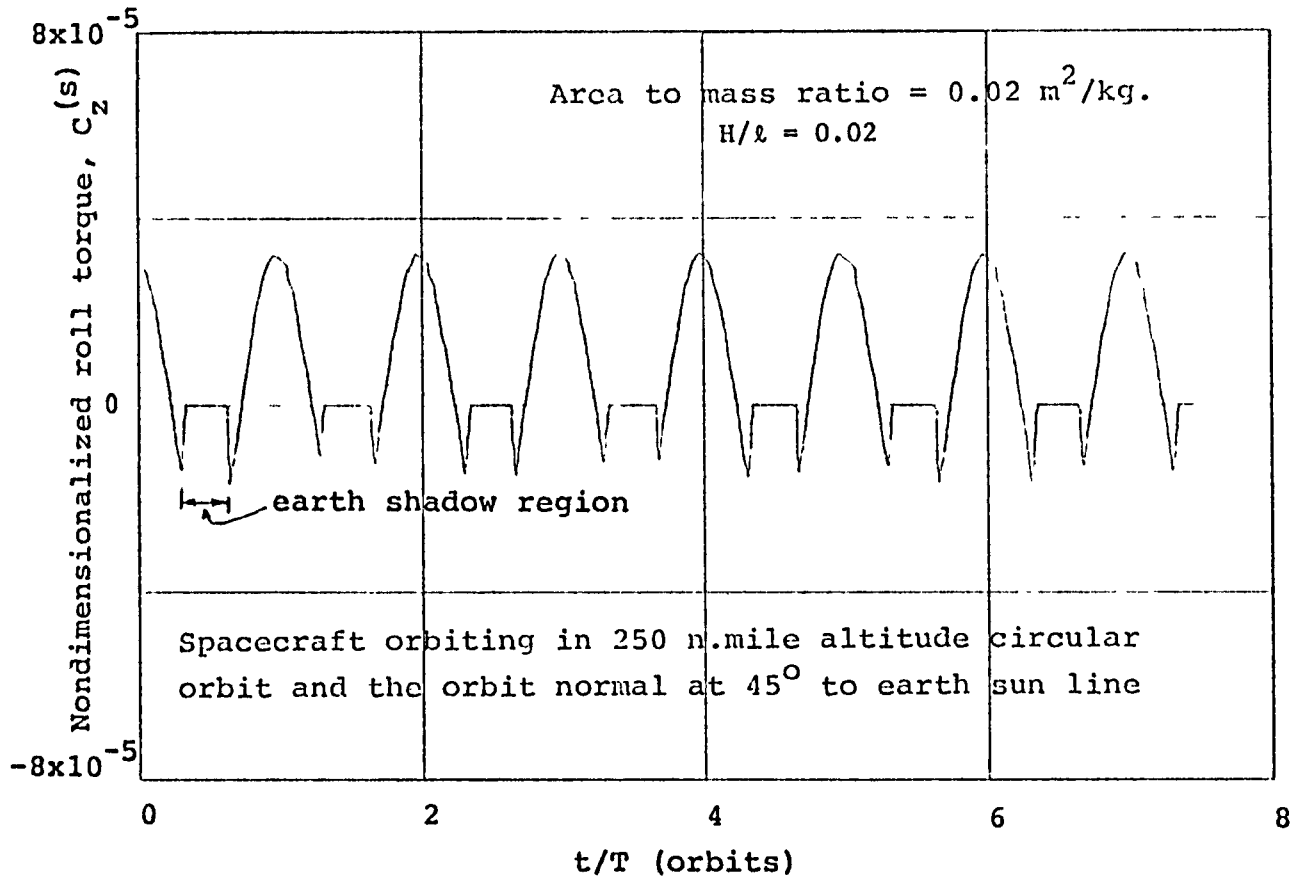

Fig. 2.7a: A Typical Variation of the Disturbance Torque, $C_z^{(s)}$, due to Solar Radiation Pressure

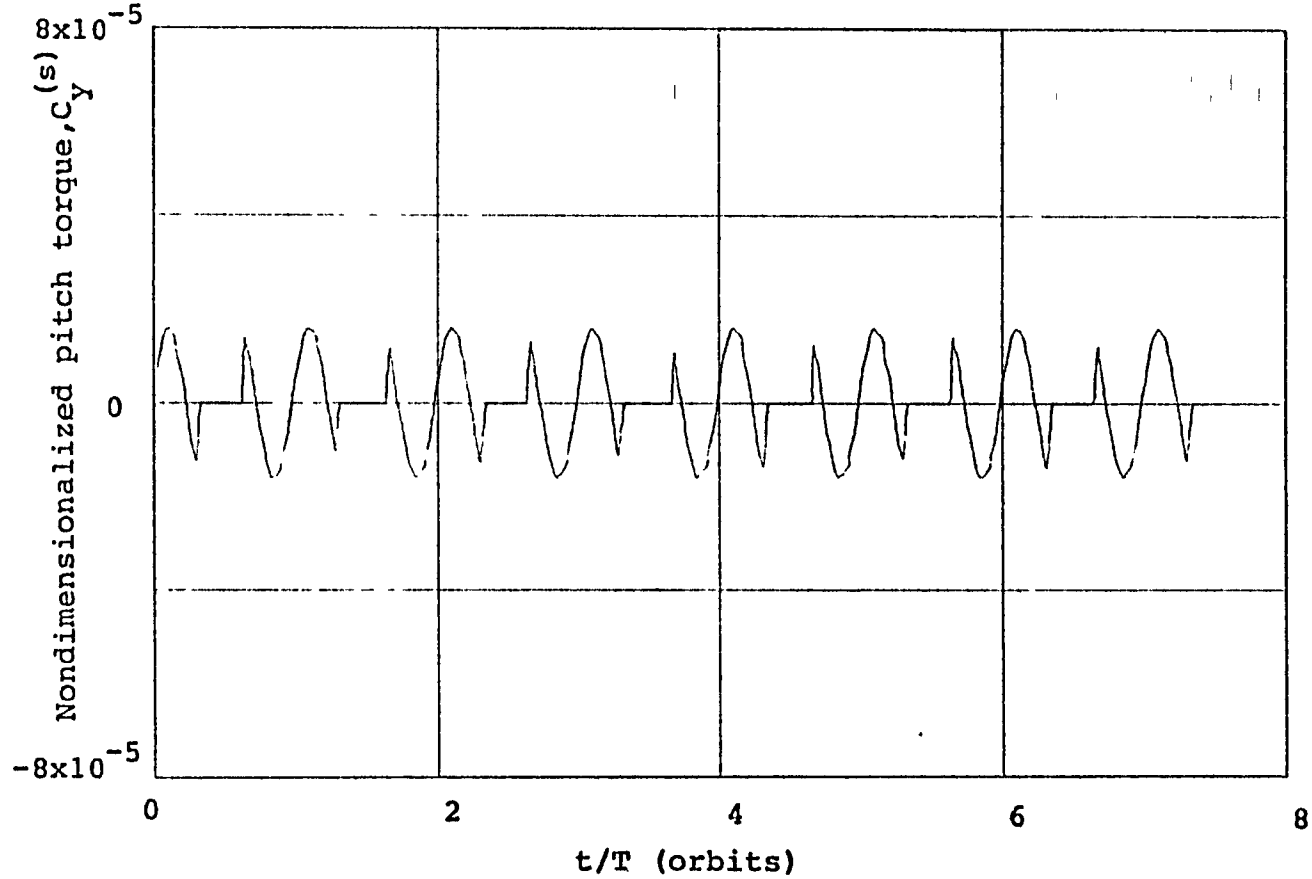

Fig. 2.7b: A Typical Variation of the Disturbance Torque, $C_y^{(s)}$, due to Solar Radiation

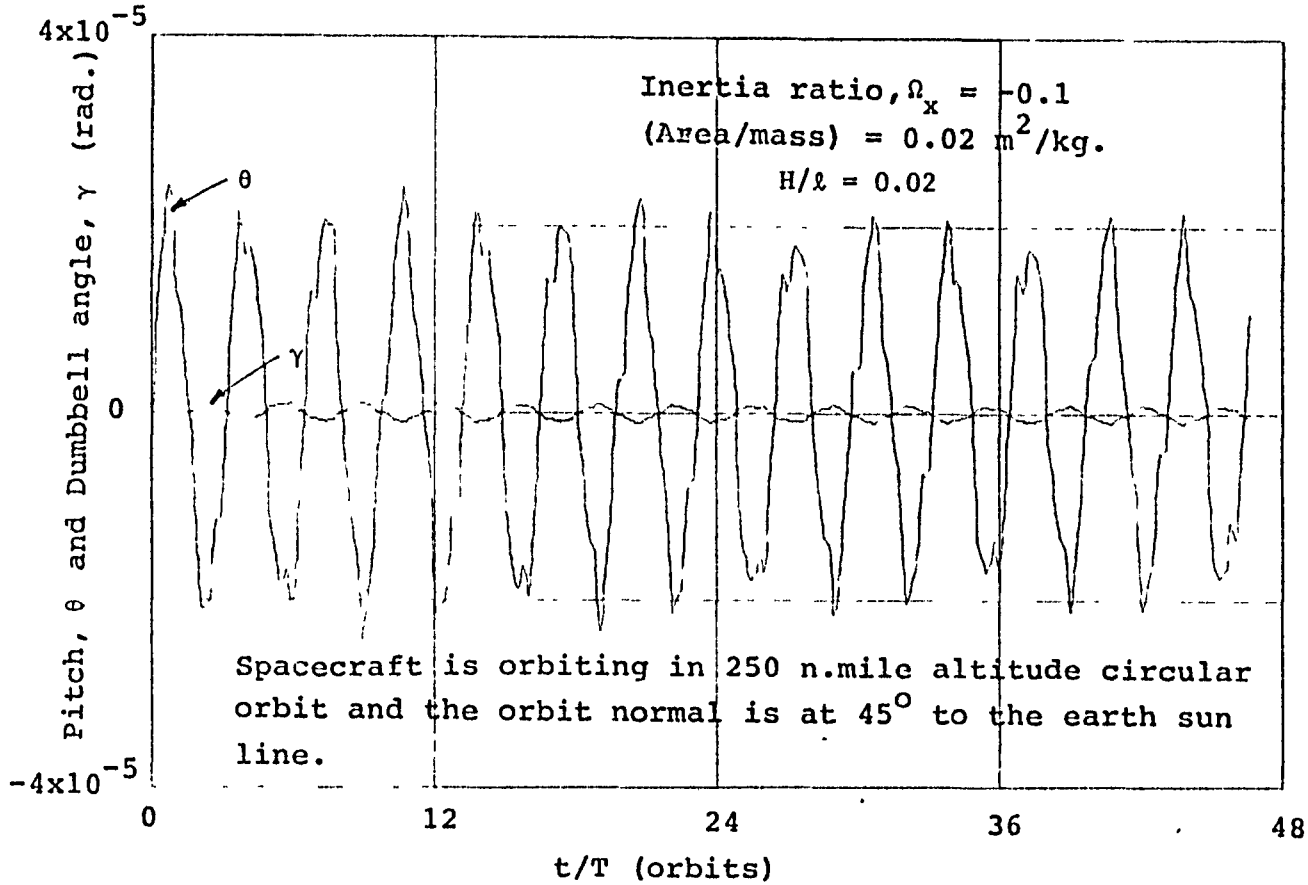

Fig. 2.8a: Forced Pitch (θ) and Dumbbell Angle (γ) Responses of the Gravitationally Stabilized Shallow Spherical Shell due to Solar Radiation Pressure

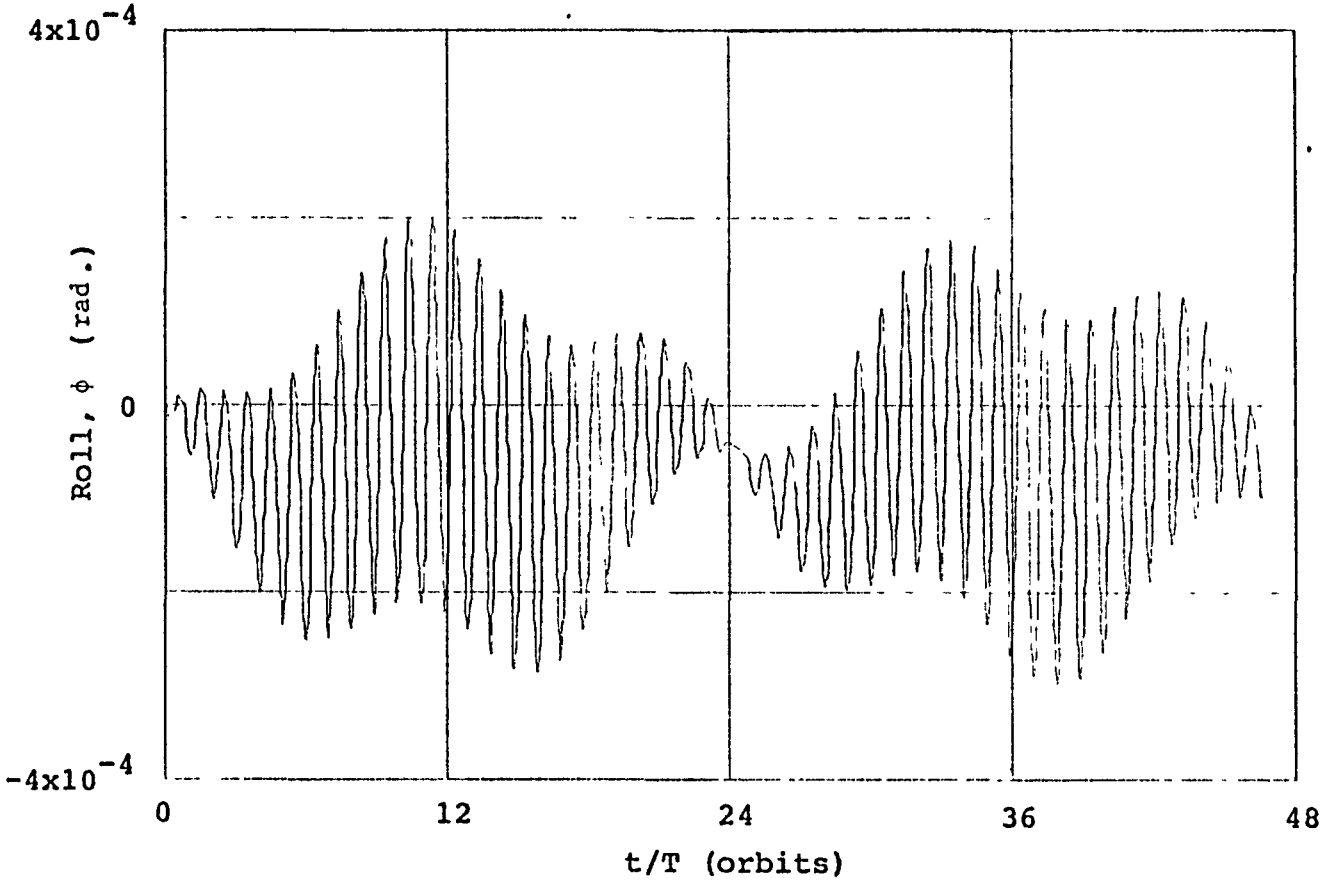

Fig. 2.8b: Forced Roll (ϕ) Response of the Gravitationally Stabilized Shallow Spherical Shell due to Solar Radiation Pressure

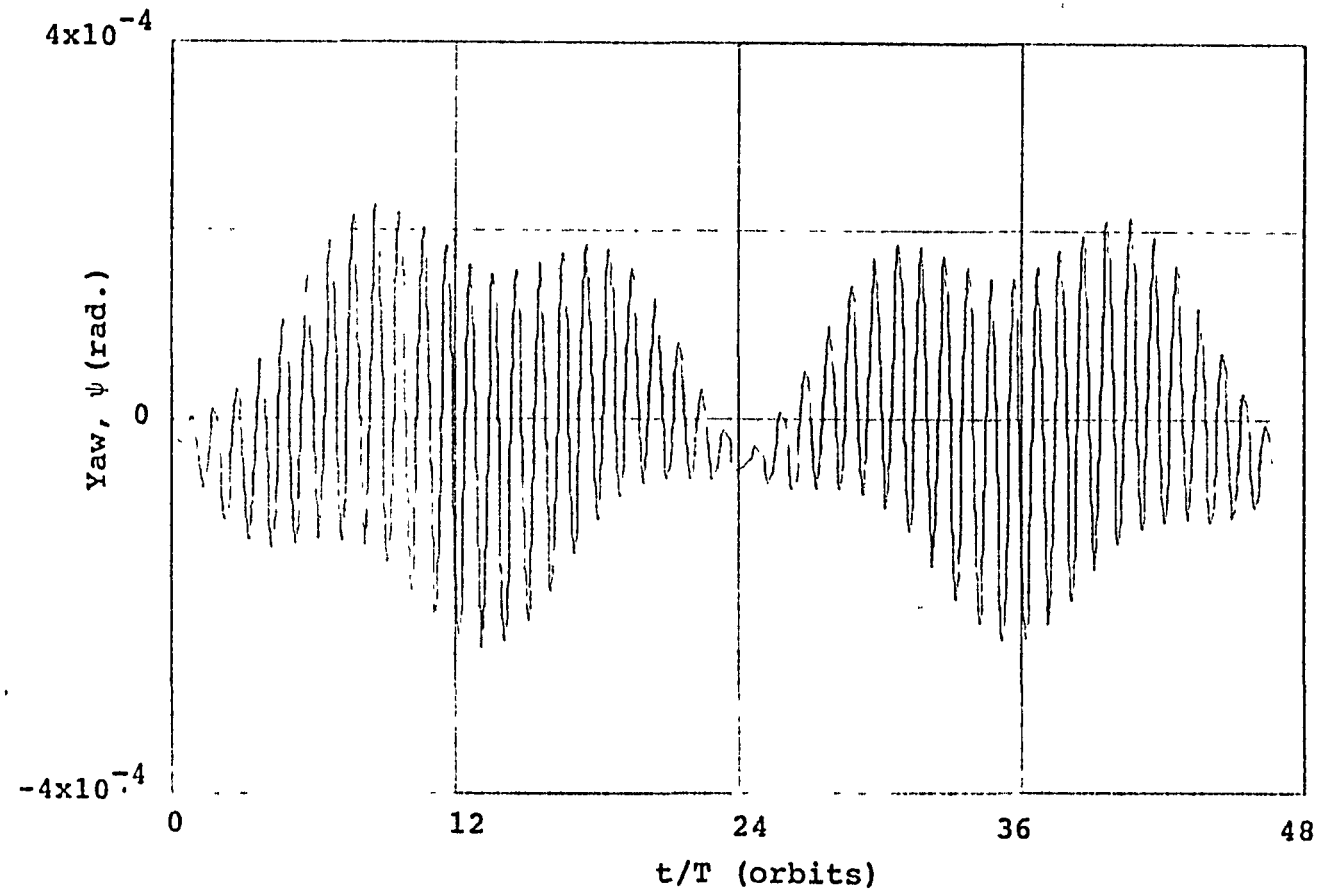

Fig. 2.8c: Forced Yaw Response of the Gravitationally Stabilized Shallow Spherical Shell due to Solar Radiation Pressure

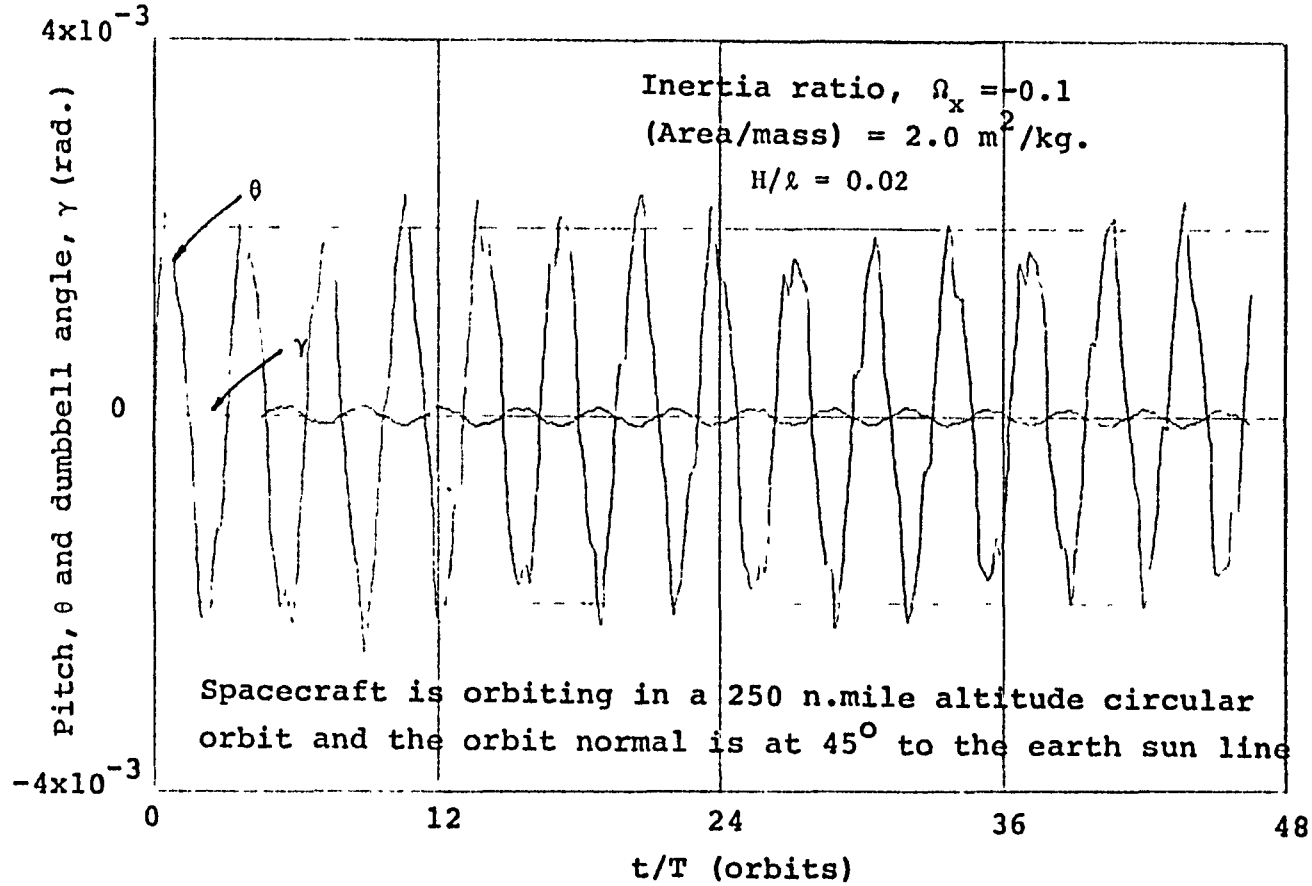

Fig. 2.9a: Forced Pitch (θ) and Dumbbell Angle (γ) Response of the Gravitationally Stabilized Shallow Spherical Shell due to Solar Radiation Pressure- Effect of increase in the area to mass ratio

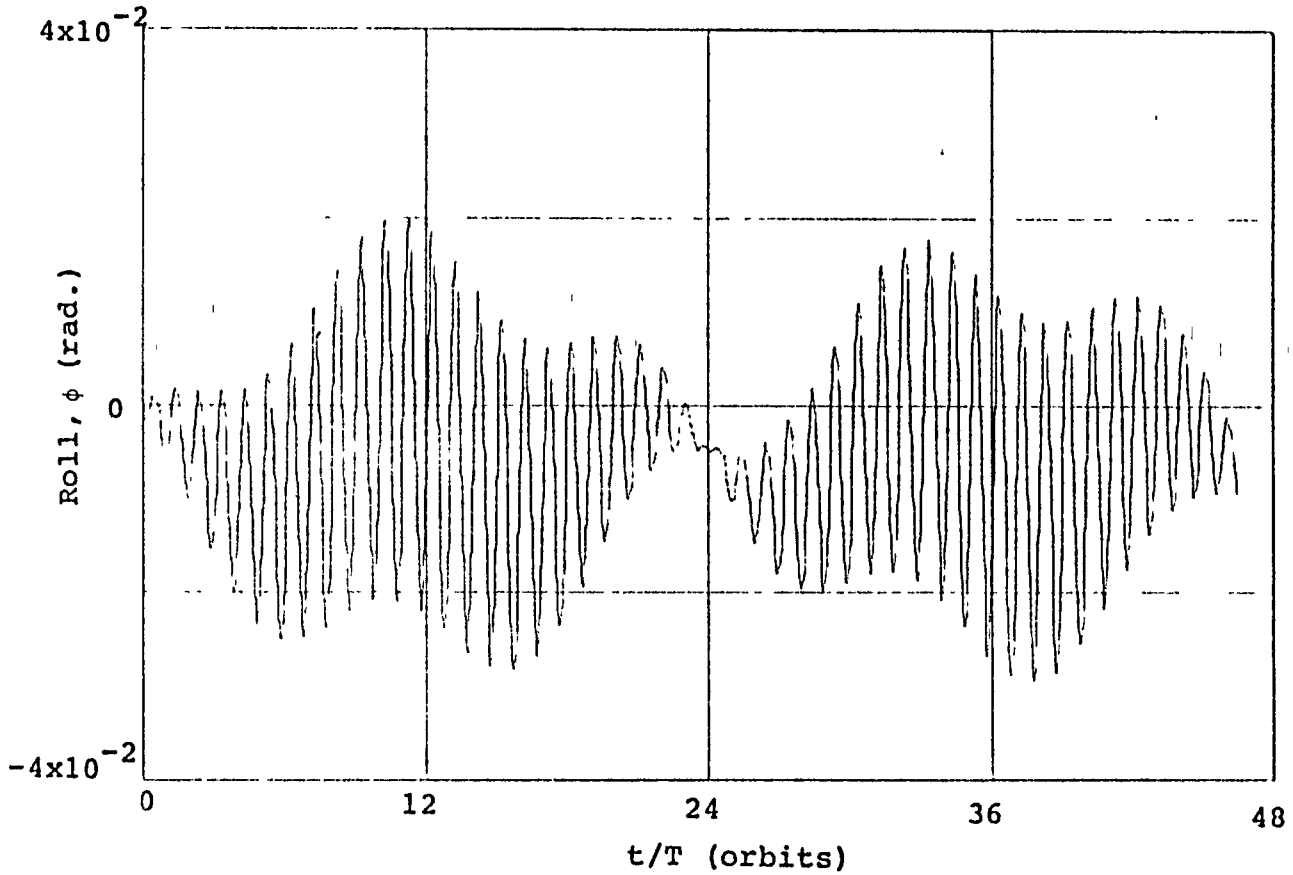

Fig. 2.9b: Forced Roll (ϕ) Response of the Gravitationally Stabilized Shallow Spherical Shell due to Solar Radiation Pressure - Effect of increase in the area to mass ratio

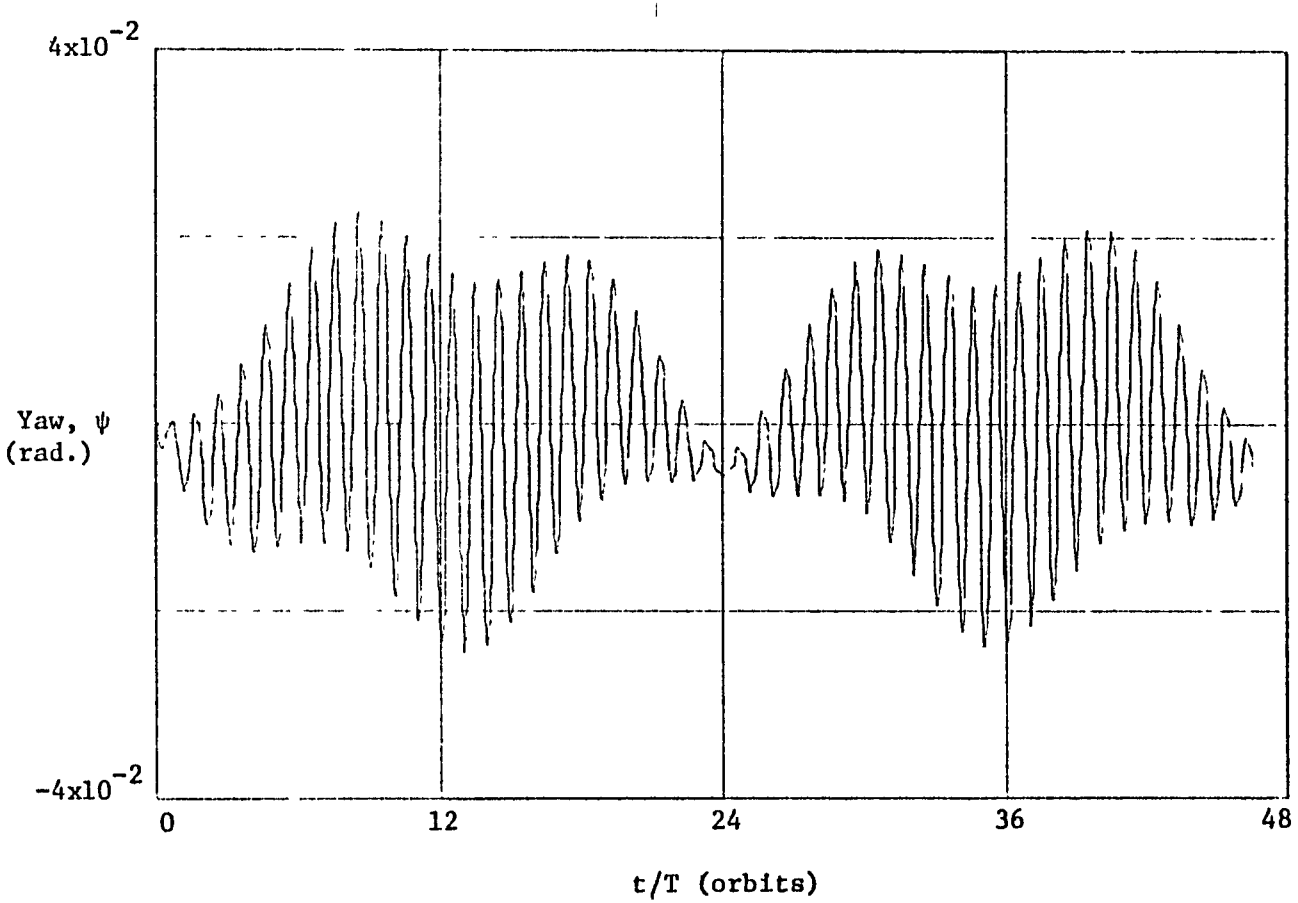

Fig. 2.9c: Forced Yaw (ψ) Response of the Gravitationally Stabilized Shallow Spherical Shell due to Solar Radiation Pressure - Effect of increase in the area to mass ratio.

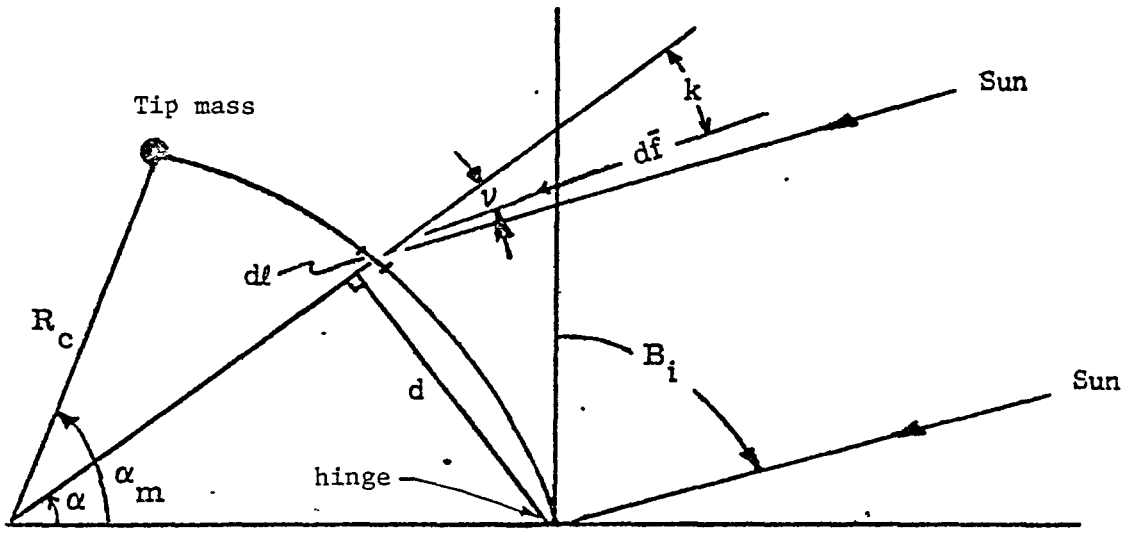

Fig. 2.10 : Boom Deflection Geometry
(only half of total boom assembly shown)

Appendix A

A brief development of the expression for the gravitational force per unit mass, $\bar{f}$, is presented here. The material presented here is extracted from Santini.*

Kinematic Relations

Fig. A.1 shows the various coordinate frames used in the development of gravity gradient force expressions. O'XYZ is an earth centered inertial reference frame (τ_o) with O'Z along the earth's spin axis and O'X along the ascending node. $Oi_1i_2i_3$ is the local intrinsic frame (τ_{10}) centered at the body center of mass, O, with Oi_1 along the local vertical and Oi_2 perpendicular to the plane ZO'O (Fig. A1). $OX_oY_oZ_o$ is an orbit fixed reference frame (τ_2) centered at the center of mass of the body, O, with OX_o along the local vertical and OY_o along the orbit normal opposite to the orbit angular momentum vector. Oxyz defines the principal axes (τ_3) of the body (not shown).

Fig. A.2 shows the sequence of Euler angle rotations adopted in going from the orbit frame, $\tau_2(X_o,Y_o,Z_o)$ to the body frame, $\tau_3(x,y,z)$. The body frame, $\tau_3(x,y,z)$ and the orbit frame, $\tau_2(X_o,Y_o,Z_o)$ are related to each other by the following transformation relation,

$$\tau_3 = T_1\tau_2 \qquad (A.1)$$

where,

$$T_1 = \begin{bmatrix} c\phi c\theta & s\phi c\psi+c\phi s\theta s\psi & s\phi s\psi-c\phi s\theta c\psi \\ -s\phi c\theta & c\phi c\psi-s\phi s\theta s\psi & c\phi s\psi+s\phi s\theta c\psi \\ s\theta & c\theta s\psi & c\theta c\psi \end{bmatrix}$$

The body angular velocity components $(\omega_x,\omega_y,\omega_z)$ and Euler angular rates $(\dot{\theta},\dot{\phi},\dot{\psi})$ are related as follows,

$$\begin{aligned} \omega_x &= \dot{\theta}s\phi+\dot{\psi}c\phi c\theta-\omega_c(s\phi c\psi+c\phi s\theta s\psi) \\ \omega_y &= \dot{\theta}c\phi-\dot{\psi}s\phi c\theta-\omega_c(c\phi c\psi-s\phi s\theta s\psi) \\ \omega_z &= \dot{\psi}s\theta+\dot{\phi}+\omega_c c\theta s\psi \end{aligned} \qquad (A.2)$$

*Santini, P., 'Stability of Flexible Spacecrafts', Acta Astronautica, Vol. 3, 1976, pp. 685-713.

Fig. A.3 shows the sequence of rotations adopted in going from the intrinsic frame, $\tau_{10}(i_1 i_2 i_3)$ to the orbit frame, τ_2 (X_o, Y_o, Z_o). The intrinsic frame, τ_{10}, is related to the orbit frame, τ_2, by the transformation relation, (see also Fig. A.1)

$$\tau_2 = T_2 \tau_{10} \tag{A.3}$$

where,

$$T_2 = \begin{bmatrix} 1 & 0 & 0 \\ 0 & c\chi & s\chi \\ 0 & -\chi & c\chi \end{bmatrix}$$

Gravity Force

One can write the gravitational potenial in the most general form as:

$$V(\rho, \eta, \omega) = \frac{\nu a^2}{\rho} + \nu a \sum_{s=1}^{\infty} \left(\frac{a}{\rho}\right)^{s+1} \Omega_s(\eta, \omega) \tag{A.4}$$

where,

$$\Omega_s(\eta,\omega) = \sum_{m=0}^{s} K_{sm}[P_s^{(m)}(\eta)\cos(m\omega+\phi_{sm})]$$

$P_s^{(m)}(\eta)$ is the m^{th} associated Legendre function of order s.

K_{sm} and ϕ_{sm} are constants to be obtained experimentally through satellite geodesy techniques.

The gravitational force per unit mass at any point in the body, $\bar{f}$, with components in the local intrinsic frame is given by,

$$\bar{F}(\rho,\eta,\omega) = F_\rho \hat{e}_\rho + F_\eta \hat{e}_\eta + F_\omega \hat{e}_\omega$$

where,

$(\hat{e}_\rho, \hat{e}_\eta, \hat{e}_\omega)$ are unit vectors in the local intrinsic frame.

$$F_\rho = \frac{\partial V}{\partial \rho} = -\frac{\nu a^2}{\rho^2} + \nu a \sum_{s=1}^{\infty} \left(\frac{a}{\rho}\right)^{s+1} \Omega_s$$

$$F_\eta = \frac{1}{\rho}\frac{\partial V}{\partial \eta} = \frac{\nu a}{\rho} \sum_{s=1}^{\infty} \left(\frac{a}{\rho}\right)^{s+1} \Omega_s'$$

$$F_\omega = \frac{1}{\rho s\eta}\frac{\partial V}{\partial \omega} = \frac{\nu a}{\rho s\eta} \sum_{s=1}^{\infty} \left(\frac{a}{\rho}\right)^{s+1} \hat{\Omega}_s$$

where, $(\ )' = \partial(\ )/\partial\eta$; $(\hat{\ }) = \partial(\ )/\partial\omega$

The gravity force per unit mass at the generic point, P, in the body as expressed in the local intrinsic frame at the center of mass of the body and for small values of $\delta\rho, \delta\eta$ and $\delta\omega$ is given by

$$\bar{F} = \bar{F}_0 + \Delta\bar{F}_0 + \frac{\partial F}{\partial(\rho,\eta,\omega)} \begin{bmatrix} \Delta\rho \\ \Delta\eta \\ \Delta\omega \end{bmatrix} + \text{H.O.T} \qquad \text{(A.5)}$$

where,

$$\Delta\bar{F}_0 = \begin{bmatrix} 0 & -F_\eta & -F_\omega s\eta \\ 0 & F_\rho & -F_\omega c\eta \\ 0 & 0 & F_\rho s\eta + F_\eta c\eta \end{bmatrix} \begin{bmatrix} \Delta\rho \\ \Delta\eta \\ \Delta\omega \end{bmatrix}$$

$\bar{F}_0$ = gravitational force per unit mass at the center of mass of the body.

After some mathematical manipulations, it can be shown that,

$$\underline{\Delta F}_0 + \frac{\partial F}{\partial(\rho,\eta,\omega)}\Big|_0 \begin{Bmatrix} \Delta\rho \\ \Delta\eta \\ \Delta\omega \end{Bmatrix} = B^* \begin{Bmatrix} \Delta\rho \\ \rho\Delta\eta \\ \rho s\eta\Delta\omega \end{Bmatrix} \qquad \text{(A.6)}$$

where,

$$B^* = \frac{\nu a^2}{\rho^3}\left[B^{(0)} + \sum_{s=1}^{\infty} \left(\frac{a}{\rho}\right)^s B^{(s)}\right]$$

$$B^{(0)} = \begin{bmatrix} 2 & 0 & 0 \\ 0 & -1 & 0 \\ 0 & 0 & -1 \end{bmatrix}$$

$$B^{(s)} = \begin{bmatrix} (s+1) & (s+2)\Omega_s & -(s+2)\Omega_s' & -s(s+2)\dfrac{\hat{\Omega}_s}{s\eta} \\ -(s+2)\Omega_s' & [\Omega_s'' - (s+1)\Omega_s] & \left(\dfrac{\hat{\Omega}_s}{s\eta}\right)' & \\ -(s+2)\dfrac{\hat{\Omega}}{s\eta} & \left(\dfrac{\hat{\Omega}_s}{s\eta}\right)' & [\Omega_s' \cot\eta - \Omega_s(s+1+\dfrac{m^2}{s^2\eta})] & \end{bmatrix}$$

To a first order approximation,

$$\begin{Bmatrix} \Delta\rho \\ \rho\Delta\eta \\ \rho s\eta\Delta\omega \end{Bmatrix} = (T_1T_2)^{-1}\bar{r} \qquad (A.7)$$

where $\bar{r}$ is the position vector expressed in the body axes frame, τ_3.

Thus, $$\bar{F} \tilde{=} \bar{F}_0 + B^*(T_1T_2)^{-1}\bar{r} \qquad (A.8)$$

The gravitational force per unit mass at the generic point, P, in the body can be expressed in the body principal axes frame, τ_3, by using the transformation, (T_1T_2) in eqn. (A.7), i.e.,

$$\bar{f} \tilde{=} \bar{f}_0 + M\,\bar{r} \qquad (A.9)$$

where,

$$\bar{f}_0 = T_1T_2\bar{F}_0$$

$$M = T_1T_2B^*\,(T_1T_2)^{-1}$$

If we write, $$M = M^{(0)} + \Sigma \left(\frac{a}{\rho_o}\right)^s M^{(s)} \qquad (A.10)$$

then,

$$M^{(0)} = T_1T_2B^{(0)}(T_1T_2)^{-1}\,\frac{\nu a^2}{\rho_o^3}$$

$$M^{(s)} = T_1T_2B^{(s)}(T_1T_2)^{-1}\,\frac{\nu a^2}{\rho_o^3}$$

For the sequence of Euler angle rotations shown in Fig. A.1,

$$M^{(0)} = \frac{\nu a^2}{\rho^3}\begin{bmatrix} 3c^2\phi c^2\theta-1 & -3s\phi c\phi c^2\theta & 3c\phi c\theta s\theta \\ -3s\phi c\phi c^2\theta & 3s^2\phi c^2\theta-1 & -3s\phi c\theta s\theta \\ 3c\phi c\theta s\theta & -3s\phi c\theta s\theta & 3s^2\theta-1 \end{bmatrix} \qquad (A.11)$$

It should be noted that the matrices, $B^{(0)}$, $M^{(0)}$, $B^{(s)}$ and $M^{(s)}$ are symmetric.

$OXYZ$ - Inertial reference frame, τ_o

$Oi_1i_2i_3$ - Local intrinsic frame at O, τ_{10}

$Pi_1i_2i_3$ - Local ontric frame at P, τ_{1P}

$OX_0Y_0Z_0$ - Orbit fixed frame, τ_2

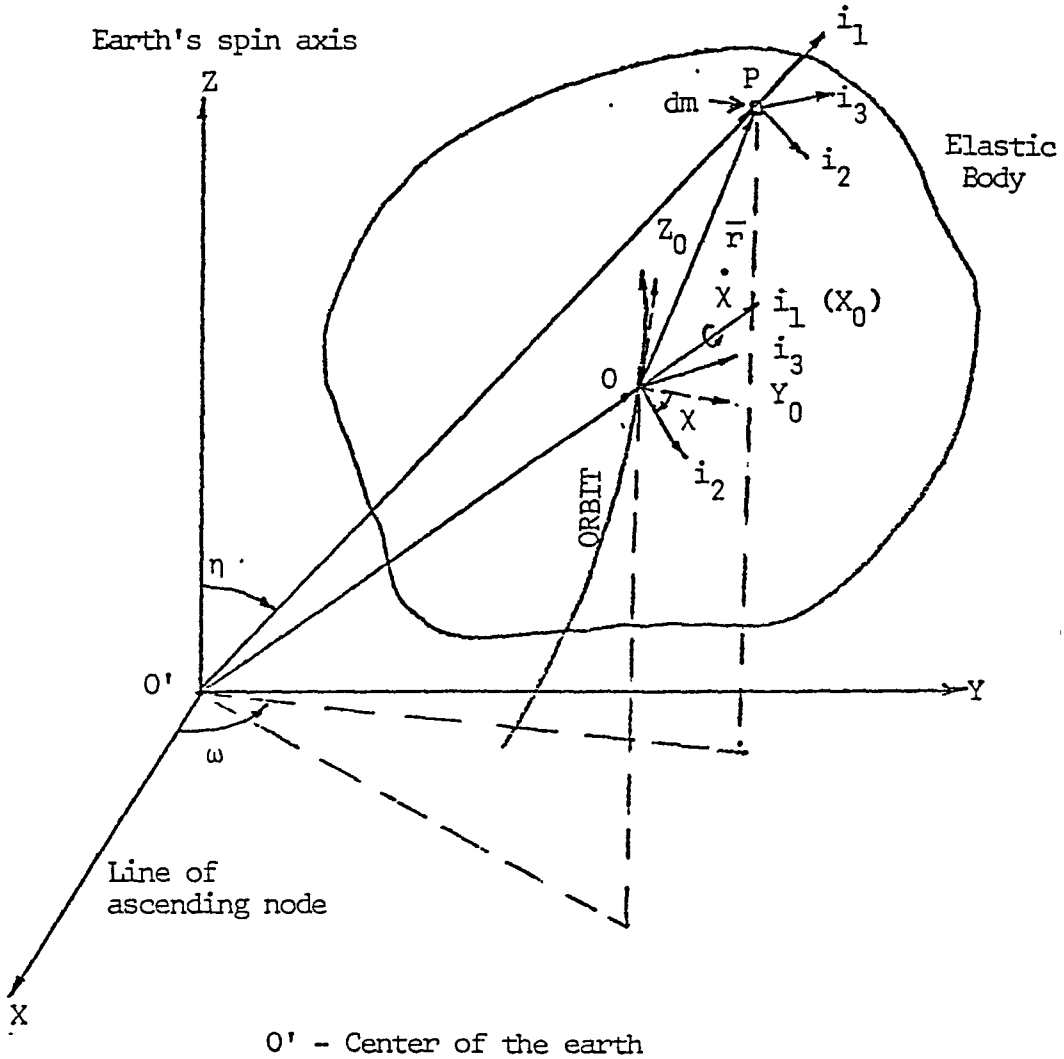

O' - Center of the earth

O - Center of mass of the body

Fig. A.1 : Coordinate Frames

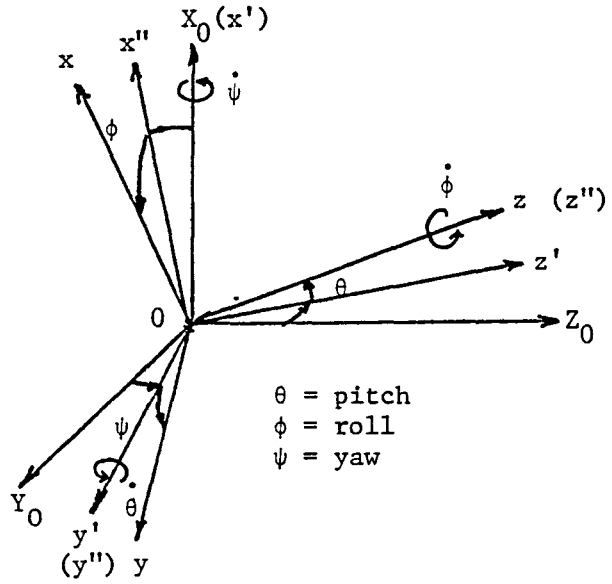

Sequence of rotations $OX_oY_oZ_o \xrightarrow{\psi} Ox'y'z' \xrightarrow{\theta} Ox"y"z" \xrightarrow{\phi} Oxyz$

Fig. A.2: Euler Angle Rotations

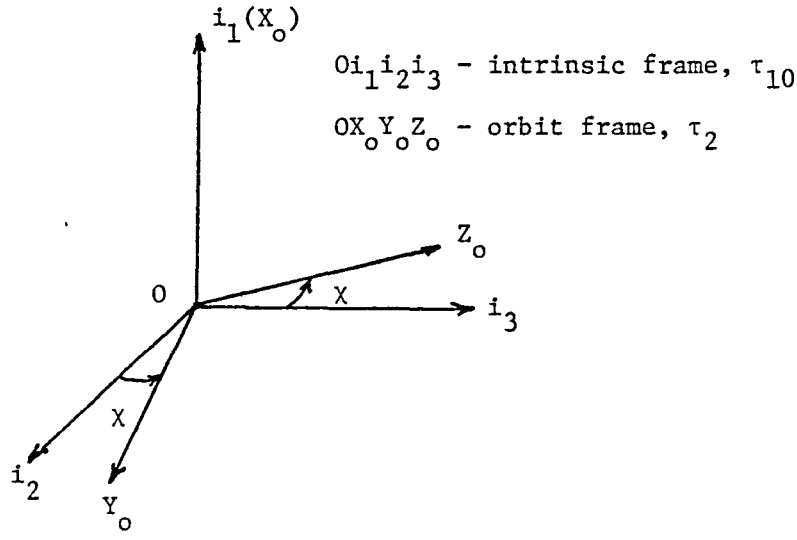

Fig. A.3: Sequence of Rotation from τ_{10} to τ_2

Appendix B

An approximate expression for, x_c (see Fig. 2.5) is derived here.

Fig. B.1 shows the cross sectional view of a shallow spherical shell with the various symbols defined. From plane geometry one notes that (see Fig. B.1),

$$AF \cdot FB = EF \cdot FJ \text{ and } CG \cdot GD = EG \cdot GJ$$

i.e. $$r_c^2 = \Delta(2R-\Delta) \text{ and } \ell^2 = H(2R-H) \qquad (B.1)$$

If it is assumed that, $H/\ell \ll 1$ (which also implies that, $H/R \ll 1$ and $\Delta/R \ll 1$) one can write,

$$\Delta \approx r_c^2/2R \text{ and } H \approx \ell^2/2R \qquad (B.2)$$

Hence, $$x_c = H - \Delta \approx (\ell^2 - r_c^2)/2R \qquad (B.3)$$

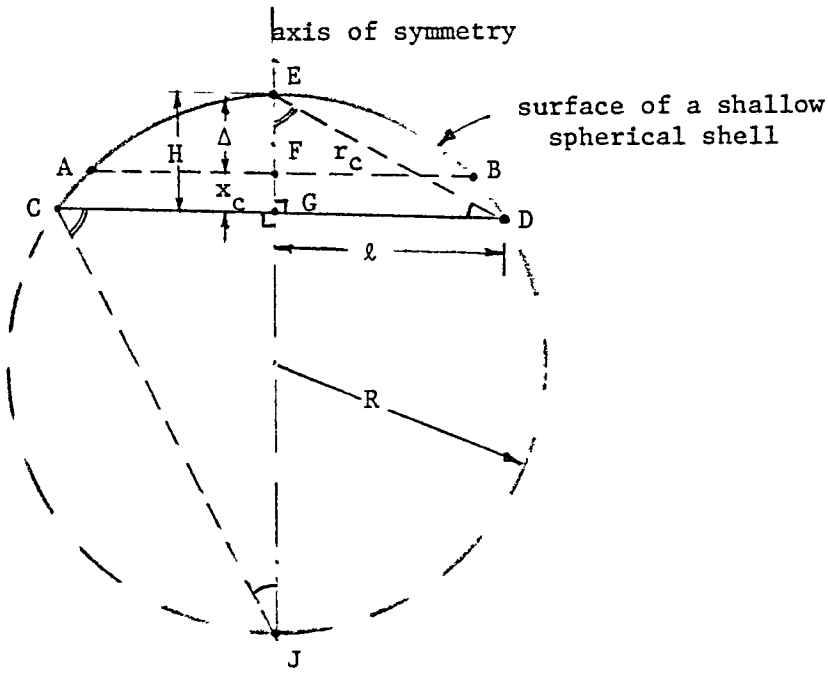

Fig. B.1: Geometry of the cross section of a shallow spherical shell.

CHAPTER III

GRAPH THEORY APPROACH TO THE EIGENVALUE PROBLEM OF LARGE SPACE STRUCTURES

Abstract

A graph theory approach for reducing a matrix to lower ordered submatrices can be utilized to find eigenvalues of a large flexible system. This approach can reduce the computational effort involved in finding the eigenvalues. The reachability matrix and term rank concepts are used to verify controllability and can be more effective than numerical rank tests of the system controllability matrix. A free-free square plate is considered as an example to illustrate these techniques.

I. Introduction

Large, flexible orbiting systems have been proposed for possible use in communications, electronic orbital based mail systems, and solar energy collection.[1,2] The size and low weight to area ratio of such systems warrant the consideration of flexibility as the main contribution to the dynamics and control problem as compared to the inherently rigid nature of earlier spacecraft systems. For such large flexible systems both orientation and surface shape control will often be required.

An analysis of the effectiveness of control systems for such missions is usually divided into: (i) a dynamic analysis of the uncontrolled flexible orbiting system; and (ii) control law selection for particular types and locations of actuators and sensors under consideration.

For a dynamic analysis it is necessary to solve the eigenvalue problem in order to determine natural (modal) frequencies and mode shapes. The eigenvalue problem for such large space structures may pose enormous numerical and computational problems for systems characterized by a state vector of large dimension.

The present paper addresses itself to approach such a problem using graph theory. The determination of the eigenvalues for many vibration problems involves the solution to a large dimensional eigenvalue problem.

In the literature there are certain methods to solve these problems using the special nature of the matrices involved in specific situations such as for rotating (gyroscopic) systems.[3,4]

In the present paper the methods available to interpret the determinant of a matrix graphically[5] are exploited to reduce the higher dimensional matrix into combinations of smaller dimensional sub-matrices, wherever possible. The union of the eigenvalues of the smaller matrices including their multiplicity results in the eigenvalues of the original matrix.[5] The reduction procedures involved employ the Boolean equivalent of the original matrices to arrive at the smaller dimensional equivalents of the original numerical matrix. As the matrix Boolean operations can be performed rapidly with comparably little memory requirements with a high speed computer, the reduction analysis has definite advantages as compared with the direct solution of the eigenvalue problem using the original system matrix. The eigenvalues found from the smaller sub-matrices will, in general, be more accurate than those calculated from the original matrix.

II. Basic Definitions and Theorems[5]

The following are some of the definitions and theorems useful in understanding graph theory as applied to matrices. These concepts will be illustrated in detail in Section III where graph theory is used to determine the eigenvalues of a free-free square plate.

1. Directed graph of a matrix: D(M) is a directed graph of the matrix, M (of order n) with n points $a_1, a_2, \ldots, a_n$, in which there is a directed line from a_i to a_j if and only if the entry m_{ij} of the matrix is not zero, and, in addition, there is a directed line from each point to itself.

2. A directed graph is strongly connected or more briefly, is strong, if, for any two points, a and b, there exists a directed path from a to b and a directed path from b to a.

3. A strong component of a directed graph is a maximal strong sub-graph.

4. The points of any directed graph are partitioned into mutually exclusive strong components. However, not every line of a directed graph necessarily lies in a strong component.

Graphical Interpretation of a Determinant: The following assertions are useful in interpreting the determinant of a matrix graphically.

Lemma 1: The lines of D(M), corresponding to the entries of M whose product is a non-zero term of $|M|$ ($|M|$ is the determinant of matrix, M), constitute a collection of disjoint directed cycles within the directed graph, D(M).

Lemma 2: Every line of D(M) which occurs in a directed cycle appears in a strong component of D(M).

Lemma 3: Each line of D(M) which does not lie in a strong component of D(M) is coordinated with an entry of M which does not occur in any non-zero terms of $|M|$.

Lemma 4: The product of the determinants of the sub-matrices of M associated with the strong components of D(M) gives, up to the sign, the value of the determinant of M.
The proofs of Lemmas 1-4 are provided in Ref. 5.

The following theorem can be used to test whether a matrix can be reducible to sub-matrices or not.

Theorem[6]: The matrix $M=(m_{ij})$ of order n is irreducible if and only if $n=1$ or if $n>1$, and for any i and j such that $1\leq i\leq n$, $1\leq j\leq n$ and $i\neq j$, either $m_{ij}\neq 0$ or there exist $i_1, i_2, \ldots, i_s$ such that $m_{i,i_1} m_{i_1,i_2} \ldots m_{i_s,j}\neq 0$. i.e. there is a path between the i and j nodes in a digraph sense.

Theorem on Eigenvalues[5]:

Let E(M) be the collection of all the eigenvalues of M, including all multiple eigenvalues counted separately. With the construction of sub-matrices, M_1, used in Lemma 4, then let $E(M_1)$ have the corresponding meaning for the collection of eigenvalues of the sub-matrix, M_1.

Theorem: Using the above notation for E(M), the eigenvalues of M are given by $E(M)=E(M_1)\cup E(M_2)\ldots\cup E(M_r)$, including multiplicity. In words, the set of eigenvalues of the matrix is the union (including multiplicity) of the sets of the eigenvalues of the sub-matrices corresponding to the strong components of the directed graph of the matrix. (The proof of this theorem is given in Ref. 5.)

III. Algorithm for Matrix Reduction

An algorithm is given here to find the sub-matrices corresponding to the strong components of a directed graph of a matrix M(order n).

Step 1: Replace the diagonal elements (whether zero or non-zero) by unity and replace all non-zero non-diagonal elements by unity. We obtain an adjacency matrix, A, of the digraph, D(M). We observe that A is a Boolean matrix - i.e. contains only "zeros" and "ones" as elements.

Step 2: Find the matrix A^i by Boolean[7] multiplication where i is either determined by $A^i=A^{i-1}$ (i.e. 1+1=1, 1+0=1, 0+0=0 rules) or $i=n-1$. This matrix is called the reachability matrix (or path matrix) and is denoted by R.

Step 3: Let S_1 be the collection of all the indices, i, such that there appears the number "1" in both the i^{th} place of the first row of R and of the first column of R.

These indices name the points of D(M) in the same strong component as a_1. Delete from the matrix, R, all rows and columns whose indices are in the set, S_1, but preserve the original row and column indices from R in the resulting sub-matrix of R.

Step 4: Repeat step 3 on this resulting sub-matrix, obtaining the collection of sets of indices $S_2, S_3, \ldots, S_r$. Then, clearly $S_1, S_2, \ldots, S_r$ are pairwise disjoint sets of indices whose union is $\{1,2,\ldots,n\}$ and each set, S_k, contains all the indices which belong to the points in one strong component of D(M).

Step 5: Let M_i be the n_i by n_i sub-matrix formed from the rows and columns that are in the set S_i. Then by the Theorem on the Eigenvalues and Lemma 4, the original matrix, M, is completely reduced to the matrices, M_i, and each M_i is irreducible. Also, the eigenvalues of M are the union of the sets of eigenvalues of the sub-matrices M_i (including multiplicity).

The numerical effort involved in reducing the original matrix is nominal as the matrices involved are Boolean. The multiplications can be done row by column wise using an assembly level language. The memory involved is also nominal as every element can be stored in a bit instead of a word. Thus, this procedure is very attractive for large dimensional systems. The above graphical procedure is applied to a mathematical model of a free free square plate.[8,9]

IV. Example of a Free-Free Square Homogeneous Plate

The transverse displacement of the free-free square plate may be represented by[8]:

$$W(x,y,t) = \sum_{j=1}^{J} \sum_{n=1}^{N} \phi_j(x)\psi_n(y)\Gamma_r(t) \qquad (1)$$

where $\phi_j(n)$, $\psi_n(y)$ are free-free beam functions

$\Gamma_r(t)$ is a time dependent function

$r = n+(j-1)N$ with $n = 1,2,\ldots N$
$j = 1,2,\ldots J$
$r = 1,2,\ldots JN$

The dynamic equations of the plate are given by[8]:

$$M\ddot{g}+Kg = qf(t) \qquad (2)$$

where $M = mI$, m = mass of the plate

$$g^T = [\Gamma_1, \Gamma_2, \ldots] \; ; \; q^T = [q_1, q_2, \ldots]$$

With p(x,y) as the spatial distribution of the control force, then,

$$q_r = \int_0^a \int_0^b p(x,y)\phi_j(x)\psi_n(y)\, dydx$$

and the general element of the stiffness matrix may be expressed

$$K_{rs} = \frac{D}{ab}\left[\delta_{rs}\left\{\frac{b^2}{a^2}\alpha_j^4 + \frac{a^2}{b^2}\beta_n^4\right\}\right.$$

$$\left. + \nu\,[I_{jj'}I_{nn'} + I_{j'j}I_{n'n}] + 2(1-\nu)J_{jj'}J_{nn'}\right]$$

$$s = n' + (j'-1)N$$

$$I_{jj'} = a\int_0^a \frac{d^2\phi_j}{dx^2}\,\phi_{j'}\,dx \;;\; I_{nn'} = b\int_0^b \frac{d^2\psi_n}{dy^2}\,\psi_{n'}\,dy$$

$$J_{jj'} = a\int_0^a \frac{d\phi_j}{dx}\,\frac{d\phi_{j'}}{dx}\,dx;\; J_{nn'} = b\int_0^b \frac{d\psi_n}{dy}\,\frac{d\psi_{n'}}{dy}\,dy$$

α_j, β_n are the free-free beam frequencies. ν is Poisson's ratio, and D is the flexural rigidity. The non-zero elements of the K matrix are calculated[9] for m = 276800 kg, a=b=100m.

$$\alpha_1 = \beta_1 = 0.0 \;;\; \alpha_3 = \beta_3 = 4.73004 \;;\; \alpha_2 = \beta_2 = 0.0$$

$$\alpha_4 = \beta_4 = 7.85324.$$

For J = N = 4 we have 16 modes for the plate, Fig. 1 illustrates the location of the non-zero elements in the K matrix. (See Step 1, Algorithm) corresponding to the following actual numerical values (Table I)

TABLE I

The First Four Free- Free Beam Frequency Parameters:

0.0,0.0,4.73004,7.85324 (α_j,β_j)

Non-zero elements of K-matrix:

K(3,3)=34.919	K(9,3)=8.03522	K(11,3)=-5.31786	K(4,4)=265.337
K(12,4)=-19.9054	K(10,4)=17.5471	K(6,6)=13.3938	K(8,6)=15.4658
K(14,6)=15.4658	K(16,6)=17.8584	K(7,7)=34.9190	K(13,7)=17.5471
K(15,7)=-11.6130	K(6,8)=15.4658	K(8,8)=386.913	K(14,8)=56.1775
K(16,8)=96.9152	K(3,9)=8.03522	K(9,9)=34.9190	K(11,9)=-5.31786
K(4,10)=17.5471	K(10,10)=34.9190	K(12,10)=-11.6130	K(3,11)=-5.31786
K(9,11)=-5.31786	K(11,11)=76.8770	K(4,12)= -19.9054	K(10,12)=-11.6130
K(12,12)=326.604	K(7,13)=17.5471	K(13,13)= 265.337	K(15,13)=-19.9054
K(6,14)=15.4658	K(8,14)=56.1775	K(14,14)=386.913	K(16,14)=96.9152
K(7,15)=-11.6130	K(13,15)=-19.9054	K(15,15)=326.604	K(6,16)=17.8584
K(8,16)=96.9152	K(14,16)=96.9152	K(16,16)=1732.85	

Col. / Row	1	2	3	4	5	6	7	8	9	10	11	12	13	14	15	16
1																
2																
3			X						X		X					
4				X						X		X				
5												·				
6						X		X				·		X		X
7							X						X		X	
8						X		X						X		X
9			X						X		X					
10				X						X		X				
11			X						X		X					
12				X						X		X				
13							X						X		X	
14						X		X						X		X
15							X						X		X	
16						X		X						X		X

Fig. 1. Non-zero Element Pattern of the K-Matrix.
(X indicates non-zero element)

From Fig. 1 it can be seen that the isolated nodes on the digraph correspond to the indices "1", "2", and "5", since none of these correspondingly numbered rows and columns contain non-zero elements. Thus, the digraph centered at these nodes consists only of a directed line from the node to itself. As an example of a strongly connected component of a directed graph, we consider the nodes corresponding to the indices, "3", "9", and "11". It can be seen that non-zero elements appear in the third, ninth, and eleventh places in both the third row and columns, respectively. Therefore, the directed graph between any two of these nodal points is strongly connected. The remainder of the digraph is constructed based on similar reasoning. It can be verified that the Boolean equivalent[7] of K^{n-1} is the same as that for the K matrix itself. This matrix is thus the path matrix (reachability matrix) and its digraph is shown in Fig. 2.

The reachability matrix shown in Fig. 3 is subdivided following Step 3 of the algorithm. For example, there is a "one" contained in the first row and the first column of the reachability matrix. No other non-zero element appears in either the first row or the first column. Thus the subset, S_1, has, in this case, only the single index "1". By similar reasoning the second subset, S_2, associated with the "one" contained in the second row and the second column of the original matrix (the first row and the first column of the reduced matrix) also has in this case a single index, "2".

We now consider elements appearing in the i^{th} places of the third row and column, respectively, of the 14x14 matrix formed by excluding S_1 and S_2. It can be seen that the number "one" appears in the third, ninth, and eleventh places of both the third row and column of the reachability matrix. Thus the subset, S_3, now contains the three indices: "3", "9", and "11". By a similar process (repeated application of Step 4), the remaining subsets, S_4-S_7, can be obtained, and the results are summarized as follows:

S_1: 1; S_2: 2; S_3: 3,9,11; S_4: 4,10,12; S_5: 5;

S_6: 6,8,14,16; S_7: 7,13,15.

The eigenvalues are evaluated using these submatrices as well as the original matrix. The comparative values are given in Table II.

TABLE II

Eigenvalues of the K matrix:

Submatrices		Original matrix
S_1	0.0	0.0
S_2	0.0	0.0
S_3	26.88378000	26.88378620
	41.36168802	41.36169439
	78.46953198	78.46953100

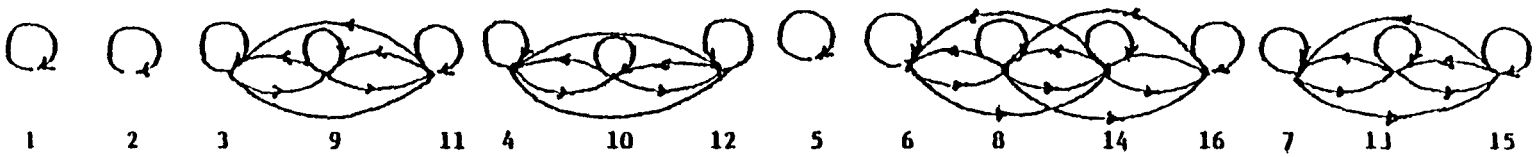

Fig. 2. Digraph of 16x16 K matrix.

Col.	1	2	3	4	5	6	7	8	9	10	11	12	13	14	15	16
Row 1	1															
2		1														
3			1						1		1					
4				1						1		1				
5					1											
6						1		1						1		1
7							1						1		1	
8						1		1						1		1
9			1						1		1					
10				1						1		1				
11			1						1		1					
12				1						1		1				
13							1						1		1	
14						1		1						1		1
15							1						1		1	
16						1		1						1		1

Fig. 3a. Reachability Matrix for Free-Free Square Plate

11x11 matrix

	4	5	6	7	8	10	12	13	14	15	16
4	1					1	1				
5		1									
6			1		1				1		
7				1				1		1	
8			1		1				1		1
10	1					1	1				
12	1					1	1				
13								1		1	
14			1		1				1		1
15				1				1		1	
16			1		1				1		1

Fig. 3b. Reachability Matrix for Free-Free Square Plate after Separation of S_1, S_2, S_3 Submatrices.

	5	6	7	8	13	14	15	16
5	1							
6		1		1		1		1
7			1		1		1	
8		1		1		1		1
13			1		1		1	
14		1		1		1		1
15			1		1		1	
16		1		1		1		1

Fig. 3c. Reachability Matrix for Free-Free Square Plate after Separation of S_1, S_2, S_3, S_4 Sub-matrices.

	7	13	15
7	1	1	1
13	1	1	1
15	1	1	1

Fig. 3d. Reachability Matrix for a Free-Free Square Plate after Separation of $S_1, S_2, S_3, S_4, S_5, S_6$ Sub-matrices.

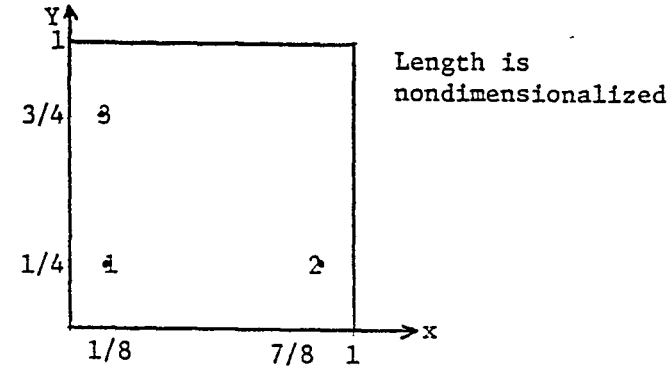

Fig. 4. Location of Actuators

TABLE II - (Continuation) - Eigenvalues of the K matrix:

Submatrices		Original matrix
S_4	33.24206125	33.24206653
	260.2368175	260.2367428
	333.3811212	333.3811150
S_5	0.0	0.0
S_6	12.21269086	12.21269085
	330.7355000	330.7355804
	429.6358695	429.6359588
	1747.485740	1747.485839
S_7	33.24206125	33.24206653
	260.2368175	260.2367428
	333.3811212	333.3811150

The eigenvalues of the system are the eigenvalues of $M^{-1}K$ and as $M=mI$, eigenvalues of $M^{-1}K=(1/m)$ times eigenvalues of K.

V. Controllability

The controllability of a dynamic system represented by $\dot{X}=AX+BU$, for a given set of actuators can be established using the path matrix obtained in the eigenvalue analysis. The two conditions to be satisfied for controllability are[10]:

(i) All states must be reachable, in a diagraph sense, form at least one input.

(ii) The required term rank tests must be satisfied.

These conditions will be discussed and fully explained in the following paragraphs.

As an example of condition (i) let us consider the system matrices

$$A = \begin{bmatrix} 1 & 1 \\ 0 & 1 \end{bmatrix} \quad ; \quad B = \begin{bmatrix} 0 \\ 1 \end{bmatrix}$$

The digraph corresponding to the A matrix can be represented as

Because of the presence of the zero element in the second row of the first column, it is observed that the directed graph between the two nodal points is not strongly connected. In addition there are also directed lines from both nodal points to the points themselves.

Now consider the control input matrix, B, which has a non-zero element in the second row. - i.e. this input directly influences the second node and via the digraph has a directed path to the first node. Therefore, all states are reachable as a result of the (control) input given by B.

In contrast suppose that the B matrix has the form: $B^T = [1\ 0]$. It is then apparent that the second node in the digraph is not reachable as a result of this (control) input.

The term rank [condition (ii)] of a matrix is the maximum rank that the matrix may have due to the locations of the non-zero elements. If the term rank of the A matrix is equal to the order of the system (n) and condition (i) is satisfied, then the system: $\dot{X}=AX+BU$ is controllable. If the term rank of the A matrix is less than n, columns of the B matrix can be used in place of selected columns of the A matrix in an attempt to augment the term rank. The number of columns of the B matrix used in this rank augmentation process is an indication of the minimum number of actuators required.

In the example of the free-free square plate the term rank and the numerical rank of the K matrix are the same (13). According to the second condition for controllability, there must be at least three actuators to control the plate since the order of the system is sixteen.

As a particular case the three actuators are selected as shown in Fig. 4 and the controllability is verified.

The closed loop equations of motion for the system can be represented as follows:

$$\begin{bmatrix} \dot{\Gamma} \\ \ddot{\Gamma} \end{bmatrix} = \left[\begin{array}{c|c} 0 & I \\ \hline \frac{-K}{m} & 0 \end{array}\right] \begin{bmatrix} \Gamma \\ \dot{\Gamma} \end{bmatrix} + \begin{bmatrix} 0 \\ \frac{B}{m} \end{bmatrix} U \qquad (3)$$

where $\Gamma = [\Gamma_1, \Gamma_2, \ldots \Gamma_{16}]$

m = mass of the plate

and the control influence matrix, B, is listed in Table III. System (3) is controllable if the pair [-K/m, B/m] is controllable.[11]

TABLE III

Elements of the B Matrix in Eq. (3)

$$\begin{bmatrix} 1.0 & 1.0 & 1.0 \\ 0.866 & 0.866 & -0.866 \\ -0.198 & -0.198 & -0.198 \\ -1.1694 & -1.1694 & 0.117445 \\ 1.2990 & -1.2990 & 1.2990 \\ 1.125 & 1.125 & 1.125 \\ -0.2577 & 0.2577 & -0.2577 \\ -1.51918 & -1.51918 & 1.52566 \\ 0.847 & 0.847 & 0.847 \\ 0.73368 & 0.73368 & -0.73368 \\ -0.168 & -0.168 & -0.168 \\ -0.99076 & -0.99076 & 0.99076 \\ 0.097396 & -0.097396 & 0.097396 \\ 0.0842 & -0.704 & -0.0842 \\ -0.01932 & +0.016129 & -0.1932 \\ -0.1139 & +0.095076 & 0.114387 \end{bmatrix}$$

For the pair [-K/m, B/m] the reachability condition (i) is very easily verified as there is no zero entry in the B/m matrix. The -K/m matrix has a term rank equal to numerical rank of 13. By supplementing the three columns of the B/m matrix, the -K/m matrix rank is augumented to 16 which, together with the reachability condition, assures the controllability of the free-free square plate for this set of actuators.

VI. Conclusions

A graph theory approach for reducing the system matrix to lower ordered sub-matrices can be utilized to find the eigenvalues. This approach can substantially reduce the numerical effort involved in finding the eigenvalues of large order flexible space systems. The reachability matrix and term rank concepts are used to verify controllability and can be computationally more effective than numerical rank tests of the system controllability matrix.

Acknowledgment

This research was supported by NASA Grant NSG-1414, Suppl 3.

References

1. Outlook for Space, NASA Report SP-386, Jan. 1976.

2. Industry Workshop on Large Space Structures, NASA CR-2709, Contract No. NAS-1-12436, for NASA LRC May 1976.

3. Meirovitch, L., "A New Method of Solution of the Eigenvalue Problem for Gyroscopic Systems," AIAA Journal, Vol. 12, No. 10, 1974, pp. 1337-1342.

4. Meirovitch, L., "A Modal Analysis for the Response of Linear Gyroscopic Systems," Journal of Applied Mechanics, Trans. of ASME, Vol. 42, No. 2, June 1975, pp. 446-450.

5. Harary, F., "A Graph Theoretic Method for the Complete Reduction of a Matrix with a View Toward Finding Its Eigenvalues," J. Mathematics and Physics, 1959, pp. 104-111.

6. Young, D.M., and Gregory, R.T., A Survey of Numerical Mathematics, Vol. II, Addison-Wesley Publishing Company, pp. 1001-1003.

7. Sorensen, P.G., and Tremblay, P.G., An Introduction to Data Structures with Applications, McGraw-Hill Book Company, 1976.

8. Warbuton, G.B., "Response Using the Rayleigh Method," Earthquake Engineering and Structural Dynamics, Vol. 7, 1979, pp. 327-334.

9. Young, D., "Vibration of Rectangular Plates by Ritz Method," ASME J. Appl. Mech., Vol. 17, 1950, pp. 448-453.

10. Schizas, C., and Evans, F.J., "Rank-Invariant Transformations and Controllability of Large Scale Systems," Electronic Letters, Vol. 16, No. 1, 3rd January 1980, pp. 19-20.

11. Balas, M.J., "Feedback Control of Flexible System," IEEE Trans. on AC., Vol. AC-23, No. 4, August 1978, pp. 673-679.

CHAPTER IV

THE CONTROL OF LARGE FLEXIBLE ORBITING SHALLOW SPHERICAL SHELL STRUCTURES

The dynamics of shallow spherical shells in orbit are studied in Ref. 1. The dumbbell is attached to the spherical shell at the apex to achieve gravitational stability of the uncontrolled system.[1] In addition if it is assumed that the dumbbell is attached to the shell with a spring loaded gimballed damping device it can also provide passive restoring and dissipative forces. The model developed in Ref. 1 is adopted and the effect of the control actuators on the system is incorporated into the model.

INTRODUCTION

The linearized equations of motion of shallow spherical shells in orbit are given by[1]*:

$$\begin{aligned}
&\psi''-\Omega_x\psi-(1+\Omega_x)\phi' = C_x/J_x\omega_c^2\\
&\phi''+4\Omega_z\phi+(1-\Omega_z)\psi' = C_z/J_z\omega_c^2\\
&\theta''-3\Omega_y\theta-2\Sigma_n\varepsilon_n' I_1^{(n)}\ell/J_y = C_y/J_y\omega_c^2\\
&\varepsilon_n''+(\Omega_n^2-3)\varepsilon_n+2\theta' I_1^{(n)}/M_n\ell = 3I_1^{(n)}/M_n\ell + \frac{E_n}{M_n\omega_c^2\ell}
\end{aligned} \qquad \text{(IV-1)}$$

The linearized equations of motion of the shallow spherical shell with the dumbbell in orbit are given by

$$\psi''-\Omega_x\psi-(1+\Omega_x)\phi' = C_x/J_x\omega_c^2$$

$$\phi''+4\Omega_z\phi+(1-\Omega_z)\psi'-\bar{c}_z\delta'-\bar{k}_z\delta-\sum_{n-1}^{N}(\bar{c}_z\varepsilon_n'+\bar{k}_z\varepsilon_n)C_y^{(n)} = C_z/J_z\omega_c^2$$

$$\theta''-3\Omega_y\theta-2\Sigma_n\varepsilon_n' I_1^{(n)}\frac{\ell}{J_y}-\bar{c}_y\gamma'-\bar{k}_y\gamma+\Sigma_n(\bar{c}_y\varepsilon_n'+\bar{k}_y\varepsilon_n)C_z^{(n)} = C_y/J_y\omega_c^2$$

$$\varepsilon_n''+(\Omega_n^2-3)\varepsilon_n+2\theta'\left(\frac{I_1^{(n)}}{M_n\ell}-\frac{3I_1^{(n)}}{M_n\ell}\right)-(\bar{c}_y\gamma'+\bar{k}_y\gamma)\frac{J_y}{M_n\ell^2}C_z^{(n)}$$

$$-(\bar{c}_z\delta'+\bar{k}_z\delta)\frac{J_z}{M_n\ell^2}C_y^{(n)}+\sum_m(\bar{c}_y\varepsilon_n'+\bar{k}_y\varepsilon_n)C_z^{mn}+\sum_m(\bar{c}_z\varepsilon_n'+\bar{k}_z\varepsilon_n)C_y^{mn} = E_n/M_n\ell\omega_c^2$$

*Note: The nomenclature for this Chapter is provided at the end of the Chapter.

$$\gamma''+\bar{c}_y(1+c_1)\gamma' + \{3+\bar{k}_y(1+c_1)\}\gamma+3(1+\Omega_y)\theta - (1+c_1)\sum_n(\bar{c}_y\varepsilon_n'+\bar{k}_y\varepsilon_n)C_z^{(n)}$$

$$+2(\sum_n\varepsilon_n' I_1^{(n)}\ell/I_y)= 0 \qquad \text{(IV-2)}$$

$$\delta''+\bar{c}_z(1+c_2)\delta' + \{4+\bar{k}_z(1+c_2)\}\delta+4(1-\Omega_z)\phi - (1-\Omega_z)\psi$$

$$-(1+c_2)\sum_n(\bar{c}_z\varepsilon_n'+\bar{k}_z\varepsilon_n)C_y^{(n)}= 0$$

The frequencies of the spherical shell are evaluated using the following identities.[2]

$$\mu = \lambda a\ [\frac{h\rho a^4}{D}\ (p^2-p_\infty^2)]^{\frac{1}{4}} \qquad \text{(IV-3)}$$

where the μ's are calculated from[2]

$$\frac{\mu}{2}\ [\ \frac{J_n(\mu)}{J_{n+1}(\mu)}\ +\ \frac{I_n(\mu)}{I_{n+1}(\mu)}\ ]\ = 1-\nu \quad \text{for n= 0,1} \qquad \text{(IV-4)}$$

where n represents the number of nodal diameters.

For n>1, Equation (IV-4) must be replaced by a more complex form as follows:

$$\frac{\mu^4}{K^4} = \frac{S_n(\mu)}{R_n(\mu)} -1 \qquad \text{(IV-5)}$$

where

$$S_n(\mu) = 4n^2(n^2-1)(1-\nu)\{\mu[J_n(\mu)I_n'(\mu)-J_n'(\mu)I_n(\mu)]$$

$$+ (n+1)(1-\nu)[I_n'(\mu)- \frac{n}{\mu}\ I_n(\mu)][J_n'(\mu)- \frac{n}{\mu}\ J_n(\mu)]\}$$

$$R_n(\mu) = \{(1-\nu)[\mu J_n'(\mu)-n^2J_n(\mu)]+\mu^2J_n(\mu)\}\{(1-\nu)n^2[\mu I_n'(\mu)$$

$$-I_n(\mu)]-\mu^3I_n'(\mu)\}-\{(1-\nu)n^2[\mu J_n'(\mu)-J_n(\mu)]+\mu^3J_n'(\mu)\}\{(1-\nu)]\mu I'_n(\mu)$$

$$-n^2I_n(\mu)]-\mu^2I_n(\mu)\}$$

Eq. (1V-4) or Eq. (IV-5) is satisfied by an infinite number of the parameter, μ, for every value of n. For the sample calculations in this chapter, we will consider only three such values of μ (j = 1,2,) for the cases where n = 0,1.

For the following numerical values considered (Fig. IV-1):

$H = 1m$; $a = 100$ m; $\rho = 27.68$ Kg/mr^2; $h = 1cm$

$D = Eh^3/12(I-\nu^2)$

$E = 0.744x10$ Kg/mr^2;

$R = 5000.0$ mrs; $p_\infty^2 = 0.107572254$

$p^2 = 0.252122471x10^{-6}\mu^4 + 0.107572254$

the frequencies are then calculated, with the results summarized as follows:

Table IV-1 - Frequencies of the Shell (Six Modes)

# of nodal diameters (n)	# of nodal circles (j)	μ^2	$p^2(H_z^2)$
0	1	9.076	0.107593022
1	1	20.52	0.107678417
0	2	38.52	0.107946351
1	2	59.86	0.108475664
0	3	87.82	0.109516711
1	3	119.0	0.11114256

It is observed that all the frequencies are grouped with only a difference of 3% between the maximum and minimum values of the flexible frequencies considered in this model. This close grouping is due to the dominance of the curvature of the shell on the assumed model.

The point actuators are modelled as follows. An actuator located at (x,y,z) with components (f_x, f_y, f_z) provides the following torques,

$$\begin{aligned} T_x &= yf_z - zf_y \\ T_y &= -xf_z + zf_x \\ T_z &= xf_y - yf_x \end{aligned} \qquad \text{(IV-6)}$$

and the corresponding generic force in the nth mode,

$$E_n = \int \Phi_n \cdot \bar{f}\, dm \qquad \text{(IV-7)}$$

For the shallow spherical shell it is assumed that the major elastic displacement occurs in a direction normal to the base (y,z) plane. - i.e. $\Phi_n \tilde{=} \phi_n \hat{i}$. Thus for a point actuator located at (x,y,z)

$$E_n \tilde{=} \phi_n(x,y,z) f_x M_n \qquad \text{(IV-8)}$$

where $\phi_n(x,y,z)^3$ is the n <u>th</u> modal shape function evaluated at (x,y,z), f_x represents the component of $\bar{f}$ in a direction normal to the base plane, and M_n is the modal mass, here considered to be the total mass of the shell, since the shell mode shape functions have each been normalized with respect to the mass of the shell.

After defining the state vector for the spherical shell, with and without dumbbell, as:

$$X^T = [\psi, \phi, \theta, \varepsilon_1, \varepsilon_2, \varepsilon_3, \varepsilon_4, \varepsilon_5, \varepsilon_6, \psi', \phi', \theta', \varepsilon_1', \varepsilon_2', \varepsilon_3', \varepsilon_4', \varepsilon_5', \varepsilon_6'] \text{ (without dumbbell)}$$

$$X^T = [\gamma, \delta, \psi, \phi, \theta, \varepsilon_1, \varepsilon_2, \varepsilon_3, \varepsilon_4, \varepsilon_5, \varepsilon_6, \gamma', \delta', \psi', \phi', \theta', \varepsilon_1', \varepsilon_2', \varepsilon_3', \varepsilon_4', \varepsilon_5', \varepsilon_6'] \text{ (with dumbbell)}$$

the equations of motion can be written in the state vector form:

$$\dot{X} = AX + BU \qquad \text{(IV-9)}$$

The B matrix is evaluated using the locations of the actuators together with the direciton cosines of the actuators.

Six actuators are assumed to be present and are located on the surface of the shell as illustrated in Fig. IV-1.

The location of these actuators and the directions of the forces that each provides are listed in Table IV-2

Table IV-2 - Actuator Locations and Force Directions

	β_o	β_1	x	y	z
1)	90^o	0.28	f_1	0	0
2)	90^o	0.57	f_2	0	0
3)	90^o	0.84	f_3	0	f_3
4)	270^o	0.28	f_4	0	f_4
5)	270^o	0.57	f_5	f_5	0
6)	270^o	0.84	f_6	f_6	f_6

The physical parameters of the shell are the same as those used in the frequency calculation. The corresponding non-zero elements of the A and B matrices are listed as follows:

A&B matrices for the case without Dumbbell

A(I, I+9) = 1.0 for I = 1,9

A(11,2)= 4.0; A(12,3)= 3.0, A(13,4)= -40219.81; A(14,5) = -40251.73;

A(15,6)= -40351.89; A(16,7)= -40549.78; A(17,8)= -40938.97;

A(18,9)= -41652.59; A(10,11)= 1.0; A(11,10)= -2.0; A(12,13)= 0.02339;

A(12,14)= -0.0026; A(12,15)= 0.000751; A(13,12)= -0.005846;

A(14,13)= 0.00066; A(15,14)= -0.00018

Lower half part of B matrix

0.000000E 0	0.000000E 0	0.147176E -3	-0.147175E -3	-0.230309E -6	-0.147410E -3	
0.000000E 0	0.000000E 0	0.312783E -3	0.166085E -3	0.468683E -6	0.313252E -3	
-0.298381E -3	-0.298381E -3	-0.298381E -3	0.298381E -3	0.735356E -6	-0.188416E -6	
0.120552E -1	0.581697E -2	-0.238711E -2	0.120552E -1	0.581697E -2	-0.238711E -2	
0.110381E -1	-0.624600E -2	-0.496221E -2	0.110381E -1	-0.624600E -2	-0.496221E -2	
0.899069E -3	-0.768770E -2	0.774266E -2	0.899069E -3	-0.768770E -2	0.774266E -2	
0.127603E -1	0.138451E -1	0.199142E -2	-0.127602E -1	-0.138450E -1	-0.199142E -2	
0.205133E -1	-0.303690E -3	-0.969612E -2	-0.205132E -1	0.303690E -3	0.969610E -2	
0.179646E -1	-0.142969E -1	0.100699E -1	-0.179646E -1	0.142969E -1	-0.100699E -1	

Non-zero elements of A with dumbbell

A(I, I+11)= 1.0 for I = 1, 11

A(12,1)= -193.0; A(12,5)= 6.0; A(12,7)= 576.32; A(12,9)= 3647.6;

A(12,11)= 6088.63, A(12,12)= -2.7568, A(12,17)= -0.0234;

A(12,18)= 8.365; A(12,19)= -0.000751; A(12,20)= 52.93; A(12,22)= 88.3432;

A(13,2)= -194.0; A(13,3)= 2.0; A(13,4)= -8.0, A(13,13)= -2.757;

A(14,15)= 1.0; A(15,2)=100.0; A(15,4)= 4.0; A(15,13)=1.451;

A(15,14)= -2.0, A(16,1)= 100.0; A(16,5)= 3.0; A(16,7)= -303.33;

A(16,9)= -1919.8; A(16,11)= -3204.54; A(16,16)= 1.451; A(16,17)= 0.0234;

A(16,18)= -4.4038; A(16,19)= 0.000751; A(16,20)= -27.8554; A(16,22)= -46.496;

A(17,6)= -40216.81; A(17,16)= -0.00585; A(18,1)= 75.834; A(18,7)= -56712.312;

A(18,12)= 1.10032; A(18,16)= 0.00066; A(18,18)= -238.88; A(19,8)= -40348.9;

A(19,16)= -0.0001878; A(20,1)= 479.97; A(20,9)= -144747.31; A(20,12)= 6.9641;

A(20,20)= -1511.9; A(21,10)= -40935.97; A(22,1)= 801.16; A(22,11)= -215581.68;

A(22,12)= 11.6245; A(22,22)= -2523.672.

The B matrix of the shell with the dumbbell is $\left[\frac{0_{13x6}}{B}\right]$ where B is the lower part of the B matrix of the shell without the dumbbell. The locations of the non-zero elements in the matrices of the spherical shell with and without the dumbbell, respectively, are shown in Figs. IV-2 and IV-3.

Control laws are selected using pole clustering techniques[4] for the spherical shell without the dumbbell. This same control law is then applied to the case of the shell with the dumbbell, i.e.- it is assumed that the dumbbell position and rate information may not be directly observable and is not included in the control law. (As long as the dumbbell-shell system is controllable and stabilizable, the dumbbell will return to its desired local vertical equilibrium orientation after the transients have been removed.

It is possible to design a control law for the dumbbell-shell system that results in a controllable-stabilizable system without including the dumbbell information within the control law.)

A typical time history of the required control forces for the shell without the dumbbell is shown in Fig. IV-4 for non-dimensional initial position displacements in all state components of 0.01, with the control law based on placement of all the poles so as to have a dimensionless negative real part of (-1.72). This will provide a system time constant of 461 seconds in all modes. A similar response was generated using the same control law for the case of the shell with the dumbbell where the dumbbell inertia ratios (c_1=c_2) were assumed to be 0.9, the dumbbell spring constants, $\bar{k}_y$=$\bar{k}_z$=100, and damping coefficients selected so as to provide 0.1 critical damping. A comparison of the maximum force amplitude in each of the actuators and also of the total force impulse required is given in Table IV-3 for the two cases. It can be seen that although there is little difference in the maximum force amplitudes, there is approximately a 25 percent savings in fuel consumption by using the shell-dumbbell system.

Table IV 3: Maximum Force Amplitudes of the Shell with 6 Actuators

	Without dumbbell	With dumbbell
f_1	103.411	103.410
f_2	105.398	105.398
f_3	317.83	317.83
f_4	107.55	107.55
f_5	77.09	77.09
f_6	127.32	127.318
Total		
Force impulse:	432.8 N-Seconds	320.49 N-Seconds

Initial Conditions

$\theta_0 = \phi_0 = \psi_0 = \varepsilon_{1(0)} = \cdots = \varepsilon_{6(0)} = 0.01$

$\dot{\theta}_0 = \dot{\phi}_0 = \dot{\psi}_0 = \dot{\varepsilon}_{1(0)} = \cdots = \dot{\varepsilon}_{6(0)} = 0.0$

with dumbbell

$\gamma_0 = \delta_0 = \gamma_0' = \delta_0' = 0.0$

25% saving with dumbbell.

References - Chapter IV

1. Bainum, P.M. and Kumar, V.K., "The Dynamics and Control of Large Flexible Space Structures - III, Part B: The Modelling, Dynamics, and Stability of Large Earth Pointing Orbiting Structures," Final Report NASA Grant: NSG-1414, Suppl. 2, Sept. 1980.

2. Johnson, M.W., and Reissner, E., "On Transverse Vibrations of Shallow Spherical Shells," Quarterly of Applied Mathematics, pp. 367-380, Vol. 15, No. 4, 1958.

3. Itao, K. and Crandall, S.H., "Natural Modes and Natural Frequencies of Uniform, Circular, Free-Edge Plates," Trans. of the ASME, Journal of Applied Mechanics, pp. 448-453, Vol. 46, June 1979.

4. Armstrong, E.S., "QRACLS - A System for Linear-Quadratic-Gaussian Control Law Design," NASA Technical Paper 1106, April 1978.

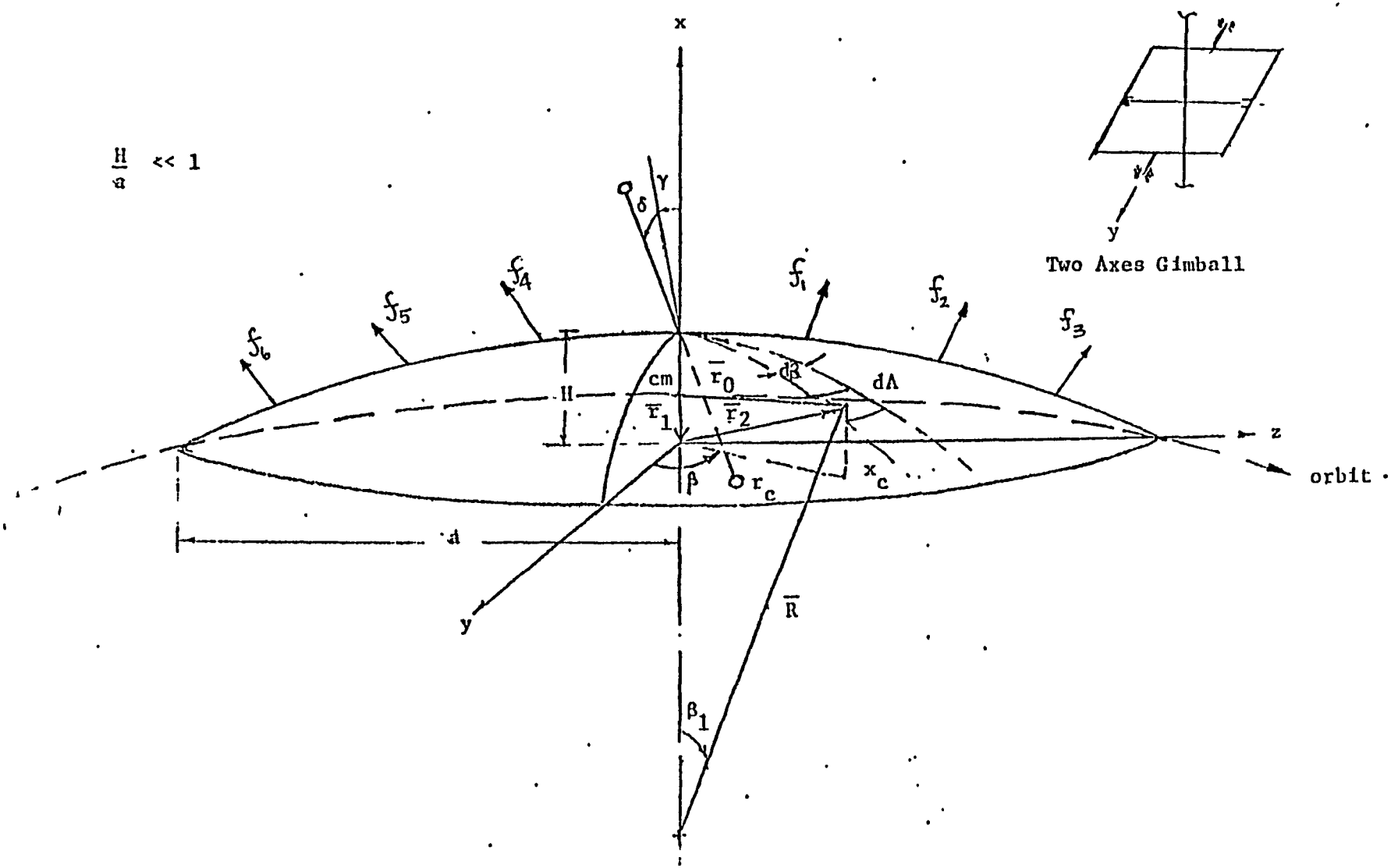

Fig. IV-1 : Shallow Spherical Shell with dumbbell

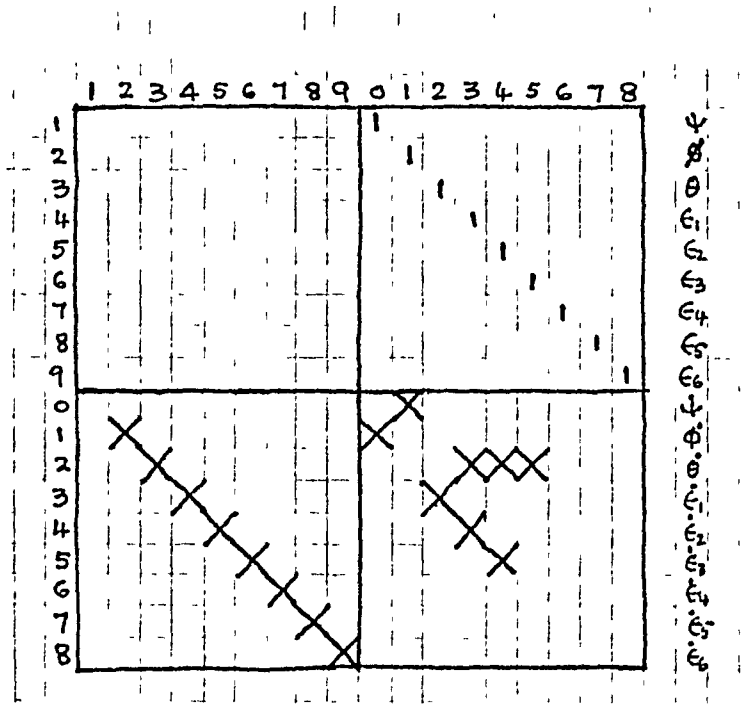

Fig. IV-2: Location of the Non-zero Elements of the "A" Matrix of Shell without the Dumbbell.

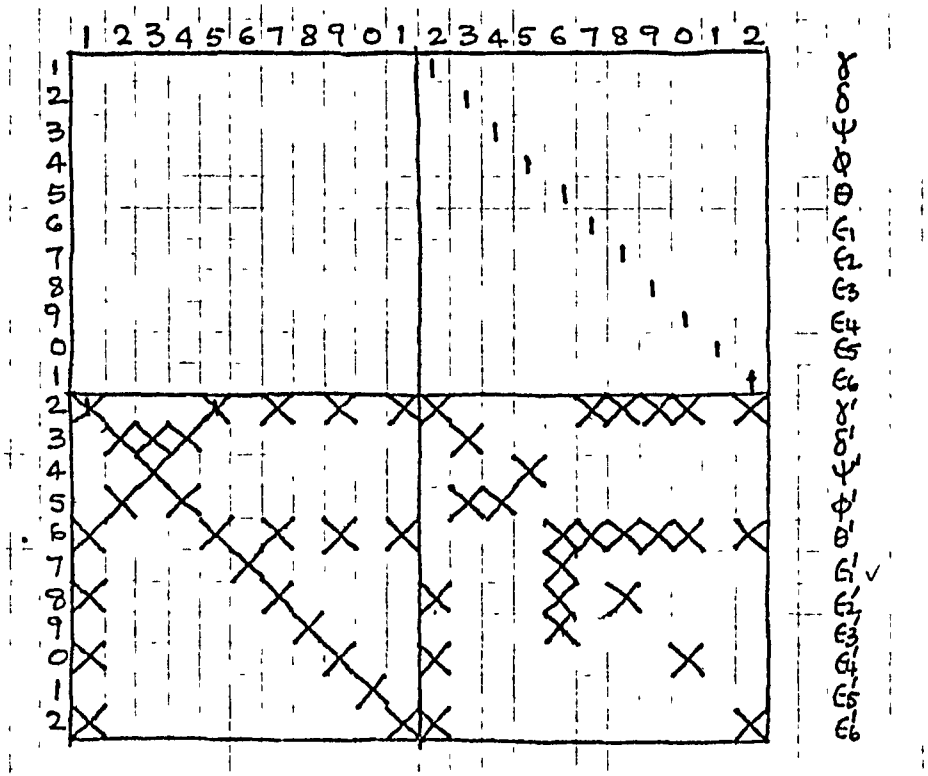

Fig. IV-3: Location of Non-zero Elements of the "A" Matrix of the Shell with the Dumbbell.

H = 1m h = 1cm a = 100 m
m = 869679.8058 kgs.

$\theta_0 = \psi_0 = \varepsilon_{10} = \ldots = \varepsilon_{60} = 0.01$

Control law based on pole placement-negative real part = -1.72 (dimensionless)
time constant = 461 seconds

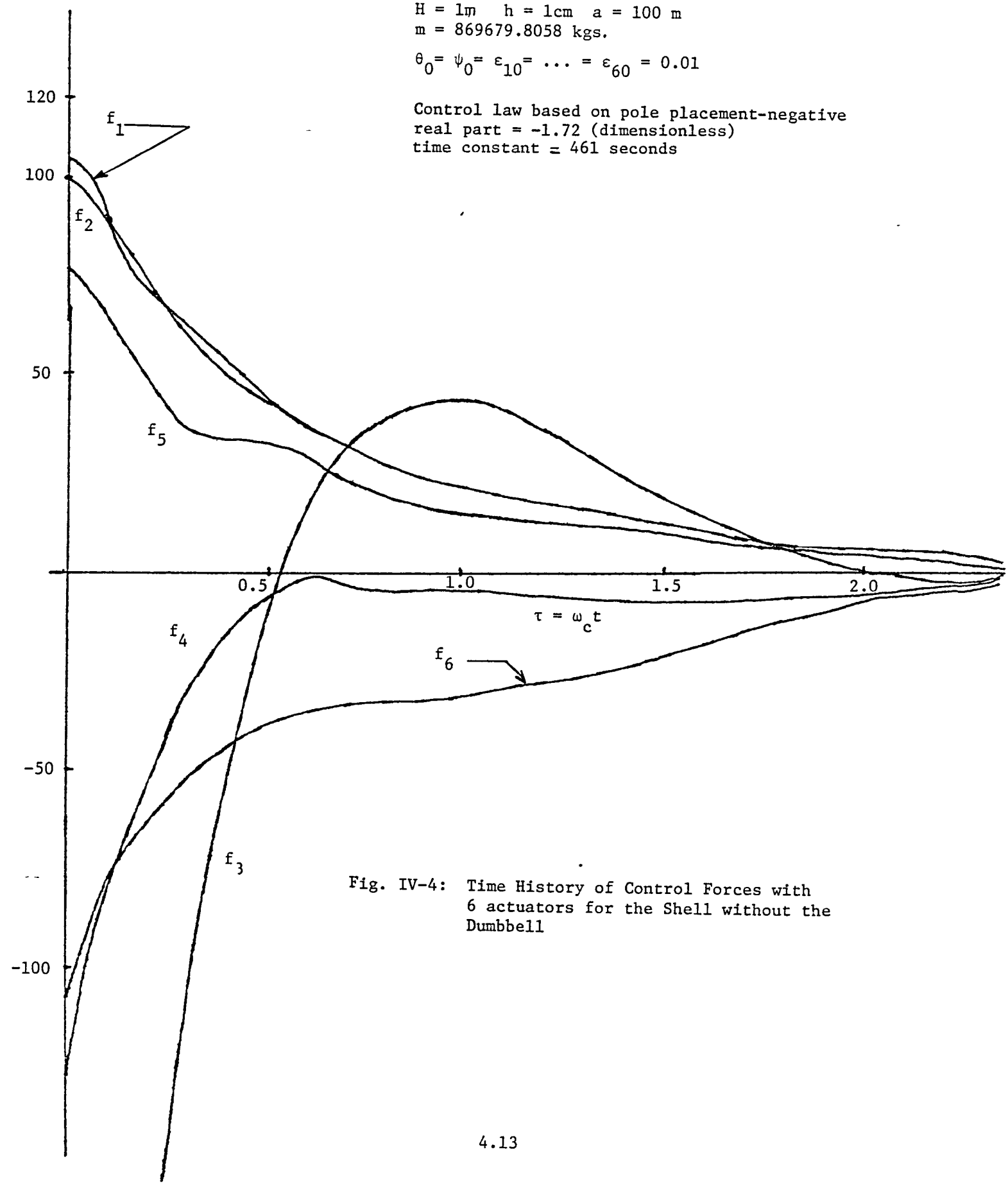

Fig. IV-4: Time History of Control Forces with 6 actuators for the Shell without the Dumbbell

NOMENCLATURE - CHAPTER IV

A_n	:	modal amplitudes
$\bar{C}$	:	external torques with components (C_x, C_y, C_z)
c, c_y, c_z	:	co-efficients of viscous damping
$\bar{c}, \bar{c}_y, \bar{c}_z$	:	$c/J_y\omega_c$, $c_y/J_y\omega_c$, $c_z/J_z\omega_c$, respectively
$C_y^{(n)}, C_z^{(n)}$	:	$\frac{\ell \partial \phi_x^{(n)}}{\partial y}(0,0)$, $\frac{\ell \partial \phi_x^{(n)}}{\partial z}(0,0)$, respectively
$C_y^{(mn)}, C_z^{(mn)}$	:	$\frac{J_y}{M_m \ell^2} C_y^{(m)} C_y^{(n)}$, $\frac{J_z}{M_m \ell^2} C_z^{(m)} C_z^{(n)}$
c_1	:	J_y/I_d
c_2	:	J_z/I_d
c_3	:	$J_y/m\ell^2$
E_n	:	modal component of external forces
I_d	:	moment of inertia of the dumbbell
J_x, J_y, J_z	:	principal moments of inertia of the undeformed shell
k, k_y, k_z	:	torsional spring constants
$\bar{k}, \bar{k}_y, \bar{k}_z$	:	$k/J_y\omega_c^2$, $k_y/J_y\omega_c^2$, $k_z/J_z\omega_c^2$, respectively
ℓ	:	characteristic length
$2\ell_d$	:	length of the dumbbell
M_n	:	modal mass of n^{th} mode
m	:	mass of shell
m_d	:	tip mass of the dumbbell
R	:	radius of curvature of the shell
$\bar{r}_1$	:	vector from the mass center of the shell to the origin of $(x_c y_c z_c)$
$\bar{r}_2$	:	position vector of a generic point on undeformed shell $(x_c y_c z_c)$
r_c	:	radial distance of the shell element from the symmetry axis of the shell

t	:	time
β	:	polar angle
β_o	:	phase angle
(γ,δ)	:	dumbbell deflection angles
ε_n	:	A_n/ℓ
ζ	:	damping ratio
θ,ψ,ϕ	:	pitch, yaw and roll angles, respectively
ρ	:	mass density
τ	:	$\omega_c t$
τ_c	:	coordinate frame, $(x_c y_c z_c)$
τ_d	:	dumbbell frame $(x_d y_d z_d)$
$\bar{\omega}$	:	body angular velocity vector, $(\omega_x \omega_y \omega_z)$ or $(\omega_r \omega_\beta \omega_x)$
ω_c	:	orbit angular velocity
ω_n	:	natural frequency of n^{th} mode
$\Omega_x,\Omega_y,\Omega_z$	:	$(J_z-J_y)/J_x$, $(J_x-J_z)/J_y$, $(J_y-J_x)/J_z$, respectively
$(\cdot)$	:	$\frac{d}{dt}$
$(\,)'$	:	$\frac{d}{d\tau}$

CHAPTER V

THE DYNAMICS OF LARGE FLEXIBLE EARTH POINTING STRUCTURES WITH A HYBRID CONTROL SYSTEM

INTRODUCTION

Proposed future applications of large space structures include: space based power generation and transmission (to earth); communications; earth resource observation missions; and electronic mail systems. The applications described here all require that the largest surface (length) of the system be nominally oriented along the orbital tangent or normal to the local vertical. In order to satisfy the mission requirements for some of these applications control of the shape of the structure as well as the orientation will be required.

Previously, the equations of motion of a general arbitrary flexible spacecraft in orbit have been developed.[1,2] As a specific example, the dynamics and stability of a long, flexible beam constrained to move only in the orbital plane without control was considered, with the principal emphasis placed on the motion about the nominal earth pointing (local vertical) orientation.[2]

It was observed that for small amplitude pitch and flexural oscillations, the rigid pitch mode was not affected by the elastic modes, and that the elastic motion was coupled to the pitch mode and described by a Mathieu equation. The possibility of parametric instability at very low natural elastic frequencies was demonstrated.

In a recent paper[3] the work of Ref. 2 was extended to consider: (1) the motion and stability of the beam about a nominal local horizontal orientation; and (2) the dynamics of free-free homogeneous platforms in orbit with emphasis placed on a circular plate structure. Both models included only the presence of an articulated passive damping device.

It is well known that, due to an unfavorable moment of inertia ratio, a rigid orbiting thin beam, when displaced from a local horizontal orientation, will not tend to return to this orientation in the absence of external control forces. This tendency is also observed when the flexural dynamics are added to the model. Such a structure can be gravitationally stabilized by using a rigid dumbbell with proper moment of inertia (Fig. 1). In Ref. 3 the dumbbell was assumed to be attached at the center of beam by a spring loaded hinge with viscous damping also present. It was seen that the pitch motion, the dumbbell librational motion, and the anti-symmetric elastic modes of the beam were all coupled. Within the linear range, the beam's symmetric elastic modes were decoupled from the pitch and dumbbell motions. The frequencies of the symmetric elastic modes were adjusted to include the effect of the dumbbell. Using the Routh-Hurwitz criteria, stability conditions were derived and limits on key system parameters established. A parametric study of the least damped mode characteristics for different system parameters was carried out. In Ref. 3 the three dimensional equations of motion for a flat plate in orbit with a two-degree-of-freedom gimballed dumbbell were also developed and, within the linear range, it was seen that only certain of the elastic modes were influenced by the dumbbell motion. Thus, in order to damp the motion of such systems nominally oriented along the local horizontal in all the modes generally contained within any truncated system model, it was concluded that the use of active devices would also be required. However, it was thought that with the use of the passive gimballed dumbbell together with the active controllers, the fuel consumption could be significantly reduced without exceeding the previous limits on the peak forces.

The present paper examines the dynamics and control of such large flexible earth pointing structures in orbit under the influence of a hybrid control system consisting of the passive gimballed dumbbell together with active point thrusters.

A THIN UNIFORM BEAM IN ORBIT NOMINALLY ORIENTED ALONG THE LOCAL HORIZONTAL

The Mathematical Modelling of a Flexible Orbiting Beam - Local Horizontal Orientation

The equations of motion for a thin uniform beam in orbit with its axis nominally along the local horizontal (Fig. 1a) is developed in Ref. 3. The beam is assumed to undergo only inplane angular motions and deformations and it is assumed also that the center of mass of the beam follows a circular orbit. The beam's elastic motions are considered to be unconstrained and the longitudinal vibrations of the beam are assumed to be negligible in comparison with the transverse vibrations. For the case of small amplitude pitch oscillations of the beam, the linearized equations of motion are derived as[3],

$$\theta''-3\theta = C_y/J_y\omega_c^2 \qquad (1)$$

$$\varepsilon_n'' + [(\omega_n/\omega_c)^2-3]\varepsilon_n = E_n/M_n\omega_c^2\ell \qquad (2)$$

where

ℓ = undeformed beam length

θ = pitch angle

ω_c = orbital angular velocity

C_y = external torque about the pitch axis

J_y = beam pitch axis moment of inertia

A_n = n^{th} flexural modal amplitude

ε_n = A_n/ℓ nondimensionalized n^{th} flexural modal amplitude

M_n = n^{th} modal mass

$( )' = \frac{d}{d\tau}$ where $\tau = \omega_c t$

t = time

As can be seen from Eq. (1), the uncontrolled local horizontal orientation of the beam represents an unstable motion. This unstable configuration of the beam can be stabilized either by providing active control torques or by adjusting the moment of inertia distribution of the system such that the resulting gravity-gradient torques provide stabilization. A gravitationally stabilized system using a connected rigid dumbbell will be considered in the next section. Eqs. (1) and (2) can be represented in a state vector form for a ready application of linear control theory.

After defining the coordinates according to:

$$\theta = x_1, \quad \varepsilon_1 = x_2, \quad \varepsilon_2 = x_3, \quad \ldots, \quad \varepsilon_{n-1} = x_n \tag{3}$$

and $\theta' = x_{n+1}$, $\varepsilon_1' = x_{n+2}$, $\varepsilon_2' = x_{n+3}$, $\ldots$, $\varepsilon_{n-1}' = x_{2n}$, then Eqs. (1) and (2) take the form

$$\dot{X} = AX + B_c U_c \tag{4}$$

where $X = [x_1, x_2, \ldots x_n, x_{n+1}, \ldots x_{2n}]^T$

$$A = \begin{bmatrix} \underset{\sim}{0} & I_1 \\ A_1 & \underset{\sim}{0} \end{bmatrix} \tag{5}$$

where

$\underset{\sim}{0}$ = nxn null matrix; I_1 = nxn identity matrix

A_1 = diag. $[-3 \ -(\omega_1/\omega_c)^2+3 \ \ldots \ -(\omega_{n-1}/\omega_c)^2+3]$

$B_c = \begin{bmatrix} 0 \\ -- \\ I \end{bmatrix}$ 0 = null vector of order n; I = identity vector of order n

$U_c = [C_y/J_y\omega_c^2, \ E_1/M_1\omega_c^2\ell, \ \ldots, E_{n-1}/M_{n-1}\ell\omega_c^2]^T$

Dumbbell Stabilized Flexible Beam in Orbit with the Longitudinal Beam Axis Nominally Along the Local Horizontal

A passive stabilization of the beam can be obtained by using a rigid dumbbell with proper moment of inertia. In Ref. 3, the equations of motion for a beam with a dumbbell assumed to be attached at the center of mass of the beam (Fig. 1b) through a spring loaded hinge and having viscous rotational damping have been developed. In addition to the assumptions made in developing Eqs. (1) and (2), it is further assumed that the dumbbell mass is concentrated at the tips and that the viscous force at the hinge is linear. With the usual assumptions of small pitch amplitude and dumbbell oscillations and flexural deformations, the linearized equations of motion in the absence of active control and external forces are obtained as[3]:

$$\theta'' + \bar{c}\theta' + (\bar{k}-3)\theta - \bar{c}\alpha' - \bar{k}\alpha + \Sigma_n(\bar{c}\varepsilon_n' + \bar{k}\varepsilon_n)C_z^{(n)} = 0 \tag{6}$$

$$\alpha'' + c_1\bar{c}\alpha' + (c_1\bar{k}+3)\alpha - c_1\bar{c}\theta' - c_1\bar{k}\theta - \Sigma_n(\bar{c}\varepsilon_n' + \bar{k}\varepsilon_n)c_1 C_z^{(n)} = 0 \tag{7}$$

$$\varepsilon_n''+(\Omega_n^2-3)\varepsilon_n - \{\bar{k}(\alpha-\theta)+\bar{c}(\alpha'-\theta')\}C_z^{(n)}J_y/M_n\ell^2+\sum_m(\bar{c}\varepsilon_m'+\bar{k}\varepsilon_m)C_z^{(nm)} = 0 \quad (8)$$

where $C_z^{(mn)} = J_y C_z^{(m)} C_z^{(n)}/M_n\ell^2$; (m,n = 1,2,...) and M_n = mass of the beam for all n.

$\bar{k}$ = $k/J_y\omega_c^2$; $\bar{c} = c/J_y\omega_c$

k = torsional restoring spring constant at the hinge

c = viscous damping coefficient

α = angle between the dumbbell axis and the local vertical

$C_z^{(n)} = \left.\dfrac{\partial\phi_x^{(n)}}{\partial z}\right|_{z=0}$

ϕ_x = beam shape function

$c_1 = J_y/I_d$, I_d = pitch moment of inertia of the dumbbell.

$\Omega_n = \omega_n/\omega_c$

The following observations can be made from a study of Eqs. (6)-(8): (a) the pitch motion of the beam, the dumbbell motion (α), and the elastic motion of the beam (ε_n) are all coupled to each other; (b) within the linear range the elastic modes for which $C_z^{(n)} = 0$ (the symmetric modes), are completely independent of the pitch and dumbbell motions. Furthermore, these modes do not influence either the pitch or dumbbell motion; (c) becuase of the presence of the dumbbell the natural frequencies and the mode shapes of the symmetric modes of the beam differ from those of the free-free beam. The frequencies and mode shapes can be easily obtained by replacing the dumbbell by a concentrated mass, equal to that of the dumbbell, at the center of the beam.[4] Eqs. (6),(7) and (8) can be rewritten in the state vector form of Eq. (4). With the inclusion of the first two free-free beam elastic modes, the eighth order matrix A has the form

$$A = \begin{bmatrix} \underset{\sim}{0} & I_1 \\ A_1 & A_2 \end{bmatrix}$$

where

$\underset{\sim}{0}$ = 4x4 null matrix

I_1 = 4x4 identity matrix

$$A_1 = \begin{bmatrix} 3-\bar{k} & \bar{k} & 0 & -\bar{k}f_2 \\ \bar{k}c_1 & -\bar{k}c_1-3 & 0 & \bar{k}c_1 f_2 \\ 0 & 0 & 3-\Omega_1^2 & 0 \\ -\bar{k}c_2 & \bar{k}c_2 & 0 & 3-\Omega_2^2-kf_2c_2 \end{bmatrix}$$

and

$f_n = c_z^{(n)}$ and $f_1 = 0$ (symmetric mode)

$c_1 = J_y/I_d$

$c_2 = f_2 J_y/M_n \ell^2$

$$A_2 = \begin{bmatrix} -c & \bar{c} & 0 & -\bar{c}f_2 \\ \bar{c}c_1 & -\bar{c}c_1 & 0 & \bar{c}c_1 f_2 \\ 0 & 0 & 0 & 0 \\ -\bar{c}c_2 & \bar{c}c_2 & 0 & -\bar{c}c_1 f_2 \end{bmatrix}$$

Modelling of the Point Actuators for the Beam

Let there be p actuators located along the beam at distances $\xi_1, \xi_2, \ldots \xi_p$ from the center of mass of the beam and the actuator forces be $f_1, f_2, \ldots f_p$, respectively. For small elastic displacements, the control torque due to the j^{th} actuator may be expressed as

$$\bar{N}_{p_j} = \bar{r} \times \bar{f}_j \qquad (10)$$

where

$\bar{f}_j \tilde{=} \bar{k} f_j \delta(\xi-\xi_j)$; i,j,k = unit vectors along the ξ,η,ζ directions.

$\bar{r} = \xi_j \bar{i} + \bar{q}_j(\xi_j)$

$\bar{q}_j = \sum_{n=1}^{\infty} \phi_z^n(\xi) A_n(t) \bar{k}$

and ϕ_z^n in the z^{th} component of the modal shape function corresponding to the n^{th} mode.

For small deflections $\bar{q}_j \approx 0$, and there are no force components along the x and y directions. Therefore,

$$\bar{N}_{p_j} = -\bar{j} f_j \xi_j \tag{11}$$

and for p actuators

$$\bar{N}_p = \Sigma_j \bar{N}_{p_j} = -j[f_1\xi_1 + f_2\xi_2 + \ldots + f_p\xi_p] \tag{12}$$

The control forces can be transformed into the corresponding modal forces by[5,2]

$$E_{nj} = \int \bar{\phi}^n \cdot \bar{f}_j dm \tag{13}$$

under the assumptions previously stated

$$E_{nj} = f_j \, \phi_z^n (\xi_j) \times (\text{a constant}) \tag{14}$$

The constant can be incorporated into f_j so that the effect of all p thrusters on the n^{th} generic mode can be expressed by

$$E_n = f_1\phi_z^{(n)}(\xi_1) + \ldots + f_p\phi_z^{(n)}(\xi_p) \tag{15}$$

The control vector, U_c, can now be related to the actuator forces, actuator locations, and modal shape functions by

$$U_c = \underset{nxp}{\begin{bmatrix} -\xi_1/J\omega_c^2, & -\xi_2/J\omega_c^2, \ldots & , -\xi_p/J\omega_c^2 \\ \phi_z^1(\xi_1)/M_1\ell\omega_c^2, & \phi_z^1(\xi_2)/M_1\ell\omega_c^2, & \ldots, \phi_z^1(\xi_p)/M_1\ell\omega_c^2 \\ \vdots & & \vdots \\ \phi_z^{n-1}(\xi_1)/M_{n-1}\ell\omega_c^2, & \ldots, & \phi_z^{n-1}(\xi_p)/M_{n-1}\ell\omega_c^2 \end{bmatrix}} \underset{pxl}{\begin{bmatrix} f_1 \\ f_2 \\ \vdots \\ f_p \end{bmatrix}} \tag{16}$$

Control of the Orbiting Beam System

Since the beam with its axis nominally along the local horizontal represents an unstable motion, active control using thrusters will have to be provided. In the case of the beam stabilized using the dumbbell, active control is still required to achieve an acceptable time response during attitude corrections and to provide damping directly into the symmetric modes.

A single actuator located at the left end of the beam is assumed to provide this control. The fundamental natural frequency of the free-free beam is taken as 0.01 Hz. and the center of mass is assumed to move in a 250 nautical mile altitude circular orbit. For this case,

$$(\omega_1/\omega_c)^2 = 3200 \quad \text{and} \quad (\omega_2/\omega_c)^2 \approx 28{,}800$$

As an example, a 100 m. long slender hollow tubular beam of aluminum (2014T6) with outside diameter of 10.79 cm, and thickness 1.06 cm would exhibit these frequencies.

The controllability of the beam without the dumbbell Eq. (1) has been studied in Ref. 5. It is shown that for a beam with an actuator at one end the necessary and sufficent conditions for controllability are (with two modes in the model)

$$\omega_1 \neq \omega_2 \; ; \quad \omega_1 \neq \sqrt{3}\,\omega_c \; ; \quad \omega_2 \neq \sqrt{3}\,\omega_c$$

The controllability of the beam with the dumbbell was verified using the ORACLS[6] computer algorithm.

First, the control law is selected for the case of the beam without the dumbbell. Then the gain values are determined so that the system response is acceptable. The same control law and gain values are then applied to the case of the beam with the dumbbell and the system response is obtained for comparison.

The rate feed-back of all the states is required in order to obtain damping in the system. Further, as can be seen from Eq. (1), there is a pole on the positive real axis indicating instability. Hence, to move this pole to the left of the imaginary axis of the complex plane a pitch position feed-back is necessary. Assuming that pitch, pitch rate and modal amplitude rates are fed-back, the closed-loop system characteristic equation for the beam with the two modes included in the model is derived as

$$\begin{aligned} & s^6 - \{aK_4 + b(K_5+K_6)\}s^5 + \{c+d-(aK_1+3)\}s^4 \\ & - \{b(dK_5+cK_6) + aK_4(c+d) - 3b(K_5+K_6)\}s^3 \\ & + \{cd-(aK_1+3)(c+d)\}s^2 - \{acdK_4 - 3b(dK_5+cK_6)\}s \\ & - (aK_1+3)cd = 0 \end{aligned} \tag{17}$$

where

$$a = \ell/2J_y\omega_c^2 \; ; \; b = 1/M_1\ell\omega_c^2$$

$$c = (\omega_1/\omega_c)^2 - 3 \; ; \quad d = (\omega_2/\omega_c)^2 - 3$$

and K_1 = pitch gain; K_4, K_5, K_6 rate gains for pitch and modal amplitudes

By inspecting the coefficients of Eq. (17), the necessary conditions for stability of the system are found to reduce to the following, noting that a,b,c, and d are all positve for the beam under consideration,

(i) $aK_1 + 3 < 0$ or $K_1 < -3/a$

(ii) K_4, K_5, K_6 should be negative.

Numerical Examples - Orbiting Beam System

By selecting $K_1 = -0.07$, $K_4 = -0.005$, $K_5 = 0.1$ and $K_6 = -0.03$, the system response was obtained using numerical integration as shown in Fig. 2. Initial errors of 5^0 in pitch and 1.5m in the two modal amplitudes were assumed. The pitch motion and the two modal oscillations are seen to be under control and the transient motion has been essentially removed in about 6 orbital periods. The maximum control force required is about 0.025 Newtons.

The same control law with identical gain values is used to obtain the response of the dumbbell stabilized system. No feed-back from the dumbbell is assumed for the sake of simplicity. The following dumbbell parameters are assumed:

$$J_y/I_d = 0.9 \; ; \; \bar{k} = 60 \; ; \; \bar{c} = 0.562.$$

Fig. 3 shows the system response obtained by numerical integration for the dumbbell stabilized system with the same initial conditions as in Fig. 2. In comparsion with Fig. 2, the pitch and the second modal oscillations of the dumbbell stabilized beam are seen to have better response characteristics. The dumbbell oscillations directly affect the asymmetric mode (second mode) and as a result the asymmetric modal oscillations are very effectively damped. The symmetric mode oscillation (first mode) is not affected by the presence of the dumbbell and is controlled mainly by the actuator. The pitch motion is also influenced by the dumbbell motion as long as there is relative motion between the dumbbell and the pitch mode - i.e. $(\theta-\alpha)$ is not zero. The peak control force required is about 0.012 Newtons. There is a total savings of about 45 percent in the force-impulse requirement as compared to the case of the beam without the dumbbell. The change in the frequencies of the beam due to the addition of the dumbbell was determined using the results of Ref. 4. Using these frequency values the response of the system for the same initial conditions was obtained. No significant change was seen from the results in Fig. 3. Other numerical results were obtained with different initial conditions (not shown here) indicating, in each case, better response and fuel savings for the dumbbell stabilized system.

A THIN UNIFORM PLATE IN ORBIT WITH ITS MAJOR SURFACE NOMINALLY IN THE LOCAL HORIZONTAL PLANE

A flat plate with its major surface in the local horizontal plane is gravitatiionally unstable in the absence of external restoring torques. In order to provide stabilizing torques, active control using thrusters can be employed or the moment of inertia distribution can be readjusted using a rigid dumbbell, as in the case of the beam. A rigid dumbbell is assumed to be attached at the center of mass of the plate (Fig. 4) by a spring loaded double gimballed joint. Here, the dumbbell would have two degrees of freedom as described by the angles γ and δ as shown in Fig. 4.

The equations of motion for a thin uniform flat plate with its major surface nominally in the local horizontal plane and carrying a rigid dumbbell at the center of mass have been derived in Ref. 3. The assumptions made in the derivation can be summarized as: (a) the plate is thin and has uniform mass and stiffness properties; (b) the center of mass of the plate is moving in a circular orbit; (c) the longitudinal vibrations of the plate are negligible; (d) the plate is unconstrained; (e) the mass of the dumbbell is concentrated at the tips of the dumbbell; (f) the center of mass of the plate and that of the dumbbell coincide; (g) the attitude angles and vibration amplitudes are small. With the above assumptions one can derive the linearized equations of motion in the following nondimensional form[3]:

$$\psi'' - \Omega_x\psi-(1+\Omega_x)\phi' = 0 \tag{18}$$

$$\phi'' - 4\phi+2\psi'-\bar{c}_z\delta'-\bar{k}_z\delta+\Sigma_n(c_z\varepsilon_n'+\bar{k}_z\varepsilon_n)C_y^{(n)} = 0 \tag{19}$$

$$\theta'' - 3\theta-\bar{c}_y\gamma'-\bar{k}_y\gamma+\Sigma_n(\bar{c}_y\varepsilon_n'+\bar{k}_y\varepsilon_n)C_z^{(n)} = 0 \tag{20}$$

$$\varepsilon_n'' + (\Omega_n^2-3)\varepsilon_n-\{(\bar{c}_y\gamma'+\bar{k}_y\gamma)J_{\bar{y}}C_z^{(n)}+(\bar{c}_z\delta'+\bar{k}_z\delta)\,J_zC_y^{(n)}\}/M_n\ell^2 +\Sigma_m\{(\bar{c}_y\varepsilon_m'+\bar{k}_y\varepsilon_m)C_z^{(nm)}+(\bar{c}_z\varepsilon_m'+\bar{k}_z\varepsilon_m)C_y^{(mn)}\} = 0 \tag{21}$$

$$\gamma'' + \bar{c}_y(1+c_1)\gamma'+\{3+\bar{k}_y(1+c_1)\}\gamma+6\theta-(1+c_1)\Sigma_n(\bar{c}_y\varepsilon_n'+\bar{k}_y\varepsilon_n)C_z^{(n)} = 0 \tag{22}$$

$$\delta'' + \bar{c}_z(1+c_2)\delta'+\{4+\bar{k}_z(1+c_2)\}\delta+8\phi-2\psi'-(1+c_2)\Sigma_n(\bar{c}_z\varepsilon_n' +\bar{k}_z\varepsilon_n)C_y^{(n)} = 0 \tag{23}$$

where, ψ, ϕ, θ = yaw, roll and pitch angles, respectively; $\varepsilon_n = A_n/\ell$; A_n = modal amplitude; M_n = n^{th} modal mass; ℓ = characteristic length (eg. radius of a circular plate or length of the side of a square plate); γ, δ = dumbbell angles; J_x, J_y, J_z = principal moments of inertia of the plate; I_d = principal moment of inertia of the dumbbell; $\Omega_x = (J_z-J_y)/J_x$; k_y, k_z = torsional spring stiffness; c_y, c_z = damping co-efficients; and,

$$c_y = J_y/I_d;\ c_2 = J_z/I_d;\ \bar{k}_y = k_y/J_y\omega_c^2;\ \bar{k}_z = k_z/J_z\omega_c^2$$

$$\bar{c}_y = c_y/J_y\omega_c;\ \bar{c}_z = c_z/J_z\omega_c;\ C_y^{(n)} = \ell\left.\frac{\partial\phi_x^{(n)}}{\partial y}\right|_{y=0,\,z=0}$$

$$C_z^{(n)} = \ell\left.\frac{\partial\phi_x^{(n)}}{\partial z}\right|_{y=0,\,z=0};\qquad C_y^{(mn)} = J_yC_y^{(m)}C_y^{(n)}/M_m\ell^2$$

$$C_z^{(mn)} = J_zC_z^{(m)}C_z^{(n)}/M_m\ell^2;\quad \Omega_n = \omega_n/\omega_c$$

ω_n = n^{th} natural frequency of the plate

ω_c = orbital angular velocity

It is interesting to note that the elastic modes for which $C_y^{(n)} = 0$ and $C_z^{(n)} = 0$, are decoupled from the ψ, ϕ, θ, γ and δ motions.

The Case of a Flexible Square Plate

As a specific example of a flat plate, a thin homogeneous square plate is considered. The natural frequencies and mode shapes of a free-free square plate have been determined in Ref. 7. The parameters of the plate were assumed to be as follows:
material of the plate is aluminum; sides of the plate = 100m; thickness of the plate = 0.01m; density = 2768.0 kg/m^3; Young's modulus = 0.7441×10^{10} kg/m^2; Poisson's ratio =0.33.

The first five nodal patterns along with the frequencies obtained for the above plate parameters are shown in Fig. 5. It may be noted that the slopes at the center of the plate in all mutually orthogonal directions for the first three modes are zero and therefore these modes are completely decoupled from the rigid body rotations (ψ,ϕ,θ) and the dumbbell motions within the linear range. Hence to see the effect of the dumbbell on the dynamics of the plate it is essential to include at least the fourth and fifth modes of the plate.

Control of the Flexible Orbiting Plate

In order to control the doubly symmetric modes (the first three modes in the present model) and to obtain better time responses in $\psi,\phi,\theta,\gamma,\delta$ and the asymmetric modes, active control using thrusters will be employed. Since the plate is homogenous with sides of equal length, $J_z = J_y$ and hence $\Omega_x = 0$, resulting in an open-loop pole at the origin. This problem will be addressed, in this paper, by providing a separate actuator, f_1 (Fig. 4) which can control the yaw motion independently, in addition to an actuator which can control the other degrees of freedom, f_2 (Figs. 4 and 5). It is assumed that actuator, f_1, has a thrust direction nominally in the plane of the undeflected plate, whereas actuator, f_2, has a thrust direction normal to the plane of the undeflected plate. f_2 is selected so that it does not lie on any of the nodal lines as shown in Fig. 5.

The effect of the actuators can be modelled as follows;

$$\text{Let} \quad \bar{t} = t_\xi \hat{i} + t_\eta \hat{j} + t_\zeta \hat{k}$$
$$\bar{r} = \xi \hat{i} + \eta \hat{j} + \zeta \hat{k} \tag{24}$$

where $\bar{r}$ defines the postion of the actuator on the plate and $\hat{i}$, $\hat{j}$, $\hat{k}$ are unit vectors along the principal axes of the plate. Then,

$$\bar{T} = \bar{r} \times \bar{f} \tag{25}$$

The generic force due to the p^{th} actuator on the r^{th} mode is given by[8]

$$E_r = \iint W_r(\xi,\eta)\hat{k} \cdot \delta(\xi-\xi_p,\eta-\eta_p) f_p(t)\hat{k} d\xi d\eta \tag{26}$$

where $W_r(\xi_p,\eta_p)$ is the r^{th} modal shape function of the deformed plate.

It can be seen that both actuators, f_1 and f_2, will produce torques that affect the rigid modes, Eq. (25), but that only f_2 could produce a generic force on the flexible modes, Eq. (26). For this application

$$E_r = W_r(\xi_2, \eta_2) f_2 \tag{27}$$

where ξ_2, η_2 are the coordinates of f_2 in the plane of the undeflected plate.

The equations of motion can be rewritten in the state vector form as in Eq. (4). The components of the state vector can be identified as,

$$x_1 = \psi,\ x_2 = \phi,\ x_3 = \theta,\ x_4 = \gamma,\ x_5 = \delta,\ x_6 = \varepsilon_1,\ x_7 = \varepsilon_2,$$

$$x_8 = \varepsilon_4,\ x_9 = \varepsilon_4,\ x_{10} = \varepsilon_5,\ x_{11} = \psi',\ \ldots, x_{20} = \varepsilon_5'.$$

The corresponding matrix, A, of order 20x20 is obtained in the form of Eq. (9). For the selected location and number of actuators the matrix B_c, of Eq. (4) becomes

$$B_c = \begin{bmatrix} 0 \\ \sim \\ B_L \end{bmatrix}$$ where, $\overset{0}{\sim}$ is a 10x2 null matrix, and

$$B_1 = \begin{bmatrix} 0.96 & 0 & 0 & 0 & 0 & 0 & 0 & 0 & 0 & 0 \\ 0 & 1.36 & -1.09 & 0 & 0 & 0.019 & 0.011 & 0.018 & 0.013 & 0.013 \end{bmatrix}$$

Parameters of the dumbbell are taken as $c_1 = c_2 = 0.9$; $\overline{k}_y = \overline{k}_z = 60.0$ and $\overline{c}_y = \overline{c}_z = 1.12$. For this system the controllability was established by using the ORACLS[6] computer alogorithm and the control $U_c = KX$ is selected such that (A-BK) has the identical negative real part in each of its eigenvalues. This algorithm was found to be useful in determining the stabilizing gains of the system. The gains were first determined for the case of the plate without the dumbbell. These gain values were then used to control the dumbbell stabilized plate. No feed-back from the dumbbell motion was included. For initial conditions of 5° in pitch and 1.5m in each of the modal amplitudes, time responses were determined for both the dumbbell stabilized plate and the plate without the dumbbell.

Fig. 6 shows the time response of the square plate without the dumbbell but under active control. After an initial overshoot in pitch, roll and yaw, respectively, the attitude errors are seen to approach zero is about six orbital periods. The first three modal amplitudes are damped out in about two orbits. The fourth and fifth modal amplitudes require about 6 orbital periods to be completely removed. The maximum control force required for the yaw actuator, f_1, is about 3 Newtons and that for the pitch-roll actuator, f_2, is about 30 Newtons.

In Fig. 6 only the combination of the absolute values of $\bar{f}_1$ and $\bar{f}_2$ is depicted. The total combined force impulse required is approximately 48000 N-sec.

Fig. 7 shows the time response for the dumbbell stabilized plate with active control and with the same gain values and initial conditions for the case of Fig. 6. The time response is shown for only two orbital periods in which the pitch, roll and yaw motions have been damped out effectively. The significant improvement in response of the fourth and fifth modal amplitudes as compared with Fig. 6 should be noted. These two modal responses (asymmetric modes) are controlled mainly by the dumbbell motion. The maximum control force for the yaw actuator, f_1, is about 3 Newtons and that for the pitch-roll actuator, f_2, is about 25 Newtons. In addition to the improvement in the responses, the dumbbell stabilized plate requires about 15 percent less total force impulse than that for the case of the plate without the dumbbell (Fig. 6) for the initial conditions and the control law considered here.

CONCLUSIONS

The dynamics and control of large flexible structures nominally oriented along the local horizontal are analysed. A thin, long flexible beam and a thin flexible square plate are considered for specific applications. Orientation and shape control is assumed to be provided by a hybrid system consisting of a passive spring loaded gimballed dumbbell damper in addition to active point thrusters. The performance of the hybrid controlled structures is compared with that of the structures having only active control. In general, substantial improvement in response and fuel consumption for the case of the hybrid systems is shown.

ACKNOWLEDGEMENT

This research was supported by NASA Grant NSG, 1414, Suppl. 3.

REFERENCES

1. P. Santini, "Stability of Flexible Spacecrafts." Acta Astronautica, Vol. 3, pp. 685-713, 1976.

2. V.K. Kumar and P.M. Bainum, "Dynamics of a Flexible Body in Orbit," Paper No. 78-1418, AIAA/AAS Astrodynamics Conf., Palo Alto, Calif., August 7-9, 1978; Also in J. of Guidance and Control, Jan.-Feb. 1980, Vol. 3, No. 1, pp. 90-92.

3. P.M. Bainum and V.K. Kumar, "On the Dynamics of Large Orbiting Flexible Beams and Platforms Oriented Along the Local Horizontal," XXXI International Astronautical Congress, Tokyo, Japan, Sept. 21-28, 1980, Paper No. 80E-230; to appear, Acta Astronautica.

4. R.L. Bisplinghoff and H. Ashley, Principles of Aeroelasticity, Addison Wesley, N.Y., 1955, pp. 80-84.

5. P.M. Bainum and A.S.S.R. Reddy, "On the Controllability of a Long Flexible Beam in Orbit," Proc. of Second VPI&SU/AIAA Symposium, Blacksburg, Virginia, June 21-23, 1979, pp. 145-159.

6. E.S. Armstrong, "ORACLS - A System for Linear-Quadratic-Gaussian Control Law Design," NASA Technical Paper 1106, April 1978.

7. P.M. Bainum, A.S.S.R. Reddy, R. Krishna and P.K. James, "The Dynamics and Control of Large Flexible Space Structures-III; Part A: Shape and Orientation Control of a Platform in Oribit Using Point Actuators," Final Report, NSG-1414, June 1980.

8. A.S.S.R. Reddy, P.M. Bainum, H.A. Hamer and R. Krishna, "Control of a Large Flexible Platform in Orbit," AIAA/AAS Astrodynamics Conference, Danvers, Ma., Aug. 11-13, 1980. Paper No. 80-1668; to appear, Journal of Guidance and Control.

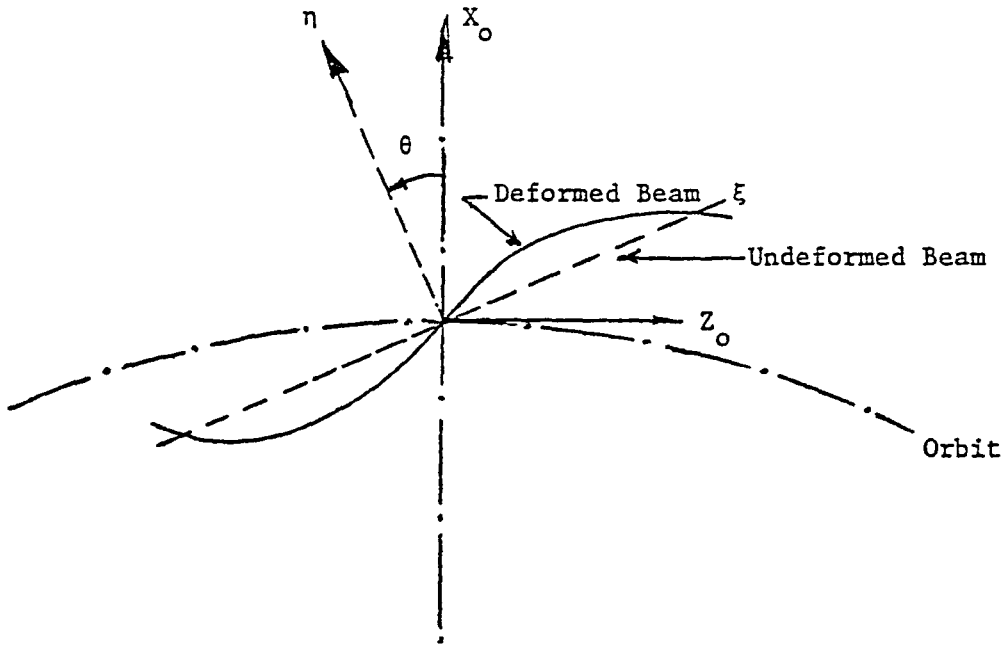

Fig. 1a. Uniform Flexible Beam Nominally Oriented Along the Local Horizontal.

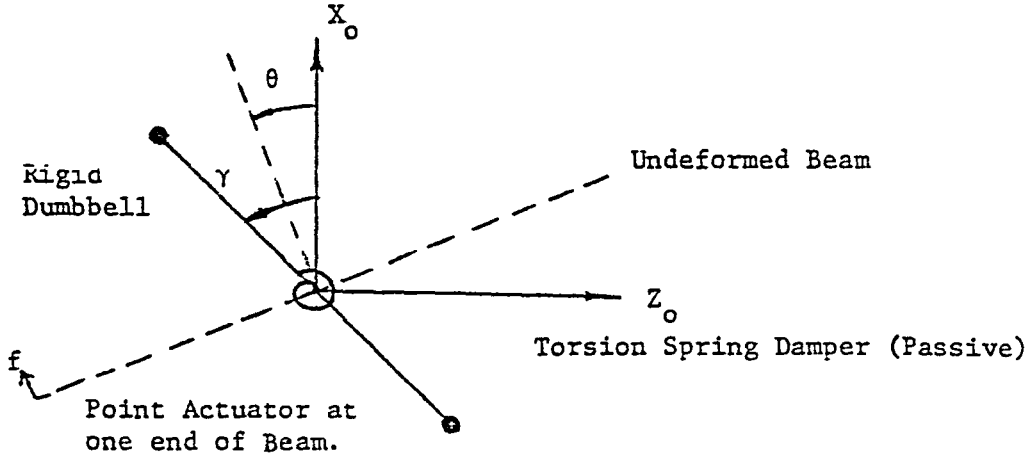

Fig. 1b. Dumbbell Stabilized Flexible Beam Nominally Oriented Along Local Horizontal with Passive and Active Controllers.

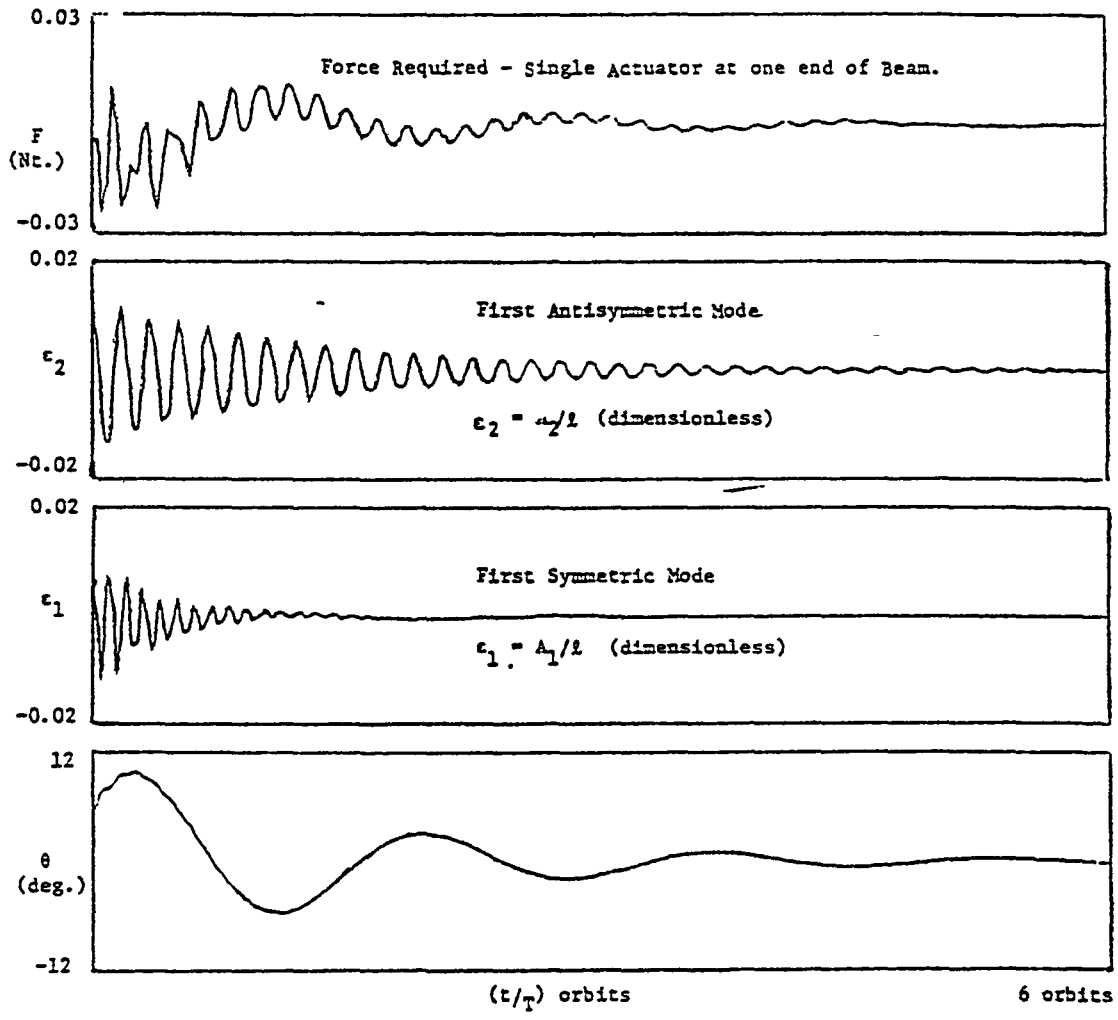

Fig. 2. Time Response of Flexible Beam with Active Control and No Dumbbell.

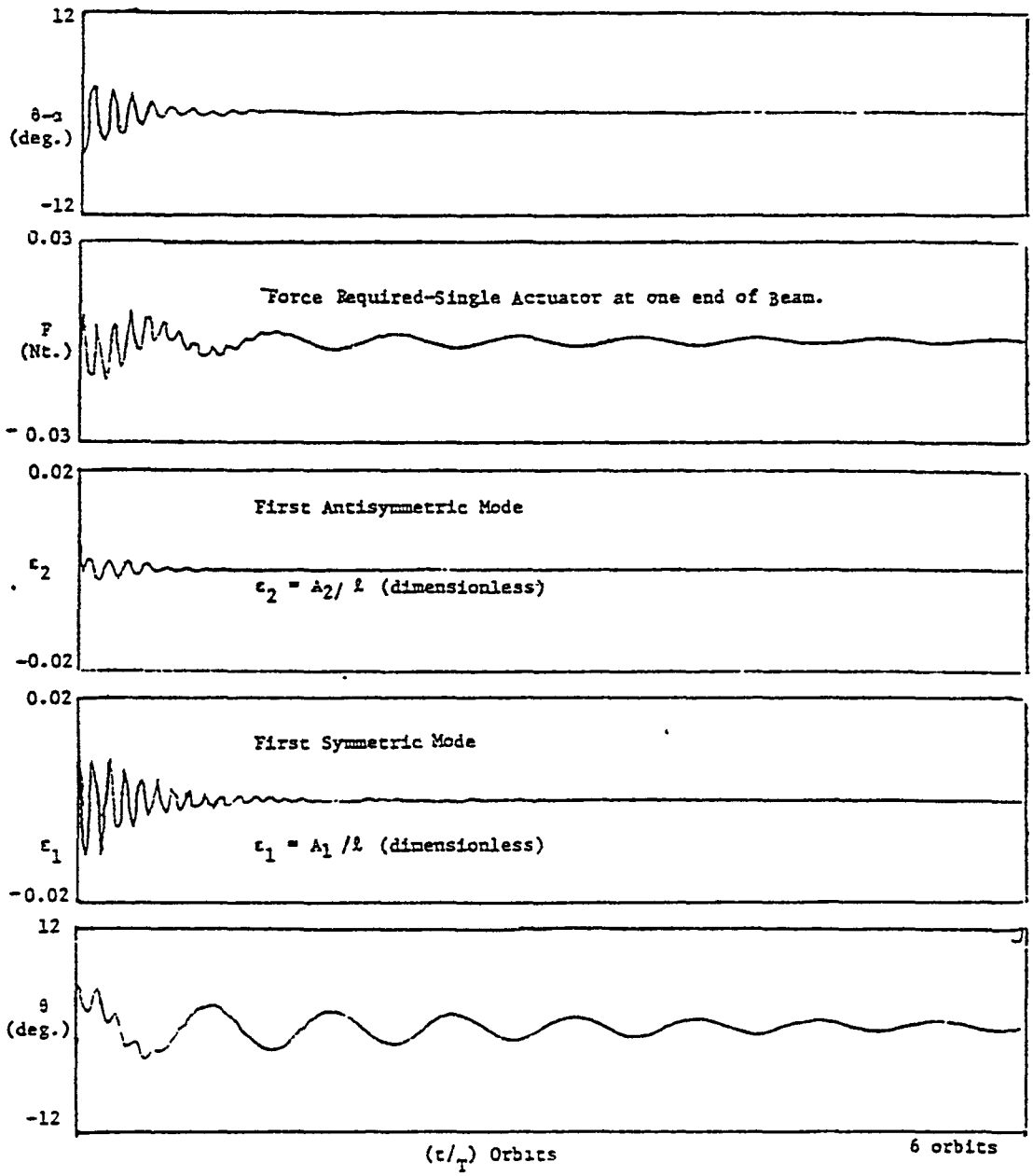

Fig. 3. Time Response of Dumbbell Stabilized Flexible Beam with Active Control.

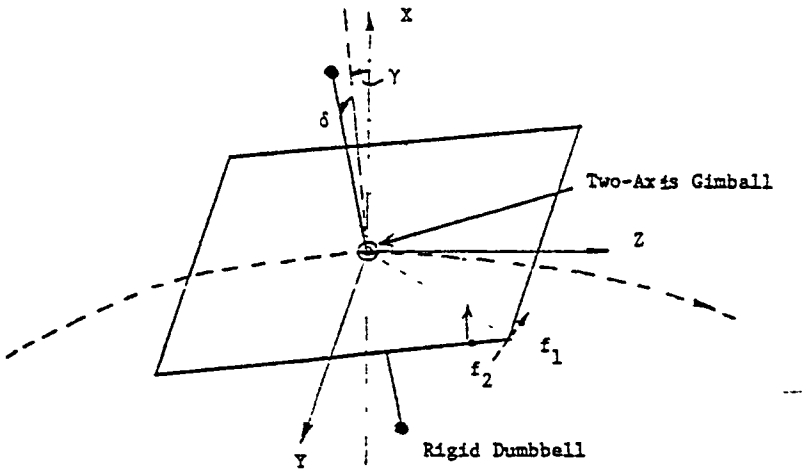

Fig. 4. Dumbbell Stabilized Square Plate in Orbit

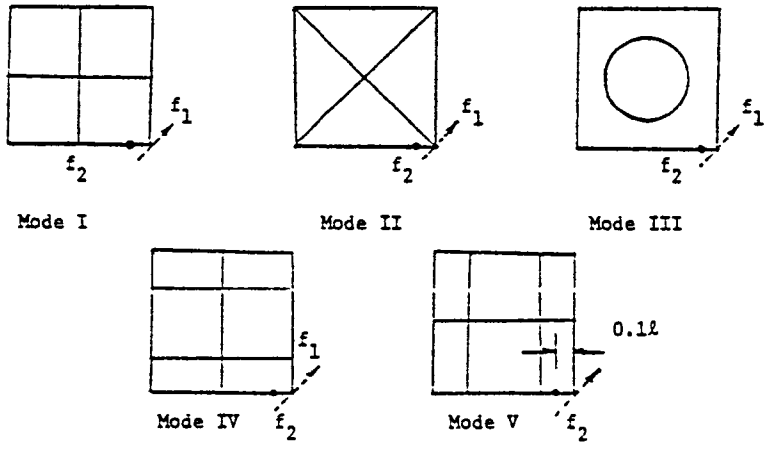

Fig. 5. Nodal Patterns of the Free-Free Square Plate and the Actuator Locations.

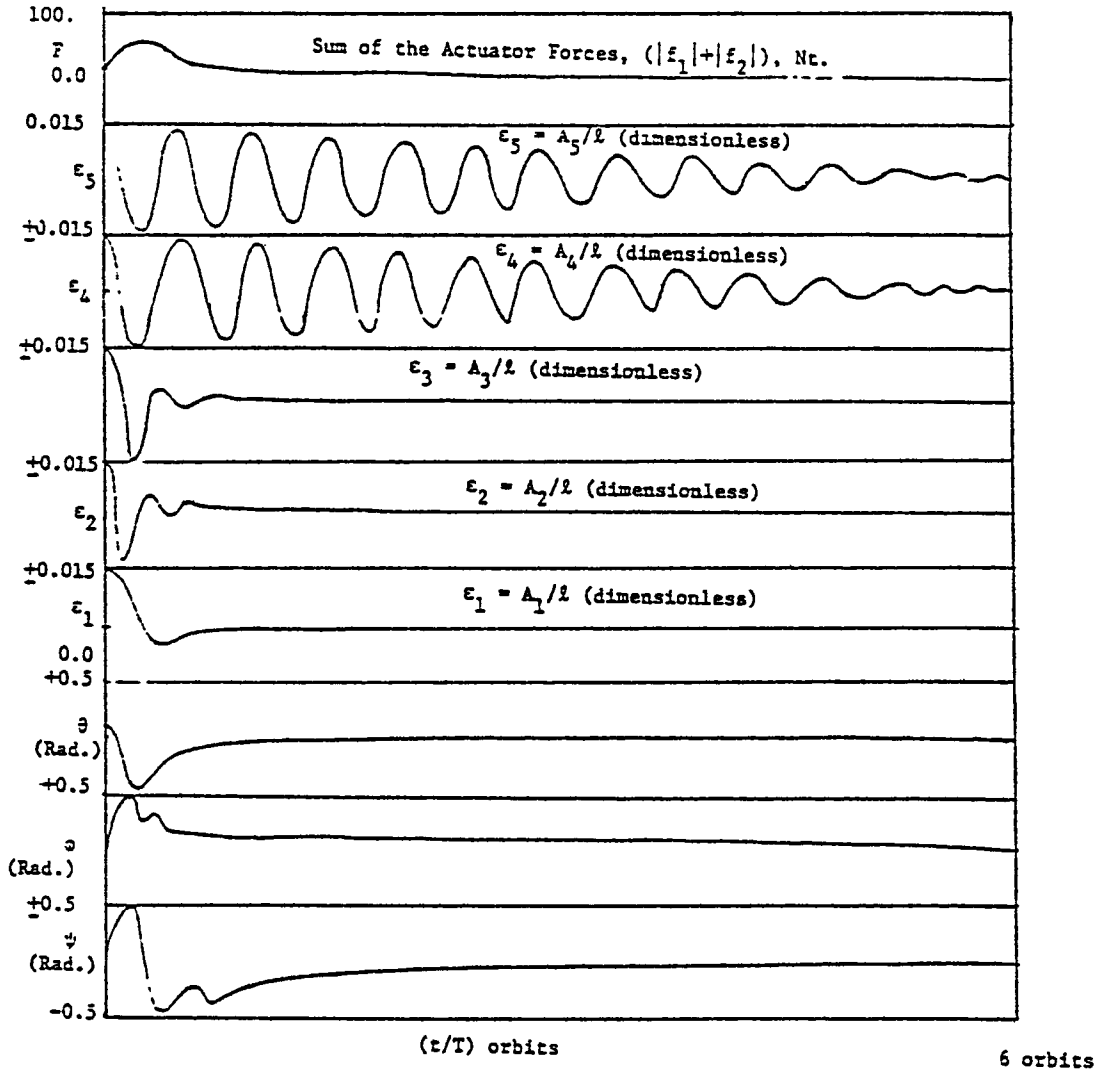

Fig. 6. Time Response of Flexible Square Plate with Active Control and No Dumbbell.

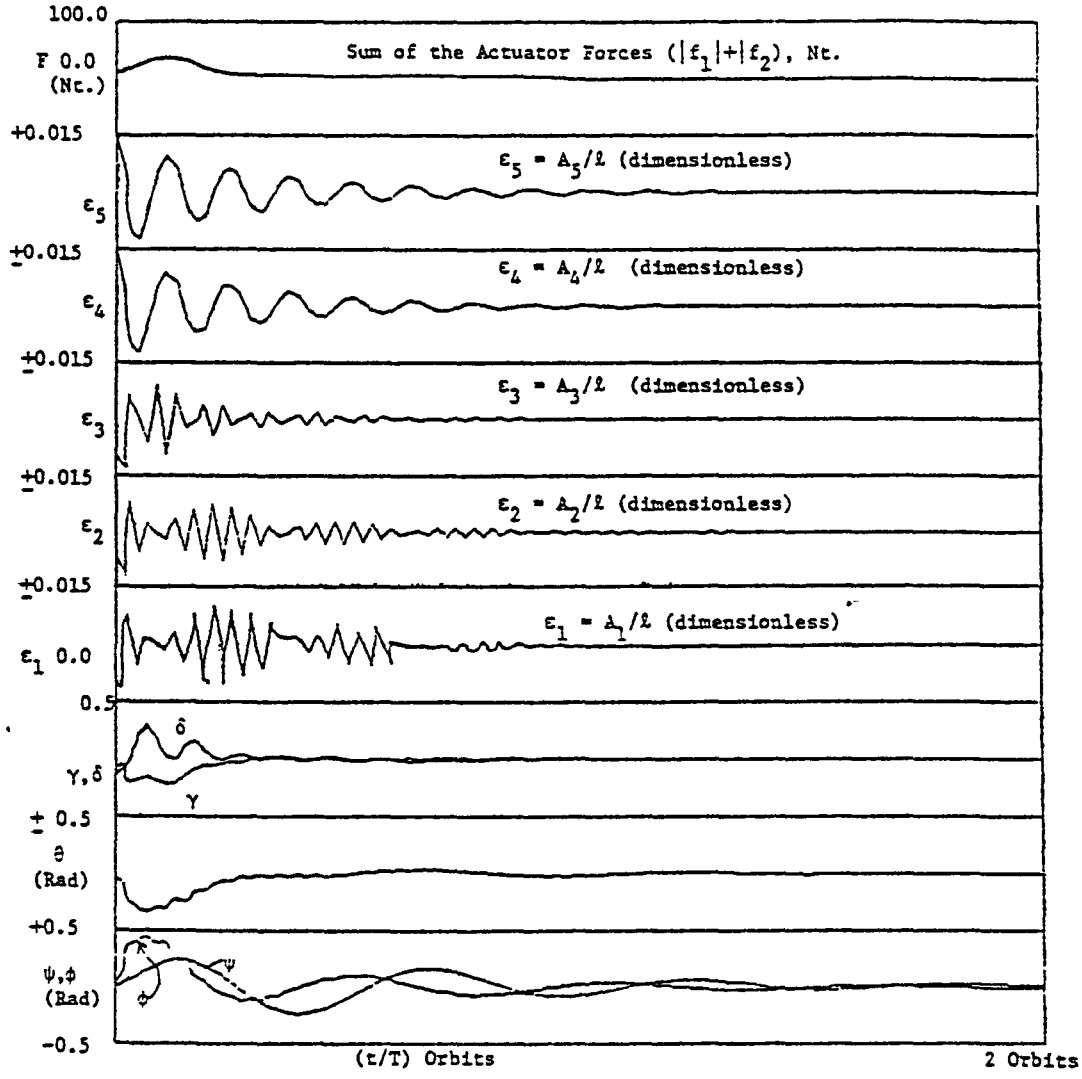

Fig. 7. Time Response of Dumbbell Stabilized Flexible Square Plate with Active Control.

VI. GENERAL CONCLUSIONS AND RECOMMENDATIONS

The effect of solar radiation pressure as the principal environmental disturbance torque has been incorporated into the model of the orbiting rigid shallow shell. For low earth orbit applications, computer simulation results indicate that within the linear range the rigid modal amplitudes are excited in direct proportion to the area to mass ratio. These amplitudes can be further amplified if the system is designed such that any of the natural frequencies are at the fundamental (or basic harmonics) of the forcing frequencies - i.e., orbital angular velocity or twice orbital angular velocity.

Graph theoretic techniques can be used for reducing the system (stiffness) matrix to lower ordered submatrices which can facilitate the calculation of eigenvalues for large ordered systems typical of LSST structures. The related reachability matrix and term rank concepts can be used to examine controllability with a reduction in the computations normally required to ascertain the rank of the system controllability matrix.

The dynamics and control of large flexible beams, plates and shells nominally oriented along the local horizontal are analyzed. Orientation and shape control is assumed to result from a hybrid system comprised of a passive spring loaded gimballed damper in addition to active point thrusters. In general, substantial improvement in response characteristics and fuel consumption is realized for the properly designed hybrid system when compared with the active system operating alone.

It should also be emphasized that the passive dumbbell system is reusable so that the savings in fuel consumption represented by a single transient response would be multiplied many times during the total mission lifetime.

Possible extensions to the work reported here could be: (1) further analysis of environmental effects on LSST systems to include the interaction of the environmental torques with the effects of flexibility; (2) a study of the sensor and actuator dynamics to include actual expected delays in these systems together with noise characteristics expected to be present in the plant as well as the measurement devices; (3) further application of the graph theory approach to consider systems with damping present and to aid in the calculation of eigenvectors as well as the eigenvalues previously considered; and (4) the adaptation of the previously developed general model of a large orbiting flexible system to more complicated, non-istropic systems such as the proposed Hoop-column Maypole configuration.

End of Document